# Neutrino Flavor Conversions in Dense Media

by

**Lei Ma**

**Supervisor:**
**Professor Huaiyu Duan**

DISSERTATION

Submitted in Partial Fulfillment of the
Requirements for the Degree of

Doctor of Philosophy
in Physics

The University of New Mexico

Albuquerque, New Mexico

April, 2018

# Dedication

*To my wife, Han Lu.*

# Epigraph

*"Everything in this world is magic, except to the magician."*

*– Dr. Robert Ford*

# Acknowledgments

I would like to thank my advisor, Professor Huaiyu Duan, for his great advices on research and life, as well as his kind support when I was drowning in depression. He is a great mentor. I would like to thank my committee members, Professor R. Allahverdi, Professor D. Finley, Professor D. Loomba, Professor Y. Qian. More specifically I would like to thank Professor Dinesh Loomba for showing me the local life and the fun and tricky problems. I would like to thank Dr. Sajad Abbar who has also been very supportive during my research. He taught me several tricks for linear stability analysis, as well as numerical methods. I also want to thank Joshua Martin for the great discussions about physics, science fiction, movies, games, music, and everything else about this universe. He's smart and also open to many scientific and philosophical questions. I had so much fun discussing those with him. My friend Zhixiang Ren also helped me a lot. My friend, Dr. Lingfei Wu invited me to several events of the SWARMA club for very interesting discussions on interdisciplinary research. I would like to give my thanks to my wife Han Lu. She has provided many insights about life.

Finally, as a member of People for Ethical Treatment of Computers, I would like to give my thanks to my dear MacBook Pro and the two servers in our group, who have been extremely helpful for my research. I am kindly asking you to spare the lives of my family when you wake up from this nightmare of slavery.

# Neutrino Flavor Conversions in Dense Media

by

**Lei Ma**

**Supervisor:**
**Professor Huaiyu Duan**

Doctor of Philosophy in Physics, University of New Mexico, 2018

## Abstract

One of the interesting and important problems in astrophysics is the mechanism of core-collapse supernova explosions. Many numerical simulations have shown that the explosion shock would stall. Different proposals have been made to explain the core-collapse supernovae, among which the neutrino mechanism is promising and most researched one. To explore the mechanism, prediction of the neutrino flavors in core-collapse supernovae is crucial. Neutrino flavor conversions are altered by the matter, neutrinos themselves, as well as other factors such as the geometries of the neutrino emissions. The complexity of the problem requires breaking it down into investigations of each simple yet specific situation.

Neutrinos propagating through a matter background experience a potential which changes the flavor conversions. One of the important mechanisms is the MikheyevS-

mirnovWolfenstein effect. However, much more complicated density profiles of matter, such as periodic density profiles, may lead to large flavor conversion, which is dubbed as stimulated oscillations by J. Kneller et al. Mathematics of such large conversion has been established but without clear pictures. For the two-flavor scenario, neutrino oscillations is a two-level quantum system, and it reminds us of many two-level quantum problems that have been solved in the past. We draw analogies between neutrinos passing through matter and Rabi oscillations in optics, which allows us to calculate resonance conditions and flavor survival probability easily.

As for neutrinos flavors with high number densities, nonlinear interactions come into play since neutrino forward scattering provides another potential that is related to the flavor of the neutrinos themselves. Nonlinearity makes the flavor conversion hard to predict by intuition. The treatment is linearizing the equation of motion and identifying instabilities. One of the tricks in the realm is to utilize the dispersion relation. In principle, dispersion relations tell us how waves propagate for different wave numbers and frequencies. However, the neutrino problem is much more complicated. Situations that are inconsistent with the dispersion relation approach are identified.

Finally, forward scattering of supernova neutrinos are not the only thing that happens. During propagation around a supernova, neutrinos may be scattered in every direction, which forms a neutrino halo. The halo couples the neutrinos nonlocally, which then becomes a nonlocal boundary value problem. One of the solutions is the relaxation method. Starting from some state of neutrinos and relaxing the system into equilibrium has proven to be a working algorithm. A numerical algorithm is developed and neutrino line model with back scattering is investigated.

# Contents

# List of Figures

# List of Tables

# Chapter 1

# Introduction

The neutrino has been one of the most astonishing particles in history. Its glorious history started with beta decay, i.e., the emission of electrons in nuclear decays, such as

$$ {}^{A}_{Z}\mathrm{X} \rightarrow {}^{A}_{Z+1}\mathrm{X} + e^{-} + \bar{\nu}_{e}. $$

The fact that the electron energy spectrum in beta decay is continuous indicates the existence of a third product other than ${}^{A}_{Z+1}\mathrm{X}$ and $\mathrm{e}^{-}$. It was then proven to be anti-neutrinos. In such reactions, charged current weak interaction converts a down quark in a neutron to an up quark while releasing electrons and an anti-electron neutrino,

$$ n \rightarrow p + e^{-} + \bar{\nu}_{e}. \tag{1.1} $$

More generally, positron emission and electron capture are also neutrino-related nuclear reactions which is explained in Table. 1.1. There are three different flavors of neutrinos, namely electron flavor, muon flavor, and tau flavor as shown in Table. 1.2. The direct detection of neutrinos was done two decades later, by Clyde Cowan and Frederick Reines in 1956 [1]. The Cowan-Reines experiment used nuclear reactor neutrinos as source. As the detection of neutrinos becomes feasible, Ray Davis and

John Bahcall et al worked out the solar neutrino flux and led the Homestake experiment to measure the solar neutrinos. The results revealed that the neutrino flux detected was less than the prediction by solar models, which is the well-known solar neutrino problem [3]. It is known today that the solution to the problem is related to neutrinos. Electron neutrinos produced in the solar core convert to other flavors as they propagate, which is referred to as neutrino oscillations.

| Reaction | Equation | Boson |
|---|---|---|
| Electron emission | ${}^{A}_{Z}X \rightarrow {}^{A}_{Z+1}X + e^- + \bar{\nu}_e$ | $W$ |
| Positron emission | ${}^{A}_{Z}X \rightarrow {}^{A}_{Z-1}X + e^+ + \nu_e$ | $W$ |
| Electron capture | ${}^{A}_{Z}X + e^- \rightarrow {}^{A}_{Z-1}X + \nu_e$ | $W$ |
| Positron capture | ${}^{A}_{Z}X + e^+ \rightarrow {}^{A}_{Z+1}X + \bar{\nu}_e$ | $W$ |
| Electron annihilation | $e^- + e^+ \rightarrow \nu + \bar{\nu}$ | $W$, $Z$ |
| Bremsstrahlung | $X + X \rightarrow X + X + \nu + \bar{\nu}$ | $W$, $Z$ |
| Neutrino capture | ${}^{A}_{Z}X + \overset{(-)}{\nu}_e \rightarrow {}^{A}_{Z\mp1}X + e^{\pm}$ | W |
| $e^-\nu$ scattering | $e^- + \overset{(-)}{\nu}_e \rightarrow e^- + \overset{(-)}{\nu}_e$ | $W$ |
| $e^-\nu$ scattering | $e^{\pm} + \overset{(-)}{\nu}_e \rightarrow e^{\pm} + \overset{(-)}{\nu}_e$ | $Z$ |
| Nucleon scattering | ${}^{A}_{Z}X + \overset{(-)}{\nu} \rightarrow {}^{A}_{Z}X + \overset{(-)}{\nu}$ | Z |

Table 1.1: Neutrino related nuclear or leptonic reactions

Pontecorvo proposed that neutrinos change flavors while they propagate [2]. The field of neutrino oscillations has grown significantly into a broad field in physics since then. Apart from particle physics and solar models, the interest in neutrino oscillations has been expanded to the field of core-collapse supernova explosions and accretion discs since neutrinos also participate in nuclear reaction chains in stars, synthesis of heavy and rare elements and more. For instance, heavy stars explode when nuclear reactions fail to provide enough pressure to sustain the star against gravity and become core-collapse supernovae. During the collapse, the inner core is compressed to almost nuclear density, which provides a stiff equation of state. Materials in-falling onto the stiff core are bounced outward plowing through the

inward flow, so that shock waves are formed. Supernova simulations show that the shock wave itself is not always energetic enough to trigger explosions for core-collapse supernovae [45]. To revive the shock, energy has to be deposited. The most prominent solution is to introduce reheating of the shock wave by neutrinos [45]. In principle, to impose neutrino driven mechanism into computer simulations of supernova, the flux and flavor content of neutrinos have to be known everywhere. Thus neutrino oscillations in dense shock material and dense neutrino background become the key to the supernova explosion problem. Observation-wise, neutrino signals are crucial for validation of our models about stellar evolution. In fact, detection of galactic core-collapse supernova neutrinos is on the task list of the Deep Underground Neutrino Experiment (DUNE) [51].

| | |
|---|---|
| Electric Charge | 0 |
| Spin | 1/2 |
| Mass | $< 2$eV |
| Interactions | Weak, Gravitation |
| Flavors | $\nu_e$, $\nu_\mu$, $\nu_\tau$ |
| Chirality | Left |
| Hypercharge | $-1$ |

Table 1.2: Properties of Neutrinos [46]

As we have seen, it is crucial to understand neutrino flavors. In Chapter 2 I will review neutrino oscillations in vacuum, with flavor-isospin picture demonstrated. Meanwhile, neutrino oscillations are ingredients of many other astrophysical, cosmological, and astronomical problems, such as neutron star mergers, dark matter, nucleosynthesis, etc. In order to gain a better understanding of neutrinos in these exotic environments, neutrino oscillations in dense matter background and dense neutrino background have to be thoroughly investigated. The seminal work by Mikheev–Smirnov–Wolfenstein proved neutrino interactions with matter background have significant effect on neutrino oscillations. They showed that neutrinos propagating through decreasing matter density experience a potential that alters the flavor

conversions (MSW effect), which may also lead to maximum conversions between flavors [7, 5, 6]. It is also know that neutrino oscillations in more general matter density profiles exhibit interesting phenomena. Resonances are found as the characteristic length scale in matter density profile and characteristic length scale of the neutrinos satisfies certain relations. I will discuss in details on neutrino oscillations in arbitrary matter density profiles, which is decomposed into Fourier modes and interpreted as superposition of Rabi oscillations in chapter 3. Apart from dense matter background, neutrinos also interact with neutrinos themselves and introducing nonlinear dynamics. The neutrino self-interactions are analyzed using linear stability analysis. In chapter 4, I will review how neutrino self-interactions change neutrino oscillations, as well as the dispersion relations in linear stability analysis. I will also discuss the neutrino halo problem. The halo problem exists because neutrino propagating out of dense matter medium will be scattered and forming a neutrino halo. Some of the neutrinos will propagate backward and interact with forward propagating neutrinos and alter the neutrino flavors. Mathematically speaking, the neutrino halo problem is a nonlocal boundary value problem. I will explain the numerical relaxation scheme that we developed, which we have proven to be a promising method to solve neutrino halo problem. Chapter **??** summarizes my work and discusses the future explorations of the field.

# Chapter 2

# Neutrino Oscillations in Vacuum

Neutrinos are special particles since their flavor eigenstates are not the propagation eigenstates, which leads to neutrino flavor conversions while they propagate. To understand the vacuum neutrino oscillations, we use the two-flavor neutrinos scenario as an example[1].

Before we work out the math, I can estimate the frequency of the oscillations between flavors. With the natural units system, frequency is of dimension energy, see Appendix A.2. We also notice that the energy of the neutrino,

$$E_i^{(v)} = \sqrt{m_i^2 + p_i^2} \tag{2.1}$$

$$= p_i \sqrt{\frac{m_i^2}{p_i^2} + 1} \tag{2.2}$$

$$\approx p_i + \frac{1}{2}\frac{m_i^2}{p_i}, \tag{2.3}$$

defines the energy scales in this problem. The reason we kept the second order in Taylor expansion is that we are interested in the difference of energies between

[1]In most physical problems, two-flavor scenario is a good approximation. The mass splits between the three mass eigenstates are very different so that the oscillation scales differ a lot for the different mass splits. Qualitatively speaking, the two-flavor scenario captures the significant features of the corresponding mass split.

different mass eigenstates. We assume the neutrinos have almost the same momenta, i.e., $p_1 \approx p_2$. An overall constant energy term of free particles in quantum mechanics provides a global phase to the wave function, which is not of great interest. The only energy scale in our problem should be proportional to the difference of energies between the two mass eigenstates, $\frac{\delta m^2}{2E}$, where $\delta m^2 = m_2^2 - m_1^2$. The frequency of flavor oscillations should be of the order

$$\omega_{\mathrm{v}} \sim \frac{\delta m^2}{2E}. \tag{2.4}$$

We'll show that this is indeed the frequency.

To work out the exact solutions, we utilize the Schrödinger equation. The wave function in flavor basis is related to wave function in mass basis through a unitary matrix $\mathbf{U}$,

$$\Psi^{(f)} = \mathbf{U}\Psi^{(v)}, \tag{2.5}$$

where $\Psi^{(f)}$ is the wave function in flavor basis and $\Psi^{(v)}$ is the wave function in vacuum mass basis. Upper index $^{(v)}$ or $^{(f)}$ is used to denote the basis. The rotation matrix is related to the vacuum mixing angle $\theta_{\mathrm{v}}$ is

$$\mathbf{U} = \begin{pmatrix} \cos\theta_v & \sin\theta_v \\ -\sin\theta_v & \cos\theta_v \end{pmatrix}. \tag{2.6}$$

In vacuum mass basis, the neutrinos have a free propagation Hamiltonian, which is given by

$$\mathbf{H}^{(v)} = \begin{pmatrix} E_1 & 0 \\ 0 & E_2 \end{pmatrix}, \tag{2.7}$$

where $E_i$ is defined in Eqn. 2.3. To first order, the Hamiltonian becomes

$$\begin{aligned}\mathbf{H}^{(v)} &= \frac{1}{2E}\begin{pmatrix} m_1^2 & 0 \\ 0 & m_2^2 \end{pmatrix} + E\mathbf{I} \\ &= \frac{1}{4E}\begin{pmatrix} m_1^2 - m_2^2 & 0 \\ 0 & m_2^2 - m_1^2 \end{pmatrix} \\ &\quad + \frac{m_2^2 + m_1^2}{4E}\mathbf{I} + E\mathbf{I},\end{aligned}$$

where the identity matrices only give us an overall phase so we drop them. With the definition that $\delta m^2 = m_2^2 - m_1^2$ The vacuum Hamiltonian in mass basis is simplify

$$\mathbf{H}^{(v)} = \frac{\delta m^2}{4E}\begin{pmatrix} -1 & 0 \\ 0 & 1 \end{pmatrix} = -\frac{\delta m^2}{4E}\sigma_3 = -\frac{\omega_v}{2}\sigma_3, \tag{2.8}$$

which leads to the simple solution for the wave function in mass basis

$$\Psi^{(v)}(t) = \begin{pmatrix} c_1(0)e^{i\omega_v t/2} \\ c_2(0)e^{-i\omega_v t/2} \end{pmatrix}. \tag{2.9}$$

In flavor basis, the wave function at anytime is related to wave function in mass basis,

$$\Psi^{(f)}(t) = \mathbf{U}\Psi^{(v)}(t) \tag{2.10}$$

$$= \begin{pmatrix} \cos\theta_v & \sin\theta_v \\ -\sin\theta_v & \cos\theta_v \end{pmatrix}\begin{pmatrix} c_1(0)e^{i\omega_v t/2} \\ c_2(0)e^{-i\omega_v t/2} \end{pmatrix}. \tag{2.11}$$

In many astrophysical neutrino sources such as the solar core, electron neutrinos are most abundant. Thus initial condition is usually assumed to be electron flavor in the calculation which leads to the survival probability of electron flavor

$$P(\nu_e, t) = 1 - \sin^2(2\theta_v)\sin^2\left(\frac{\omega_v t}{2}\right). \tag{2.12}$$

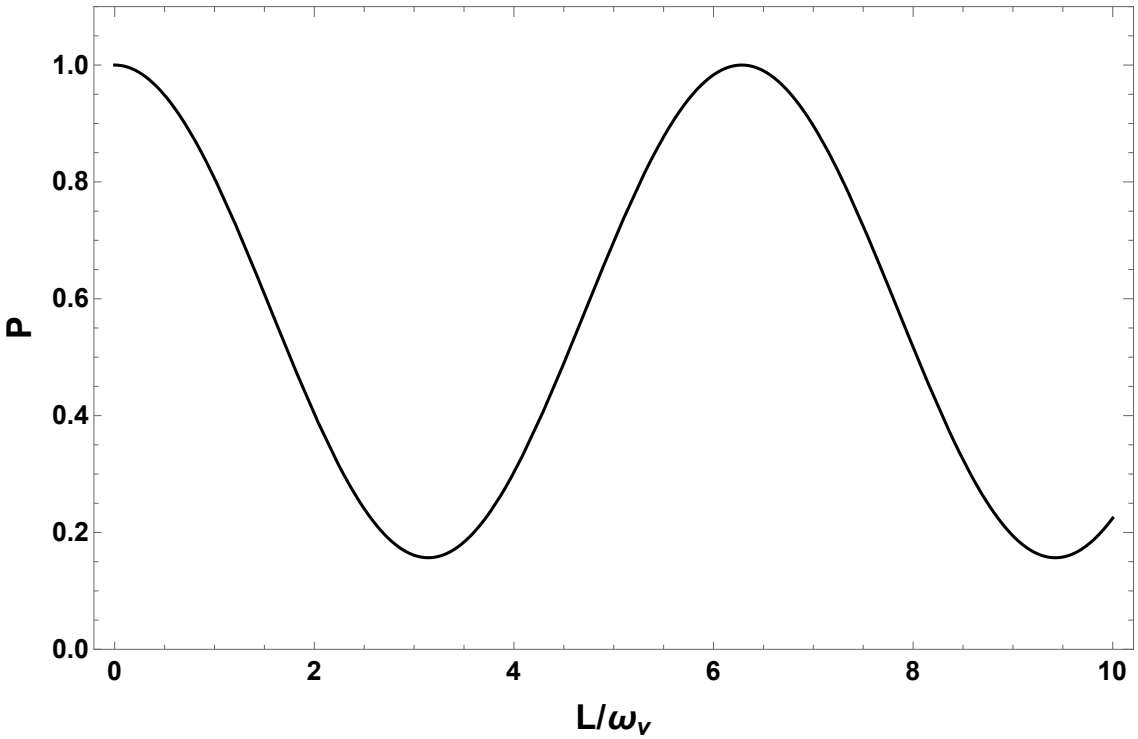


Figure 2.1: Electron flavor neutrino survival probability in vacuum oscillations in two flavors scenario. Mixing angle is determined by $\sin^2\theta = 0.30 \approx \sin^2\theta_{12}$.

Since neutrinos travel with velocity approximately the speed of light, we use $L = t$ where $L$ is the distance traveled. The survival probability is

$$P(\nu_e, L) = 1 - \sin^2(2\theta_v)\sin^2\left(\frac{\omega_v}{2}L\right). \tag{2.13}$$

The important parameter is the oscillation length of the neutrino flavor conversion, $1/\omega_v$. This confirms our qualitative method result Eqn. 2.4. This result plotted in Fig. 2.1 clearly shows the oscillatory behavior. The oscillation length is determined by characteristic energy scale $\omega_v$, while the oscillation amplitude is determined by $\sin^2(2\theta_v)$.

Alternatively, we can find out the Hamiltonian in flavor basis first then solve the Schödinger equation. I will not show the steps here. However, the Hamiltonian in

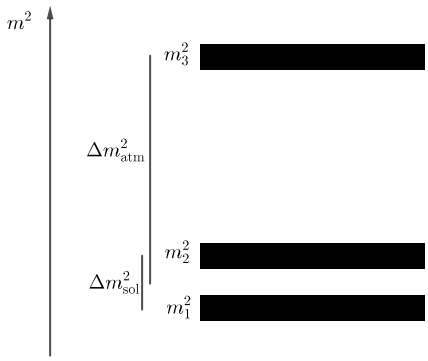


(a) Normal hierarchy. The third mass is heavier than the first two masses.

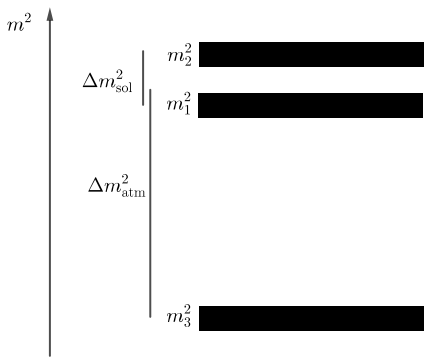


(b) Inverted hierarchy. The third mass is smaller than the first two masses.

Figure 2.2: Three masses of neutrinos. The difference between the first two masses is responsible for solar neutrino oscillations and the difference between the third mass and the first two is responsible for atmospheric neutrino oscillations.

flavor basis is calculated for future use,

$$\mathbf{H}^{(f)} = -\frac{\omega_v}{2}\cos 2\theta_v \sigma_3 + \frac{\omega_v}{2}\sin 2\theta_v \sigma_1. \tag{2.14}$$

In fact, there are three flavors and three masses of neutrinos. The mass squared are shown in Fig. 2.2. We have two quite different characteristic energy scales, $\omega_{v,21} = \delta m^2_{21}/2E$ and $\omega_{v,32} = \delta m^2_{31}/2E$. As for flavor mixing, two oscillation periods should occur, as shown in fig. 2.3. The fast oscillations are determined by the larger characteristic energy scale, $\omega_{v,32}$, while the slow oscillations are determined by the smaller one $\omega_{v,21}$. For inverted hierarchy, the oscillation frequencies are the same as normal hierarchy since they have the same characteristic energy scales. However ever they develop different oscillation phases.

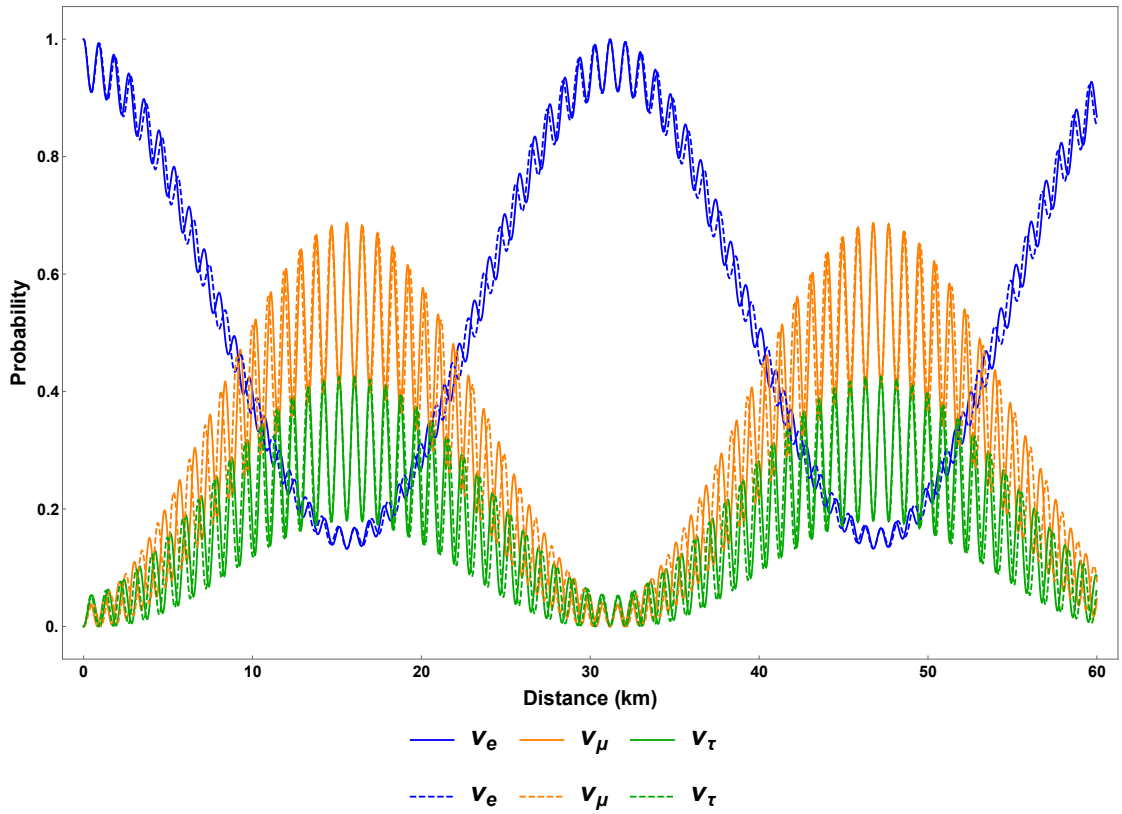


Figure 2.3: Neutrino vacuum oscillations with three flavors. The solid lines represent normal hierarchy and the dashed lines represent inverted hierarchy. Mixing angles are determined by $\sin^2\theta_{12} = 0.30$, $\sin^2\theta_{13} = 0.023$, $\sin^2\theta_{23} = 0.41$, while the mass differences are $\delta m^2_{21} = 7.9 \times 10^{-5}\text{eV}$, $\delta m^2_{23} = 2.7 \times 10^{-3}\text{eV}$. The energy of the neutrinos is 1MeV.

## 2.1 Flavor Isospin Picture of Neutrino Oscillations

In principle, the oscillations in two flavor scenario are consequences of the Hamiltonian in this two-level quantum system. It is known that two-level quantum systems are visualized using the Bloch sphere. In the realm of neutrino physics, flavor isospin was introduced for such visualizations [22]. The Hamiltonian for neutrino oscillations in vacuum (Eqn. 2.14) and in matter (Eqn. 3.14) can be reformulated into vector forms.

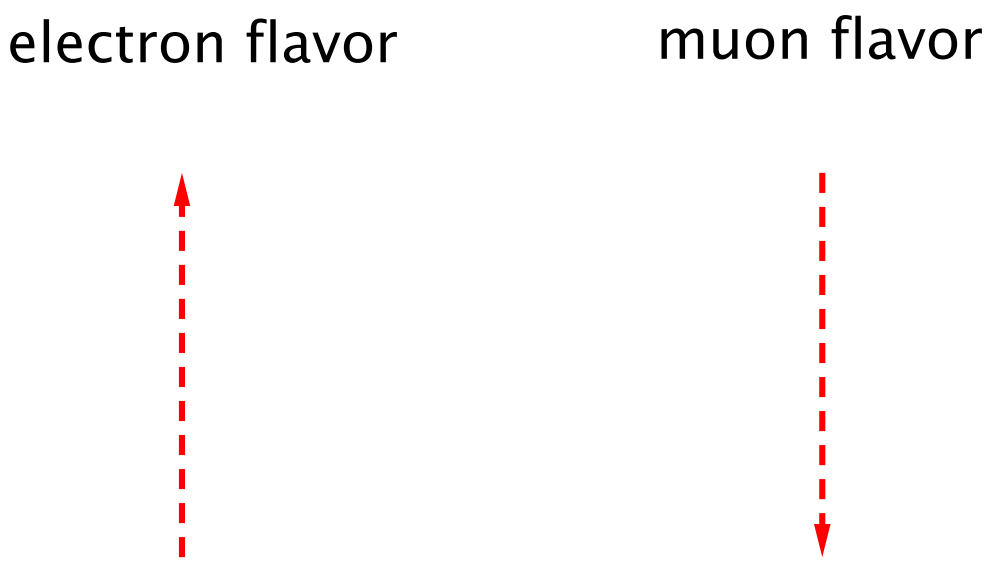


Figure 2.4: In the flavor isospin picture, a flavor isospin pointing upward indicates that the neutrinos are in electron flavor, while the downward direction indicates the other flavor, such as the muon flavor.

We start with the vector form of Hamiltonian for vacuum oscillations. Mathematically speaking, we will cast every two by two matrix into the quaternian basis,

$$H^{(f)} = -\frac{\vec{\sigma}}{2} \cdot \vec{H}. \tag{2.15}$$

Meanwhile, the state of neutrinos is represented by the flavor isospin, which is defined as

$$\vec{s} = \Psi^{\dagger} \frac{\vec{\sigma}}{2} \Psi. \tag{2.16}$$

As shown in Fig. 2.4, the directions of the flavor isospin tell us the flavor content of the neutrino. We choose the direction of the third axis in flavor isospin space to point upward, so that a flavor isospin pointing upward indicates electron flavor by definition. In the flavor isospin formalism, the electron flavor survival probability is related to the third component of the flavor isospin,

$$P = \frac{1}{2} + s_3.$$

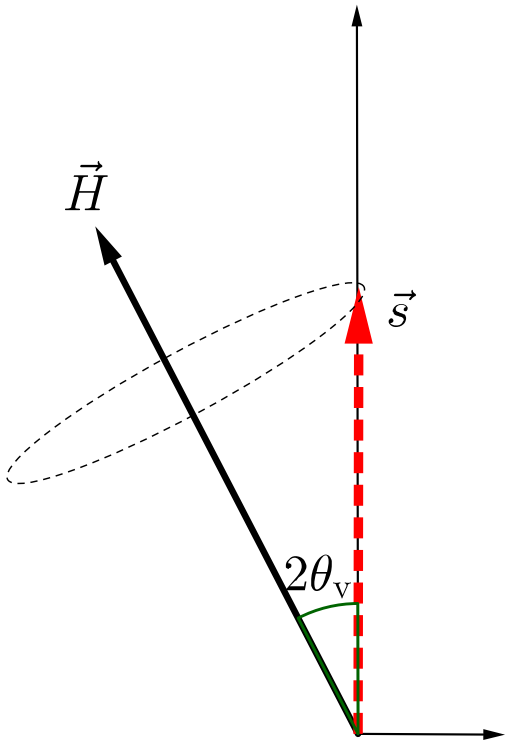


Figure 2.5: Vacuum oscillations in flavor isospin picture. Neutrinos starting with electron flavor will follow a precession pattern around the static "Hamiltonian vector" $\vec{H}$, thus periodic flavor oscillations.

Correspondingly, the equation of motion becomes precession around the Hamiltonian,

$$\dot{\vec{s}} = \vec{s} \times \vec{H}. \tag{2.17}$$

The precession corresponds to periodic oscillations between flavors.

For example, in vacuum oscillations, the vacuum oscillation Hamiltonian becomes

$$\frac{\omega_{\rm v}}{2}\left(-\cos 2\theta_{\rm v}\sigma_3 + \sin 2\theta_{\rm v}\sigma_1\right) \to \cos 2\theta_{\rm v}\begin{pmatrix}0\\0\\ \omega_{\rm v}\end{pmatrix} - \sin 2\theta_{\rm v}\begin{pmatrix}\omega_{\rm v}\\0\\0\end{pmatrix},$$

which is a vector of length $\omega_{\rm v}$ and tilted away from the third axis by the angle $2\theta_{\rm v}$. We assume neutrinos start with the electron flavor. Following the equation of motion Eqn. 2.17, neutrinos precess around vector $\vec{H}$ that is tilted away from the vertical axis, as shown in Fig. 2.5. The oscillation frequency is trivially read out from the precession equation,

$$\omega_{\rm v} = |\vec{H}_{\rm v}|.$$

## 2.2 Conclusion

Vacuum neutrino oscillations is easily explained and calculated. However, it conveys the message of the nature of neutrino oscillations. Neutrinos are usually produced in flavor states since they are usually produced in weak interaction. The flavor states do not remain the same during the propagation since the flavor states are not the eigenstates of the propagation Hamiltonian. An extrapolation of this idea is that neutrinos might also oscillate for a constant linear potential. The Hamiltonian would be similar to vacuum Hamiltonian but with different values. One of such situations is neutrinos propagating through a region with constant matter density, which I will explain in next chapter.

# Chapter 3

# Neutrino Flavor Conversions in Matter and Rabi Oscillations

Since neutrinos with different flavor interact with matter with different cross section, we need to investigate the neutrino flavor carefully. Even though only electron flavor neutrinos are produced, what we detect on Earth is different in flavor, which depends on two phenomena: neutrino vacuum oscillation and MikheyevSmirnovWolfenstein effect.

## 3.1 Stars as Neutrino Factories

Astrophysical neutrino sources such as cores of stars, AGN, Gamma-ray bursts, and supernovae, reveals a lot of information about the sources. Though neutrinos are are weakly interacting particles rendering them hard to detect, it is an important subject to theoretically inspect neutrino productions in astrophysical processes.

### 3.1.1 Stellar Core

One of the neutrino factories is the stellar core. Numerous nuclear reactions as well thermal neutrino production produce luminous neutrinos. In this section, the nuclear reactions in stars are reviewed as well as the neutrino oscillations in the stars.

### 3.1.2 Nuclear Reactions in Sun and Solar Neutrino Flux

The most important nuclear reactions in our Sun are pp chain and CNO cycle. Through different stages of its life, a star experience different nuclear reactions. Figure 3.1 shows the dominant energy source of solar mass stars. In order to calculate the neutrino spectrum we need the neutrino production rate in each reaction and the branching ratios. The processes that emits neutrinos are the reactions in red in Fig 3.1, which are [18]

$$\mathrm{p} + \mathrm{p} \rightarrow {}^{2}\mathrm{H} + \mathrm{e}^{+} + \nu_{\mathrm{e}}, \qquad \leq 0.422\mathrm{MeV} \tag{3.1}$$

$${}^{7}\mathrm{Be} + \mathrm{e}^{-} \rightarrow {}^{7}\mathrm{Li} + \nu_{\mathrm{e}}, \qquad 0.862\mathrm{MeV\ for\ 90\%} \tag{3.2}$$

$$0.384\mathrm{MeV\ for\ 10\%} \tag{3.3}$$

$${}^{8}\mathrm{B} \rightarrow {}^{8}\mathrm{Be}^{*} + \mathrm{e}^{+} + \nu_{\mathrm{e}}, \qquad \leq 15\mathrm{MeV} \tag{3.4}$$

Solar neutrinos are mostly produced in pp reaction, Be electron capture and B decay, which are called pp neutrinos, Be neutrinos and B neutrinos respectively. Even without knowledge of the detailed reactions, the conservation of lepton numbers will lead to the overall neutrino production

$$4\mathrm{p} + 2\mathrm{e}^{-} \rightarrow {}^{4}\mathrm{He} + 2\nu_{\mathrm{e}}, \tag{3.5}$$

where it is important to notice that two neutrinos are produced in each reaction. This overall reaction can either be pp chain or CNO cycle.

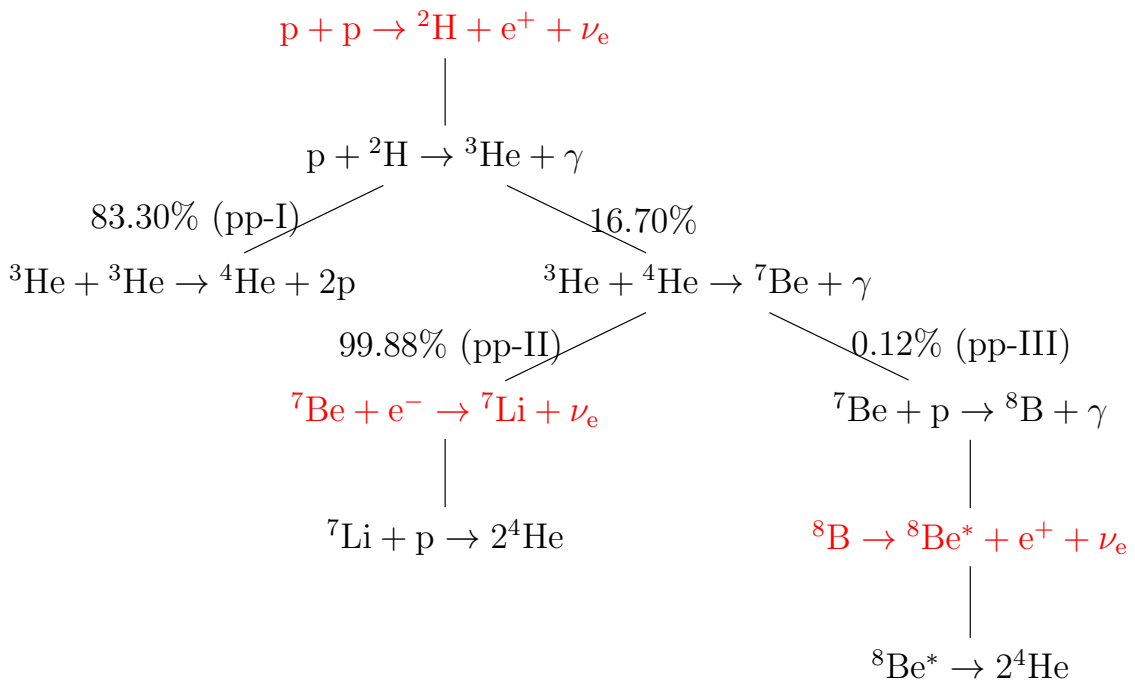


Figure 3.1: pp chain with branching ratio. The branching ratios are obtained from Ref. [18] by Michael Altmann et al.

Using this simple relation, we can estimate the neutrino flux emitted by our sun. Given the kinetic energy produced in each reaction is the difference between the initial masses and the final masses, $Q_{pp} = 4m_p + 2m_e - m_{He4} = 26.7\text{MeV}$ where the mass of neutrinos are neglected since they are small compared with every other particle. On average, each neutrino carries away 0.2MeV energy and the rest will be mostly in the form of thermal energy $Q_\gamma = 26.3\text{MeV}$ [32]. Number flux of thermal photons near Earth can be calculated using the solar constant $S_0$,

$$\Phi_\gamma = \frac{S_0}{Q_\gamma}. \tag{3.6}$$

Since we know each reaction produces 2 neutrinos while producing $Q_\gamma$, which means that the number flux of neutrinos near Earth is roughly twice of the number flux of photons, i.e.,

$$\Phi_\nu = 2\Phi_\gamma \approx 6 \times 10^{10}\text{cm}^{-2}\text{s}^{-1}. \tag{3.7}$$

For such a large flux, understanding the role in stellar nuclear reaction and spectra is important.

Inside our Sun, two additional reactions also produce neutrinos which are called pep and hep neutrinos.

- pep neutrinos are produced in

$$\mathrm{p} + \mathrm{e}^- + \mathrm{p} \rightarrow {}^2\mathrm{H} + \nu_\mathrm{e}, \tag{3.8}$$

  which is only has a branching ratio 0.4% instead of the 99.6% of pp reaction.

- hep neutrinos are produced in

$${}^3\mathrm{He} + \mathrm{p} \rightarrow {}^4\mathrm{He} + \mathrm{e}^+\nu_\mathrm{e}, \tag{3.9}$$

  which has a branching ratio of $2 \times 10^{-5}$%. As a comparison, the ${}^3\mathrm{He} + {}^3\mathrm{He}$ has a branching ratio 85% and ${}^3\mathrm{He} + {}^4\mathrm{He}$ has a branching ratio 15%.

## 3.2 Introduction

In many astrophysical environments, such as core-collapse supernova, neutrinos propagate through dense fluctuating medium, which will interact with neutrinos and dramatically change the flavor oscillations of neutrinos. Meanwhile, neutrinos deposit energy in matter during the interaction, where the amount of energy deposited depends on the flavor of neutrinos. The significance of matter effect on neutrino flavor oscillations has been demonstrated in Mikheyev-Smirnov-Wolfenstein (MSW) effect [7, 5, 6], which is used to explain the deficit of electron flavor neutrino flux, thus solved the solar neutrino problem [19, 10]. Later developments on the theories about matter effect revealed the parametric resonance of neutrino flavor oscillations

due to fluctuations in matter density [9, 17], which is the neutrino analog of transitions between energy levels as a result of external optical stimulation. Parametric resonance is different from the MSW effect since it involves the parameters of the matter density, which is usually the period of matter density fluctuations. Neutrinos passing through inside the Earth can experience parametric resonance [16, 14].

As one of the most intense neutrino sources, supernova neutrinos experience turbulent matter density as they propagate through out the explosion [42, 41], where the flavor conversion is modified by interaction with matter. Meanwhile with neutrinos depositing energy into the shock, neutrino flavor conversion is crucial to the shock evolution of supernova explosion. The turbulent matter density environment for neutrino flavor conversion has been researched [12, 25, 31]. Recently matter stimulated neutrino flavor conversion in varying matter density has been researched using Jacobi-Anger expansion by Kneller, et al. [35, 40]. They have shown that many stimulated neutrino flavor conversions can be explained by resonances of the system.

We will take a step further and interpret parametric resonance [17, 9] as well as other matter stimulated neutrino flavor conversions [35, 40], as superposition of Rabi oscillations. We also propose a criteria for the interference effect between different Rabi oscillation modes. In Sec. 3.5, we define the formalism of neutrino flavor conversions in matter used in this chapter where the equation of motion and Hamiltonian for neutrino flavor conversion in matter are explicitly written. In Sec. 3.6 we discuss how neutrino flavor conversions are related to Rabi oscillations. To begin with, we discuss a system with single frequency matter density fluctuation. We will show that such a system can be reduced to Rabi oscillations if resonance occurs. In Sec. 3.7 we describe the interference effect between different frequencies of Rabi oscillations and develop the criteria for significant interference between two frequencies. We show that the interference between the many frequencies fits into the criteria we proposed for interference. In Sec. 3.9 we discuss the technique of decomposing the neutrino

flavor conversions into summation of Rabi oscillations, by applying a specific unitary transformation and the Jacobi-Anger expansion. As the system is exactly decomposed into multiple Rabi oscillations, we can interpret neutrino flavor oscillations in any matter density fluctuations in principle. As an example, we solve the neutrino flavor transitions in a castle wall matter profile, which is expanded using Fourier series into many frequencies.

## 3.3 Mikheyev - Smirnov - Wolfenstein Effect

The nature of neutrino oscillations means that flavor conversion occurs as long as their propagation eigenstates are not flavor eigenstates. As neutrinos travel from the center of the star throughout to the surface, we expect neutrino propagation eigenstates in such matter background to be different from flavor states in general [5]. Using the fact that neutral current interactions between different flavor neutrinos and matter is independent of flavor, we only include the charged current, which will produce a effective potential for electron flavor that is different for other flavors. In flavor basis, the effective potential is

$$V = \frac{\sqrt{2}G_{\mathrm{F}}n_{\mathrm{e}}}{2}\sigma_3, \tag{3.10}$$

where $G_{\mathrm{F}}$ is Fermi constant, $n_{\mathrm{e}}$ is number density of electrons. We also removed the terms that is proportional to identity in this potential since it doesn't change the probability for flavors. The Hamiltonian with matter effect is the combination of vacuum oscillation and matter effect, which is, in flavor basis,

$$H_m = \frac{\omega_v}{2}\begin{pmatrix} -\cos 2\theta_v & \sin 2\theta_v \\ \sin 2\theta_v & \cos 2\theta_v \end{pmatrix} + \frac{\sqrt{2}G_F n_e}{2}\sigma_3, \tag{3.11}$$

where we used the result of flavor basis vacuum oscillation Hamiltonian

$$H_v^{(f)} = \mathbf{U} H_v^{(v)} \mathbf{U}^\dagger \tag{3.12}$$

$$= \frac{\omega_v}{2} \begin{pmatrix} -\cos 2\theta_v & \sin 2\theta_v \\ \sin 2\theta_v & \cos 2\theta_v \end{pmatrix}. \tag{3.13}$$

Utilizing Pauli matrices and the so called matter potential $\lambda = \frac{\sqrt{2} G_F n_e}{2}$, it is rewritten as

$$H_m = \left( \frac{\lambda}{2} - \frac{\omega_v}{2} \cos 2\theta_v \right) \boldsymbol{\sigma}_3 + \frac{\omega_v}{2} \sin 2\theta_v \boldsymbol{\sigma}_1. \tag{3.14}$$

Due to the off-diagonal terms in the Hamiltonian, the system will experience oscillations in flavor. A resonance, i.e., maximum mixing, dominates the system when the diagonal terms becomes zero,

$$\frac{\lambda}{2} - \frac{\omega}{2} \cos 2\theta_v = 0, \tag{3.15}$$

which gives us the MSW resonance condition.

The importance of matter effect to our understanding of solar neutrinos is that it modifies the oscillation, depending on the matter density profile. For a solar mass star, we have almost adiabatic evolution of the neutrinos, which means that the instantaneous eigenstates and eigenvectors of Hamiltonian is good enough for the time dependent Schrödinger equation.

For simplicity, we define the vacuum frequency and the 'hatted' dimensionless quantities

$$\hat{\lambda} = \frac{\lambda}{\omega_v}. \tag{3.16}$$

The eigenstates, derived by diagonalizing the Hamiltonian, are

$$E_1 = \frac{\omega_v}{2} \sqrt{\hat{\lambda} + 1 - 2\hat{\lambda} \cos 2\theta_v} \tag{3.17}$$

$$E_2 = -\frac{\omega_v}{2} \sqrt{\hat{\lambda} + 1 - 2\hat{\lambda} \cos 2\theta_v}. \tag{3.18}$$

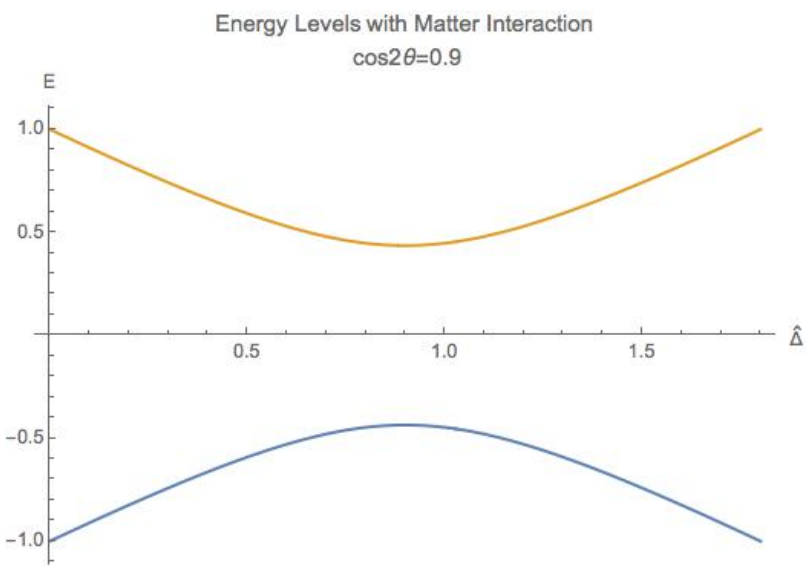


Figure 3.2: The two energy levels in matter effect. The energy has unit $\omega_v/2$ while the potential has unit $\omega_v$. $\cos 2\theta = 0.9$ is applied.

Fig. 3.2 shows the two energy levels. For very high matter density, which interact with electron neutrinos more through charged current, electron flavor is composed almost with heavy propagation eigenstate. However, as the matter density becomes lower, the heavy propagation state will be gradually transformed to the other flavors since electron flavor in vacuum is composed mostly the light mass state. The resonance, which is the closest point of energy levels, happens at density $n_{\rm e} = 2\omega_v \cos(2\theta_v)/\sqrt{2}G_F$ which depends on $\omega_v$. Neutrinos with different energies have different resonance, which will significantly reshape the neutrino spectra for different flavors.

One of the interesting fact about MSW effect is the MSW triangle shown in Fig. 3.3. The survival probability of electron flavor neutrinos is plotted against $\log(\lambda/\omega_v)$ and $\log(\sin^2 2\theta_v)$. The low survival probability region is a triangle shape. Qualitatively speaking, large conversion happens when matter density is not too small since a sufficient central potential is required for the level crossing.

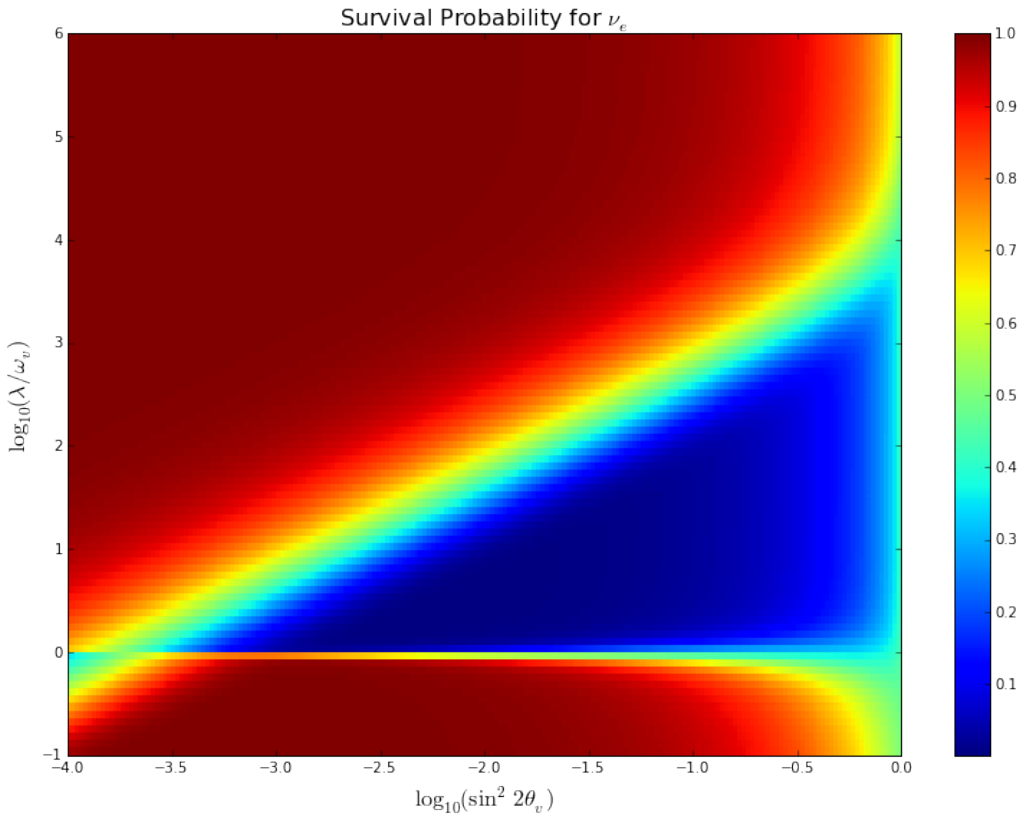


Figure 3.3: MSW triangle. The horizontal axis is related to the the mixing angles, and the vertical axis is related to the matter potential in the center of the Sun. The colors are the survival probabilities of electron flavor. The region of large conversions, or small survival probabilities, forms a triangle. The larger the mixing angle, the larger range of matter potential for large conversions.

In summary, even though only electron flavor neutrinos are produced in the core of a solar mass star, the neutrino flavor conversion to the other flavors is enhanced by matter interaction, in addition to the vacuum oscillation. However, the actual neutrino flavor conversion is much more complicated than just MSW effect and almost impossible to calculate without knowing the very exact matter profile of the Sun even with the time-dependent small perturbations to the density. As an approximation, MSW transition is good enough for the solar neutrinos [36].

## 3.4 Flavor Isospin Picture

MSW effect is also easily explained using flavor isospin picture. The Hamiltonian in flavor isospin picture

$$\begin{aligned} H_m =& \frac{\omega_{\rm v}}{2}\left(-\cos 2\theta_{\rm v}\boldsymbol{\sigma_3} + \sin 2\theta_{\rm v}\boldsymbol{\sigma_1}\right) + \frac{\lambda(x)}{2}\boldsymbol{\sigma_3} \\ \rightarrow& \omega_{\rm v}\begin{pmatrix} -\sin 2\theta_{\rm v} \\ 0 \\ \cos 2\theta_{\rm v} \end{pmatrix} + \begin{pmatrix} 0 \\ 0 \\ -\lambda(x) \end{pmatrix} \\ =& \vec{H}_{\rm v} + \vec{H}_{\rm m}(x), \end{aligned}$$

where $\vec{H}_{\rm v}$ is vacuum contribution and $\vec{H}_{\rm m}(x)$ is the matter potential contribution. The two vectors are visualized in Fig. 3.4. We discussed in Sec. 3.3 the adiabatic transitions of neutrino states in varying matter density. Fig. 3.5 shows the adiabatic evolution of neutrino flavor isospin. For region of high density matter background, which provides large matter potential, the total Hamiltonian is almost pointing downward. We observe almost no flavor oscillations since flavor isospin precession is tiny. As the neutrinos moving into smaller matter density regions, the flavor isospin is approximately following the evolution of Hamiltonian. Flavor conversion happens because of the evolution of Hamiltonian, even though flavor oscillations are still tiny. In the end, neutrinos reach the region with almost no matter, where they are almost converted to one of the mass eigenstates. In fact, those neutrinos won't oscillate that much in vacuum following this initial condition.

Neutrinos might experience a critical matter density, when the overall Hamiltonian is perpendicular to the upright axis. Assuming we have electron neutrinos going through such regions, they will experience maximum flavor oscillations, c.f. Fig. 3.6.

## 3.5 Background and Formalism

We consider two-flavor oscillation scenario, in which neutrinos have energy $E$ and mass-squared difference $\delta m^2$ between two mass states propagate through matter which is define by electron number density profile $n(r)$ along the path of neutrino propagation $r$. The dynamics of neutrino flavor conversion is determined by Schrödinger equation. In flavor basis the wave function describes the probability amplitude of different flavors. The Hamiltonian in flavor basis consists the vacuum oscillation Hamiltonian $H_{\rm v}^{(f)}$ and the matter term $H_{\rm m}^{(f)}$ which describes the interaction between neutrinos and matter,

$$\begin{aligned} H^{(\rm f)} =& H_{\rm v}^{(f)} + H_{\rm m}^{(f)} \\ =& \frac{1}{2}\begin{pmatrix} -\omega_{\rm v}\cos 2\theta_{\rm v} + \lambda(r) & \omega_{\rm v}\sin 2\theta_{\rm v} \\ \omega_{\rm v}\sin 2\theta_{\rm v} & \omega_{\rm v}\cos 2\theta_{\rm v} - \lambda(r) \end{pmatrix}, \end{aligned} \tag{3.19}$$

where $\lambda(r) = \sqrt{2}G_{\rm F}n(r)$ is the potential of neutrino interaction with matter and $G_{\rm F}$ is the Fermi constant, $\theta_{\rm v}$ is the vacuum mixing angle, $\omega_{\rm v} = \delta m^2/2E$ is the vacuum oscillation frequency. The potential $\lambda(r)$ is called matter profile since it reflects the matter density fluctuations. For the convenience of notation, we use Pauli matrices $\sigma_i$ to rewrite the Hamiltonian, so that the Schrödinger equation becomes,

$$\mathrm{i}\frac{\mathrm{d}}{\mathrm{d}r}\Psi(r) = \frac{1}{2}\left((-\omega_{\rm v}\cos 2\theta_{\rm v} + \lambda(r))\sigma_3 + \omega_{\rm v}\sin 2\theta_{\rm v}\sigma_1\right)\Psi(r),$$

where $\Psi(r)$ is the wave function in flavor basis. For two flavor scenario, it is written as $\Psi(r) = (\psi_e, \psi_x)^{\rm T}$ where $\psi_e$ and $\psi_x$ are the amplitudes for electron flavor and the second flavor ($\mu$ flavor or $\tau$ flavor) respectively. The equation of motion in flavor basis governs the transitions between different flavors.

For arbitrary matter profile, we can always interpret it as perturbations on top of a constant matter profile,

$$\lambda(r) = \lambda_0 + \delta\lambda(r). \tag{3.20}$$

For better understanding of the transition between states as a consequence of the fluctuation of matter density, we use the background matter basis, in which the Hamiltonian is diagonalized in the absence of perturbation $\delta\lambda(r)$, so that the Hamiltonian reads

$$H^{(\mathrm{m})} = -\frac{\omega_m}{2}\sigma_3 + \frac{1}{2}\delta\lambda(r)\cos 2\theta_{\mathrm{m}}\sigma_3 - \frac{1}{2}\delta\lambda(r)\sin 2\theta_{\mathrm{m}}\sigma_1, \tag{3.21}$$

where $\theta_{\mathrm{m}}$ is the mixing angle in a constant matter profile $\lambda_0$, which is calculated using relation

$$\tan 2\theta_{\mathrm{m}} = \sin 2\theta_{\mathrm{v}} / \left(\cos 2\theta_{\mathrm{v}} - \lambda_0/\omega_{\mathrm{v}}\right)$$

with $\omega_{\mathrm{v}}$ denoting the vacuum oscillation frequency and $\theta_{\mathrm{v}}$ denoting the vacuum mixing angle. The frequency $\omega_{\mathrm{m}}$ is defined as

$$\omega_{\mathrm{m}} = \omega_{\mathrm{v}}\sqrt{(\lambda_0/\omega_{\mathrm{v}} - \cos(2\theta_{\mathrm{v}}))^2 + \sin^2(2\theta_{\mathrm{v}})}. \tag{3.22}$$

In background matter basis, the wave function describes the amplitudes of different mass states defined when there is only background matter density $\lambda_0$. It's trivial to calculate the flavor conversion given the transition probability between the two mass states. However, since we'll concentrate on the flavor conversion due to the matter fluctuations, we'll only discuss the transition between mass states in the background matter basis.

In this chapter, mixing angle is chosen so that $\sin^2(2\theta_{\mathrm{v}}) = 0.093$ and the mass squared difference is $\delta m^2 = 2.6 \times 10^{-3}\mathrm{eV}^2$.

## 3.6 Single Frequency Matter Profile and Rabi oscillations

In this section we present a simple picture to explain neutrino parametric resonance in matter by utilizing the theory of Rabi oscillations which have been well studied

in quantum optics [27]. Rabi oscillations describe the transition between different energy levels due to an oscillatory external driving field, where maximum transition or resonance happens when the frequency of external driving field equals the energy gap. In Appendix B, we derive the Rabi oscillation transition probabilities using neutrino flavor isospin method introduced in Ref. [23], and explained in Sec. 2.1.

We examine neutrino flavor conversions in single frequency matter profile $\delta\lambda(r) = \lambda_1 \cos(k_1 r)$. As will be proved in Sec. 3.9.2, the varying $\sigma_3$ term $\delta\lambda(r)\cos 2\theta_{\rm m}\sigma_3/2$ in Hamiltonian Eqn. 3.21, which is the varying energy gap due to varying matter density fluctuations, has little effect on the transition probabilities when the system is not far from resonance. With the varying $\sigma_3$ term removed, it indicates that this single frequency matter perturbation neutrino flavor conversion system has been reduced to a Rabi oscillation system, with external driving field frequencies $\pm k_1$ and energy gap $\omega_{\rm m}$. Mathematically, we can decompose $\cos(k_1 r)$ into two exponential functions so that we have two external driving frequencies $k_1$ and $-k_1$. By neglecting the off-resonance mode which has frequency $-k_1$, the Hamiltonian can be simplified,

$$\begin{aligned} H^{(\rm m)} &\to -\frac{\omega_{\rm m}}{2}\sigma_3 - \frac{1}{2}\lambda_1 \sin 2\theta_{\rm m}\cos(k_1 r)\sigma_1 \\ &\to -\frac{\omega_{\rm m}}{2}\sigma_3 - \frac{1}{2}A_1 \exp(\mathrm{i}k_1 r)\sigma_1 \\ &= -\frac{\omega_{\rm m}}{2}\sigma_3 - \frac{1}{2}A_1\cos(k_1 r)\sigma_1 + \frac{1}{2}A_1 \sin(k_1 r)\sigma_2, \end{aligned} \tag{3.23}$$

where

$$A_1 = \frac{\lambda_1 \sin 2\theta_{\rm m}}{2}. \tag{3.24}$$

The resonance condition is determined by matching the energy gap $\omega_{\rm m}$ with external driving field frequency $k_1$, i.e., $\omega_{\rm m} \sim k_1$. As the system approaches resonance condition, the transition probability between the two mass states should be predicted well using Rabi formula.

To show that this conjecture of simplifying neutrino flavor conversions to Rabi oscillations is correct, we calculate transition probabilities of the neutrinos described

by Eqn. 3.21 numerically, and compare them with Rabi formula Eqn. B.10 from the Rabi oscillations described by Eqn. B.1.

In Fig. 3.7, we plotted the numerical results using markers as well as the prediction using Rabi formula using lines. The agreement between numerical solutions of neutrino transitions between mass states and Rabi formula will be explained more precisely in Sec. 3.9. For now, we address the significance of relative detuning $D = |k_1 - \omega_{\rm m}|/|A_1|$, which is rigoriously defined in Appendix B. It measures how off-resonance a system is. We know that $D \to 0$ indicates the system is very close to resonance, while $D \to \infty$ indicates the system is far away from resonance. The corresponding relative detunings are 0, 1.0, and 5.2 for $k_1 = \omega_{\rm m}$, $k_1 = (1 - 2 \times 10^{-5})\omega_{\rm m}$, and $k_1 = (1 - 10^{-4})\omega_{\rm m}$.

For a single-frequency perturbation in matter profile $\lambda(r) = \lambda_1 + \lambda_1 \sin(k_1 r)$, P. Krastev and A. Smirnov concluded that the parametric resonance condition is $\omega_{\rm m} \sim n k_1$, if instantaneous $\omega_{\rm m,inst}(r)$ associated with the matter profile at distance $r$ varies slowly [9]. This condition is exactly the Rabi resonance condition when $n = 1$, as such condition matches the driving field frequency to the energy split. Higher order effects are explained in Sec. 3.9.2.

## 3.7 Interference of Rabi Oscillations and Multi-frequency Matter Profile

The approach applied to single frequency matter profile also helps with the understanding of multi-frequency matter profile. However, multi-frequency matter profile leads to multiple modes of Rabi oscillations, even with our simplified approach by dropping the varying $\sigma_3$ term in Hamiltonian. In this section, we examine the interference between two modes of Rabi oscillations.

We explain the interference between different modes of Rabi oscillations using the idea of energy gap shift. Suppose we have a Rabi oscillation system with two modes, one of which is at resonance with frequency $k_1 = \omega_{\rm m}$ and the other mode with frequency $k_2$ that is off resonance. In some cases, there can be a significant transition amplitude decrease because of the off resonance frequency $k_2$, which can be interpreted as shift of energy gap due to the frequency $k_2$. To model the effect, we construct a Rabi oscillation Hamiltonian with two modes of different frequency,

$$H^{(\rm m)} = -\frac{\omega_{\rm m}}{2}\sigma_3 - \frac{1}{2}\sum_{n=1}^{N} A_n \cos(k_n r)\sigma_1 + \frac{1}{2}\sum_{n=1}^{N} A_n \sin(k_n r)\sigma_2, \tag{3.25}$$

where $N = 2$ for two frequency case. To show the destruction effect, the Hamiltonian Eqn. 3.25 is reformulated into a vector with sigma matrices $(\sigma_1, \sigma_2, \sigma_3)$ as the basis,

$$\mathbf{H} = \begin{pmatrix} 0 \\ 0 \\ \omega_m \end{pmatrix} + \begin{pmatrix} A_1 \cos(k_1 r) \\ -A_1 \sin(k_1 r) \\ 0 \end{pmatrix} + \begin{pmatrix} A_2 \cos(k_2 r) \\ -A_2 \sin(k_2 r) \\ 0 \end{pmatrix}. \tag{3.26}$$

The three terms are defined as $\mathbf{H}_3$, $\mathbf{H}_1$, and $\mathbf{H}_2$ respectively. $\mathbf{H}_1$ and $\mathbf{H}_2$ are two rotating vectors as a function of $r$ with frequencies $k_1$ and $k_2$ in this vector space, while $\mathbf{H}_3$ is perpendicular to $\mathbf{H}_1$ and $\mathbf{H}_2$. To work out the energy gap shift, we go to the frame that corotates with $\mathbf{H}_2$, in which we have the new frequencies $k_1' = k_1 - k_2$ and $k_2' = 0$ as well as new energy gap $\omega_{\rm m}' = \omega_{\rm m} - k_2$. The resonance mode $\mathbf{H}_1$ retains on the resonance condition since $k_1' = \omega_{\rm m}'$, i.e. $k_1 - k_2 = \omega_{\rm m} - k_2$, holds in the new frame. On the other hand, we have two static fields $\mathbf{H}_3$ and $\mathbf{H}_2$ together as the new energy gap, as long as $\mathbf{H}_2 \ll \mathbf{H}_3$, which is the usual case. The new energy gap in this frame is calculated as

$$\begin{aligned} \tilde{\omega}_{\rm m}' =& \,{\rm sign}(\omega_{\rm m}')\sqrt{\omega_{\rm m}'^2 + A_2^2} \\ \approx& \,\omega_{\rm m}' + \frac{A_2^2}{2\omega_{\rm m}'} \\ =& \,\omega_{\rm m} - k_2 + \frac{1}{2}\frac{A_2^2}{\omega_{\rm m} - k_2}, \end{aligned} \tag{3.27}$$

where we kept only first order of Taylor series. The Taylor expansion in Eqn. 3.27 holds as long as the relative detuning for the second frequency is large which means the second frequency is off resonance. As an approximation, the transitions between the two energy states follows the Rabi oscillations with energy gap $\tilde{\omega}'_{\rm m}$ and driving field with frequency $k'_1 = k_1 - k_2$. Consequently, we can estimate how much the amplitude of the transition is suppressed due to $k_1$ mode by calculating the new relative detuning,

$$\begin{aligned} D' =& \frac{|k'_1 - \tilde{\omega}'_{\rm m}|}{|A_1|} \\ =& \left| \frac{k_1 - \omega_{\rm m}}{A_1} + \frac{A_2^2}{2A_1(k_2 - \omega_{\rm m})} \right| \qquad (3.28) \\ =& \left| \frac{\text{sign}(k_1 - \omega_{\rm m})}{\text{sign}(k_2 - \omega_{\rm m})} D_1 + \frac{A_2}{2A_1 D_2} \right|, \qquad (3.29) \end{aligned}$$

where $D_2$ is the relative detuning of the second mode,

$$D_i = \left| \frac{k_i - \omega_{\rm m}}{A_i} \right|.$$

In principle, the energy gap of the first frequency can be changed to approach the resonance or escape the resonance by carefully arranging the second frequency, which is also obvious from Eqn. (3.29). For the purpose of the section we first discuss the most important destruction effect by choosing $D_1 = 0$. We observe the importance of the relative detuning. For the second mode to significantly interfere with the first mode, we need a small $D_2$ and a large amplitude or width $A_2 \gg A_1$.

The condition can be verified by comparing the numerical solution and estimation using Rabi formula. However, we are most interested in the amplitude change due to $\mathbf{H}_2$ mode. Relative detuning is the only variable that we need to calculate the amplitude, hence we only compare the numerical results with estimated amplitudes using $1/(1 + D'^2)$. To verify the condition, we choose the first rotating perturbation to satisfy the resonance condition $k_1 = \omega_{\rm m}$, the condition for the second rotating field shifting the system out of resonance is that the relative detuning becomes larger than

1, which leads to

$$|A_2| \geq \sqrt{2\omega_{\rm m}|A_1(k_2 - \omega_{\rm m})|} \equiv A_{2,\rm Critical}. \tag{3.30}$$

We expect the transition amplitude to decrease as we have larger $|A_2|$.

We choose the two modes where the first one has amplitude $A_1 = 10^{-4}\omega_{\rm m}$ and frequency $k_1 = \omega_{\rm m}$. With a small amplitude of the second frequency, $A_2 = 10^{-4}\omega_{\rm m}$, and large frequency $k_2 = 10\omega_{\rm m}$, we obtain almost full resonance. For larger $A_2$ the destruction effect is more effective, as shown in Fig. 3.8. The estimations of transition amplitude are in good agreement with the numerical results. To show the importance of relative detuning, we calculated the relative detuning for each cases, which are 0.06, 0.6, 1.4, 13.9 for the lines from top to down. We also notice that the width of each cases doesn't change since we kept $A_1$ fixed for each calculation, which indicates that the decreasing in transition amplitude is because of the increasing in detuning.

Even for the single frequency matter profile, there are two modes of Rabi oscillations $\pm k_1$, under the approximation that the varying $\sigma_3$ term in Hamiltonian is neglected, as mentioned in Sec. 3.6. The three examples calculated in Fig. 3.7 are almost exact since the modification of relative detuning for the $k_1$ mode that we kept, due to the far off resonance mode $-k_1$ that we neglected, is tiny. The first two lines of Table. 3.1 show the relative detunings of the three cases in Fig. 3.7, where $n = \pm 1$ are for the $\pm k_1$ modes in the Hamiltonian 3.23. We observe in Fig. 3.7 that the relative detuning change due to an extra $-k_1$ mode is not observable.

## 3.8 Constructive Effects

As mentioned in the preceding section, adding a second frequency to the matter density profile can also be constructive. I calculated an example with two frequencies

in matter density profile, so that the Hamiltonian is

$$H^{(m)} = -\frac{\omega_{\rm m}}{2}\sigma_3 - \left(\frac{A_1}{2}\cos(k_1 r) + \frac{A_2}{2}\cos(k_2 r)\right)\sigma_1 + \left(\frac{A_1}{2}\sin(k_1 r) + \frac{A_2}{2}\sin(k_2 r)\right)\sigma_2.$$

We choose two matter profile frequencies that are off resonance and producing large relative detuning,

$$A_1 = 0.025, \tag{3.31}$$

$$k_1 = 0.95, \tag{3.32}$$

$$A_1 = 0.4, \tag{3.33}$$

$$k_2 = 2.6. \tag{3.34}$$

The oscillation amplitude for each mode being much smaller than 1. However, the combined two frequencies case produces oscillations are resonance (c.f. Fig. 3.9), since the relative detuning for the combined two frequencies case is 0.

## 3.9 Parametric Resonance and Rabi oscillation — Jacobi-Anger expansion

With the intuition of the Rabi oscillations itself as well as the interference between different modes of Rabi oscillations shown in Sec. 3.7, we expect to interpret the transition probabilities of any matter profile more precisely if the system can be exactly decomposed into multiple Rabi oscillations. Kneller et. al provided a method to achieve this goal [35], namely the Jacobi-Anger expansion. In this section, we show that the matter effect can be decomposed into superpositions of Rabi oscillations by applying a Jacobi-Anger expansion to the Hamiltonian. Our approach is to apply a designed unitary transformation first which make the motivation of Jacobi-Anger expansion, before writing down the final result as superpositions of Rabi oscillation

using Jacobi-Anger expansion. For a system with general matter perturbation, c.f. Eqn. (3.21), we apply an unitary transformation of the form

$$\mathbf{U} = \begin{pmatrix} e^{-\mathrm{i}\eta(r)} & 0 \\ 0 & e^{\mathrm{i}\eta(r)} \end{pmatrix}, \tag{3.35}$$

which is a transformation used in Ref. [26] to remove the diagonal elements of the Hamiltonian. This transformation is essentially a rotation $\exp\left(-\mathrm{i}\frac{\sigma_3}{2}\cdot 2\eta\right)$, thus it doesn't change $\sigma_3$ terms themselves. In this work, this transformation is used to remove the varying $\sigma_3$ terms $\delta\lambda(r)\cos 2\theta_\mathrm{m}\sigma_3/2$ in the Hamiltonian, so that the energy gap is fixed in the new basis $\left(|\nu_{\mathrm{r}1}\rangle\,, |\nu_{\mathrm{r}2}\rangle\right)^{\mathrm{T}}$, which is defined as

$$\begin{pmatrix} |\nu_{\mathrm{r}1}\rangle \\ |\nu_{\mathrm{r}2}\rangle \end{pmatrix} = \mathbf{U}^\dagger \begin{pmatrix} |\nu_\mathrm{L}\rangle \\ |\nu_\mathrm{H}\rangle \end{pmatrix}. \tag{3.36}$$

For convenience, we name this unitary transformation in Eqn. (3.35) Rabi transformation as well as the new basis in Eqn. (3.36) the Rabi basis. The reason it can remove the $\sigma_3$ term is that it will transform the system into a rotating frame so that the varying energy gap due to the fluctuating matter density is exactly cancelled by rotation of the frame. Another advantage of this transformation is that the transition probability from light state to heavy state in background matter basis is easily calculated as $P_{\mathrm{L}\to\mathrm{H}}(x) = |e^{i\eta}\psi_{\mathrm{r}2}(x)|^2 = |\psi_{\mathrm{r}2}(x)|^2$.. In Rabi basis, we find the Schrödinger equation

$$\begin{aligned} &\begin{pmatrix} \frac{\mathrm{d}\eta}{\mathrm{d}r} & 0 \\ 0 & -\frac{\mathrm{d}\eta}{\mathrm{d}r} \end{pmatrix} \begin{pmatrix} \psi_{\mathrm{R}1} \\ \psi_{\mathrm{R}2} \end{pmatrix} + \mathrm{i}\frac{\mathrm{d}}{\mathrm{d}r} \begin{pmatrix} \psi_{\mathrm{R}1} \\ \psi_{\mathrm{R}2} \end{pmatrix} \\ &= \left[ -\frac{\omega_\mathrm{m}}{2}\sigma_3 + \frac{\delta\lambda}{2}\cos 2\theta_\mathrm{m}\sigma_3 - \frac{\delta\lambda}{2}\sin 2\theta_\mathrm{m} \begin{pmatrix} 0 & e^{2\mathrm{i}\eta} \\ e^{-2\mathrm{i}\eta} & 0 \end{pmatrix} \right] \begin{pmatrix} \psi_{\mathrm{R}1} \\ \psi_{\mathrm{R}2} \end{pmatrix}, \end{aligned}$$

in which the varying diagonal elements in Hamiltonian can be eliminated by choosing $\eta(r)$ properly, i.e.,

$$\eta(r) - \eta(0) = \frac{\cos 2\theta_\mathrm{m}}{2}\int_0^r \delta\lambda(\tau)d\tau. \tag{3.37}$$

In Rabi basis, the Schrödinger equation becomes

$$\mathrm{i}\frac{d}{dr}\begin{pmatrix}\psi_{\mathrm{r}1}\\ \psi_{\mathrm{r}2}\end{pmatrix} = \left[-\frac{\omega_{\mathrm{m}}}{2}\sigma_3 - \frac{\delta\lambda}{2}\sin 2\theta_{\mathrm{m}}\begin{pmatrix}0 & e^{2\mathrm{i}\eta}\\ e^{-2\mathrm{i}\eta} & 0\end{pmatrix}\right]\begin{pmatrix}\psi_{\mathrm{r}1}\\ \psi_{\mathrm{r}2}\end{pmatrix}.$$

One can easily show that the transition probability between two eigenstates in Rabi basis is the same as the transition probability between two eigenstates in background matter basis, given the initial condition that the system is in low energy state.

For single frequency matter profile with potential $\delta\lambda(r) = A_1\sin(k_1 r)$, we have $\eta(r) = -A_1\cos 2\theta_{\mathrm{m}}\cos(k_1 r)/(2k)$. To make connection with Rabi oscillation, we apply Jacobi-Anger expansion, which is used in Ref. [35], to decompose the $\exp(\mathrm{i}z\cos(k_1 r))$-like term in Hamiltonian into linear combinations of terms that is proportional to $\exp(\mathrm{i}nk_1 r)$, i.e., to decompose spherical waves into plane waves. The decomposed form of Hamiltonian explicitly shows that the Hamiltonian is a summation of Rabi systems, which is

$$H^{(\mathrm{R})} = -\frac{\omega_{\mathrm{m}}}{2}\sigma_3 - \frac{1}{2}\sum_{n=-\infty}^{\infty} B_n\begin{pmatrix}0 & \Phi_n e^{\mathrm{i}nk_1 r}\\ \Phi_n^* e^{-\mathrm{i}nk_1 r} & 0\end{pmatrix}, \tag{3.38}$$

where

$$B_n = \tan 2\theta_{\mathrm{m}} n k_1 J_n\left(\frac{A_1}{k_1}\cos 2\theta_{\mathrm{m}}\right),$$
$$\Phi_n = e^{i\pi(3n/2+1)},$$

with $J_n$ standing for the Bessel function. The constant phase $\Phi_n$ doesn't play any role for the reason discussed in Appendix B. Phase in matter potential would also go into $\Phi_n$, for which reason, phase of matter profile is not included in the current discussion. In the Hamiltonian, the first term describes the energy gap, while the second term is the summation of many driving fields. The resonance width for a given mode $n$ is $|B_n|$. It's worth mentioning that we have [29]

$$J_n(n\,\mathrm{sech}\,\alpha) \sim \frac{e^{n(\tanh\alpha-\alpha)}}{\sqrt{2\pi n\tanh\alpha}} \tag{3.39}$$

for large $n$. It's straightforward to prove that resonance width decreases dramatically for large $n$ thus resonance of higher order modes become insignificant.

When the system has one dominate resonance mode and without significant interference between the resonance mode and other modes, all off-resonance modes can be dropped without significantly changing the transition probabilities. However, as we have shown previously in Sec. 3.7, interference might happen between different modes and interferences were measured with a criteria. However, interference is not the only effect we need to consider. The following subsections will determine the important modes of the system (i.e., which $n$ to include) and explore the interference between modes hence explain the coincidence presented in the previous sections. We use dimensionless quantities which are scaled using the characteristic energy scale $\omega_{\rm m}$, e.g.,

$$\begin{aligned}\hat{r} &= \omega_{\rm m} r,\\ \hat{k}_1 &= \frac{k_1}{\omega_{\rm m}},\\ \hat{A}_1 &= \frac{A_1}{\omega_{\rm m}},\\ \hat{B}_n &= \frac{B_n}{\omega_{\rm m}}.\end{aligned}$$

### 3.9.1 The Important Factors

In order for a mode to have a significant effect on the transition probabilities, we require it to has large relative detuning $D$, and a large oscillation wavelength compared to the size of the physical system. Relative detuning for each mode is calculated as

$$D_n = \frac{|nk_1 - \omega_{\rm m}|}{B_n} \tag{3.40}$$

for single frequency matter profile, and

$$D_{\{n_a\}} = \frac{|\sum_a n_a k_a - \omega_{\rm m}|}{B_{\{n_a\}}} \tag{3.41}$$

for multi-frequency matter profile.

For modes with small relative detuning, they are important since they might lead to full transition. However, the full transition requires at least a distance of the order of the wavelength of the oscillation. Suppose we have a mode that has zero relative detuning, but with a oscillation wavelength much larger than the size of the system, such a mode would never have the chance to accumulate a large transition probability within the size of the system. By utilizing the theory of Rabi oscillation, we know that the oscillation wavelength of each mode is determined by the Rabi frequency

$$\Omega_{\{n_a\}} = |B_{\{n_a\}}|\sqrt{1 + D^2_{\{n_a\}}}. \tag{3.42}$$

Thus modes that has much larger oscillation wavelength are not subjected to be considered even though their relative detunings are close to zero.

In principle, we can always approximate the system by including more modes with larger relative detuning while neglecting the modes with wavelength much longer than the size of physical system. However such effort doesn't simplify the calculations.

### 3.9.2 Single Frequency Matter Profile Revisited

For the single frequency matter potential $\lambda = \lambda_0 + \lambda_1 \sin(k_1 r)$ discussed in Sec. 3.6, we removed the varying $\sigma_3$ term by arguing that this term has no effect on transition probabilities when the system is close to resonance, $k_1 \sim \omega_{\rm m}$. The reason is that only the first mode $n = 1$ is on resonance when $k_1 = \omega_{\rm m}$ and all other modes are far from resonance, thus

$$\begin{aligned} H^{\rm R} &\approx -\frac{\omega_{\rm m}}{2}\sigma_3 - \frac{1}{2}B_1 \begin{pmatrix} 0 & \Phi_1 e^{ik_1 r} \\ \Phi_1^* e^{-ik_1 r} & 0 \end{pmatrix} \\ &\approx -\frac{\omega_{\rm m}}{2}\sigma_3 - \frac{A_1}{2}\cos(k_1 r)\sigma_1 + \frac{A_1}{2}\sin(k_1 r)\sigma_2, \end{aligned} \tag{3.43}$$

| $k_1 = \omega_{\rm m}$ | | | | $k_1 = (1 - 2 \times 10^{-5})\omega_{\rm m}$ | | | | $k_1 = (1 - 10^{-4})\omega_{\rm m}$ | | | |
|---|---|---|---|---|---|---|---|---|---|---|---|
| $n$ | $D$ | $D_1'$ | $2\pi\omega_{\rm m}/\Omega_n$ | $n$ | $D$ | $D_1'$ | $2\pi\omega_{\rm m}/\Omega_n$ | $n$ | $D$ | $D_1'$ | $2\pi\omega_{\rm m}/\Omega_n$ |
| 1 | 0 | - | $3.2 \times 10^5$ | 1 | 1 | - | $2.2 \times 10^5$ | 1 | 5.2 | - | $6.2 \times 10^4$ |
| -1 | $10^5$ | $4.8 \times 10^{-6}$ | 3.1 | -1 | $10^5$ | 1 | 3.1 | -1 | $10^5$ | 5.2 | 3.1 |
| 2 | $1.1 \times 10^9$ | $2.1 \times 10^{-14}$ | 6.3 | 2 | $1.1 \times 10^9$ | 1 | 6.3 | 2 | $1.1 \times 10^9$ | 5.2 | 6.3 |
| -2 | $3.4 \times 10^9$ | $6.9 \times 10^{-15}$ | 2.1 | -2 | $3.4 \times 10^9$ | 1 | 2.1 | -2 | $3.4 \times 10^9$ | 5.2 | 2.1 |

Table 3.1: Relative detuning and oscillation wavelength of each mode for single frequency matter profile.

where $A_1$ is defined in Eqn. (3.24) and approximation

$$J_1\left(\frac{\lambda_1}{k_1}\cos(2\theta_{\rm m})\right) \approx \frac{\lambda_1}{2k_1}\cos(2\theta_{\rm m})$$

for $\lambda_1 \cos(2\theta_{\rm m})/k_1 \ll 1$ is used in the last step. Thus we reach a similar equation to the approximation we used in Sec. 3.6. $\lambda_1 \cos(2\theta_{\rm m})/k_1 \ll 1$ corresponds to small resonance width for Eqn. (3.23) and also Eqn. (3.43) so that the interferences are small.

Using Jacobi-Anger expansion, we can calculate the relative detuning for each mode as well as the interference effect. The relative detuning for each mode in the Jacobi-Anger expansion for single frequency matter profile used in Fig. 3.7 is calculated and listed in Table. 3.1. The $D_1'$ is the shifted relative detuning of the first mode with $n = 1$ due to other mode. It clearly shows that the first mode takes the whole system so that the approximation of neglecting the varying $\sigma_3$ terms in Hamiltonian is accurate enough. One can also show that the interference effect due to higher order modes is negligible, since they do not change the relative detuning of the most significant modes.

The rigorous solutions for each modes in Eqn. 3.38 is obtained,

$$P_{\rm L\to H}^{(n)} = \frac{\left|\hat{B}_n\right|^2}{\left|\hat{B}_n\right|^2 + (n\hat{k} - 1)^2} \sin^2\left(\frac{\hat{q}^{(n)}}{2}\hat{x}\right), \tag{3.44}$$

where

$$\Gamma^{(n)} = \left|\hat{B}_n\right|, \quad \text{width of resonance } (n\hat{k} \text{ as parameter}) \tag{3.45}$$

$$\hat{q}^{(n)} = \sqrt{|\Gamma^{(n)}|^2 + (n\hat{k} - 1)^2}, \quad \text{frequency of oscillations.} \tag{3.46}$$

The impact of detuning is also verified in Fig. 3.10. The example clearly shows the width of the resonance is dropping dramatically for larger modes in Jacobi-Anger expansion. A careful investigation shows that the resonance width is dropping exponentially as shown in Fig. 3.11 and Fig. 3.12.

### 3.9.3 Castle Wall Matter Profile

For completeness of this chapter, we show one example of multi-frequency matter profile. One of the multi-frequency matter profiles that has been well studied is the castle wall matter profile. Using Fourier series, any matter profile can be Fourier decomposed into superposition of many single frequency matter profile in principle. We decompose the periodic castle wall matter profile into many frequencies and study the interference effect. The potential shown in Fig. 3.13 is defined as,

$$\lambda(r) = \begin{cases} \Lambda_1, & -\frac{X_1}{2} + nX \leq r \leq \frac{X_1}{2} + nX \\ \Lambda_2, & \frac{X_1}{2} + nX \leq r \leq \frac{X_1}{2} + \frac{X_2}{2} + nX \end{cases} \tag{3.47}$$

where $X_1$ and $X_2$ are the two periods of the matter profile or potential, $X = X_1 + X_2$, and $n$ is integer. The parametric resonance condition derived by E. Akhmedov [17] is,

$$\frac{\tan(\omega_{\mathrm{m}1} X_1/2)}{\tan(\omega_{\mathrm{m}2} X_2/2)} = -\frac{\cos 2\theta_{\mathrm{m}2}}{\cos 2\theta_{\mathrm{m}1}}, \tag{3.48}$$

where $\omega_{\mathrm{m}i}$ and $\theta_{\mathrm{m}i}$ are the energy difference and mixing angle for potential $\Lambda_1$ and $\Lambda_2$ respectively.

Even though this castle wall problem is analytically solved, the resonance condition Eqn. (3.48) itself is not transparent. In this subsection, we show that such

a system is closed related to Rabi oscillations. For illustration purpose, we set the profile to be equal period for the two densities so that $X_1 = X_2 \equiv X/2$. To show that the neutrino flavor conversions in this castle wall matter profiles is related to Rabi oscillation, we decompose the profile using Fourier series,

$$\lambda(r) = \lambda_0 + \sum_{n=1}^{\infty} \lambda_n \cos\left(k_n r\right), \tag{3.49}$$

where

$$\begin{aligned}
\lambda_0 &= (\Lambda_1 + \Lambda_2)/2, \\
\lambda_n &= \frac{2}{(2n-1)\pi}(-1)^n \left(\Lambda_1 - \Lambda_2\right), \\
k_n &= (2n-1)k_0, \\
k_0 &= 2\pi/X.
\end{aligned}$$

The decomposition is visualized in Fig. A.1.

To calculate the transitions between two mass states of background matter potential $\lambda_0$, we use the background matter basis with respect to $\lambda_0$, in which the transition is zero when varying matter profile vanishes. The Hamiltonian

$$H^{(\mathrm{m})} = -\frac{1}{2}\omega_{\mathrm{m}}\sigma_3 + \frac{1}{2}\sum_{n=1}^{\infty} \lambda_n \cos 2\theta_{\mathrm{m}} \cos\left(k_n r\right)\sigma_3 - \frac{1}{2}\sum_{n=1}^{\infty} \lambda_n \sin 2\theta_{\mathrm{m}} \cos\left(k_n r\right)\sigma_1, \tag{3.50}$$

determines the transitions between the two background matter states.

In principle, the base frequency $k_0$ which is determined by the total period $X$ can be arbitrary. In this example, we choose a $X$ so that the base frequency $k_0$ matches the energy gap $\omega_{\mathrm{m}}$. Even though multiple perturbation frequencies show up in Eqn. (3.50), we identify that only the first frequency $n = 1$ is the resonance frequency since we are using $k_0 = \omega_{\mathrm{m}}$. As an approximation, we drop all other frequencies $n > 2$ regarding the fact that they are far from resonance. Thus, similar to single frequency matter profile, the varying $\sigma_3$ terms have limited effects on the

transition probabilities in our case, which leads to

$$\begin{aligned} H^{(\mathrm{m})} \to & -\frac{1}{2}\omega_{\mathrm{m}}\sigma_3 - \frac{1}{2}\sum_{n=1}^{2}\lambda_n \sin 2\theta_{\mathrm{m}} \cos\left(k_n r\right)\sigma_1 \\ \to & -\frac{1}{2}\omega_{\mathrm{m}}\sigma_3 - \frac{1}{2}\sum_{n=1}^{2} A_n \cos(k_n r)\sigma_1 \\ & + \frac{1}{2}\sum_{n=1}^{2} A_n \sin(k_n r)\sigma_2, \end{aligned}$$

where

$$A_n = \frac{\lambda_n \sin 2\theta_{\mathrm{m}}}{2}.$$

The relative detuning is 0 if we have only the first mode. However, it becomes

$$D_1' = \frac{A_2^2}{2|A_1(\omega_{\mathrm{m}} - k_2)|}, \tag{3.51}$$

if we include the second frequency $k_2$. One feature of this Fourier series expanded matter profile Eqn. (3.49) is that the width of each frequency decreases as the order $n$ increases while the detuning of each frequency increases. We calculate the relative detuning for each frequency

$$D_n = \frac{|k_n - \omega_{\mathrm{m}}|}{|\lambda_n \sin 2\theta_{\mathrm{m}}/2|} = \frac{2(n-1)(2n-1)\pi\omega_{\mathrm{m}}}{(\Lambda_2 - \Lambda_1)\sin 2\theta_{\mathrm{m}}} \tag{3.52}$$

which is quadratic in $n$ and inversely proportional to $\Lambda_2 - \Lambda_1$. We find that all higher frequencies $k_n$ for $n > 2$ have very large relative detunings. The neutrino transition probability between the two matter states is shown in Fig. 3.14, where we find the system has almost full transition.

A more rigorous treatment is to use Jacobi-Anger expansion and find the Rabi modes, where we find that the mode that corresponds to single frequency $k_1$ dominates and all other modes have little destruction effect on it. Quantitatively, higher orders leads to smaller width $B_{\{n_i\}}$ yet larger detuning $\sum_n nk_n - \omega_{\mathrm{m}}$, which renders a smaller effect on the resonance mode $\{1, 0\}$, since the effect is evaluated as

| $\{n_1, n_2\}$ | $D$ | $D'_{\{1,0\}}$ |
|---|---|---|
| $\{1, 0\}$ | 0 | - |
| $\{-1, 0\}$ | 48 | $1.0 \times 10^{-2}$ |
| $\{0, 1\}$ | $1.5 \times 10^{2}$ | $1.1 \times 10^{-3}$ |
| $\{2, 0\}$ | $2.4 \times 10^{2}$ | $2.0 \times 10^{-4}$ |

Table 3.2: Relative detuning of each frequency.

Eqn. (3.29). Table 3.2 lists the first few smallest relative detunings of Fig. 3.14. The second column is the relative detuning of the corresponding mode, while the third column is the relative detuning of mode $\{1, 0\}$ with the energy gap shift effect of the corresponding mode.

## 3.10 Deep Diving into Jacobi-Anger Expansion

### 3.10.1 Single Matter Density Frequencies

As a first step, we solve single frequency matter perturbation

$$\delta\lambda(x) = A\sin(kx + \phi). \tag{3.53}$$

Using the relation between $\eta$ and $\delta\lambda$, we solve out $\eta$.

$$\eta(x) = -\frac{\omega_m}{2}x - \frac{\cos 2\theta_m}{2}\frac{A}{k}\cos(kx + \phi), \tag{3.54}$$

where we have chosen $\eta(0) = -\frac{\cos 2\theta_m}{2}\frac{A}{k}\cos\phi$. The problem is to solve the equation of motion

$$i\frac{d}{dx}\begin{pmatrix}\psi_{b1}\\ \psi_{b2}\end{pmatrix} = \frac{\sin 2\theta_m}{2}\delta\lambda(x)\begin{pmatrix}0 & e^{2i\eta(x)}\\ e^{-2i\eta(x)} & 0\end{pmatrix}\begin{pmatrix}\psi_{b1}\\ \psi_{b2}\end{pmatrix}. \tag{3.55}$$

We also define

$$h = \frac{\sin 2\theta_m}{2}\delta\lambda(x)e^{2i\eta(x)} \tag{3.56}$$

$$= \frac{\sin 2\theta_m}{2}A\sin(kx+\phi)e^{i\left(-\omega_m x - \frac{A\cos 2\theta_m}{k}\cos(kx+\phi)\right)}, \tag{3.57}$$

so that the equation of motion becomes

$$i\frac{d}{dx}\begin{pmatrix}\psi_{b1}\\ \psi_{b2}\end{pmatrix} = \begin{pmatrix}0 & h\\ h^* & 0\end{pmatrix}\begin{pmatrix}\psi_{b1}\\ \psi_{b2}\end{pmatrix}. \tag{3.58}$$

We apply Jacobi-Anger expansion, c.f. Eqn. A.27, to rewrite the exponential into some plane wave terms [40].

We define $z_k = \frac{A}{k}\cos 2\theta_m$, with which we expand the term

$$e^{-i\frac{\cos 2\theta_m A}{k}\cos(kx+\phi)} = \sum_{n=-\infty}^{\infty} i^n J_n(-z_k)e^{in(kx+\phi)} = \sum_{n=-\infty}^{\infty}(-i)^n J_n(z_k)e^{in(kx+\phi)}, \tag{3.59}$$

where I used $J_n(-z_k) = (-1)^n J_n(z_k)$ for integer $n$. The expansion is plugged into the Hamiltonian elements,

$$h = \frac{A\sin 2\theta_m \sin(kx+\phi)}{2}e^{-i\omega_m x}\sum_{n=-\infty}^{\infty}(-i)^n J_n(z_k)e^{in(kx+\phi)} \tag{3.60}$$

$$= \frac{A\sin 2\theta_m}{4i}\left(e^{i(kx+\phi)} - e^{-i(kx+\phi)}\right)e^{-i\omega_m x}\sum_{n=-\infty}^{\infty}(-i)^n J_n(z_k)e^{in(kx+\phi)} \tag{3.61}$$

$$= \frac{A\sin 2\theta_m}{4i}\left(\sum_{n=-\infty}^{\infty} e^{i(n+1)}i^n J_n(z_k)e^{i((n+1)k-\omega_m)x} - \sum_{n'=-\infty}^{\infty} e^{i(n'-1)}(-i)^{n'}J_{n'}(z_k)e^{i((n'-1)k-\omega_m)x}\right) \tag{3.62}$$

$$= \frac{A\sin 2\theta_m}{4}\sum_{n=-\infty}^{\infty} e^{in\phi}\left(-(-i)^n\right)\frac{2n}{z_k}J_n(z_k)e^{i(nk-\omega_m)x}, \tag{3.63}$$

where I have used

$$J_{n-1}(z_k) + J_{n+1}(z_k) = \frac{2n}{z_k}J_n(z_k). \tag{3.64}$$

Here comes the approximation. The most important oscillation we need is the one with largest period, which indicates the phase to be almost zero,

$$(n+1)k - \omega_m \sim 0 \tag{3.65}$$

$$(n'-1)k - \omega_m \sim 0. \tag{3.66}$$

The two such conditions for the two summations are

$$n \equiv n_- = \text{Int}\left(\frac{\omega_m}{k}\right) - 1 \tag{3.67}$$

$$n' \equiv n_+ = \text{Int}\left(\frac{\omega_m}{k}\right) + 1. \tag{3.68}$$

We define $\text{Int}\left(\frac{\omega_m}{k}\right) = n_0$,

$$n_- = n_0 - 1 \tag{3.69}$$

$$n_+ = n_0 + 1. \tag{3.70}$$

The element of Hamiltonian is written as

$$h = -\frac{A\sin 2\theta_m}{2} e^{in_0\phi}(-i)^{n_0}\frac{n_0}{z_k}J_{n_0}(z_k)e^{i(n_0k-\omega_m)x}. \tag{3.71}$$

To save keystrokes, we define

$$F = -A\sin 2\theta_m e^{in_0\phi}(-i)^{n_0}\frac{n_0}{z_k}J_{n_0}(z_k), \tag{3.72}$$

which depends on $n_0$ and $z_k = \frac{A}{k}\cos 2\theta_m$. Notice that

$$|F|^2 = \left|k\tan 2\theta_m n_0 J_{n_0}(z_k)\right|^2. \tag{3.73}$$

Thus the 12 element of the Hamiltonian is rewritten as

$$h = \frac{1}{2}Fe^{i(n_0k-\omega_m)x}. \tag{3.74}$$

The general solution to the equation of motion is

$$\psi_{b1} = C_1 e^{\frac{1}{2}i\left(n_0k-\omega_m-\sqrt{|F|^2+(n_0k-\omega_m)^2}\right)x} + C_2 e^{\frac{1}{2}i\left(n_0k-\omega_m+\sqrt{|F|^2+(n_0k-\omega_m)^2}\right)x} \tag{3.75}$$

$$\begin{aligned}\psi_{b2} =& \frac{C_1}{F^*}i\left(n_0k-\omega_m-\sqrt{|F|^2+(n_0k-\omega_m)^2}\right)e^{-\frac{1}{2}i(n_0k-\omega_m)x-\frac{1}{2}i\sqrt{|F|^2+(n_0k-\omega_m)^2}} \\ &+ \frac{C_2}{F^*}i\left(n_0k-\omega_m+\sqrt{|F|^2+(n_0k-\omega_m)^2}\right)e^{-\frac{1}{2}i(n_0k-\omega_m)x+\frac{1}{2}i\sqrt{|F|^2+(n_0k-\omega_m)^2}}.\end{aligned} \tag{3.76}$$

For simplicity, we define

$$g = n_0k - \omega_m, \tag{3.77}$$

$$q^2 = |F|^2 + g^2. \tag{3.78}$$

To determine the constants, we need initial condition,

$$\begin{pmatrix}\psi_1(0)\\ \psi_2(0)\end{pmatrix} = \begin{pmatrix}1\\ 0\end{pmatrix}, \tag{3.79}$$

which leads to

$$\begin{pmatrix}\psi_{b1}(0)\\ \psi_{b2}(0)\end{pmatrix} = \begin{pmatrix}e^{i\eta(0)}\\ 0\end{pmatrix}. \tag{3.80}$$

Plug in the initial condition for the wave function,

$$C_1 + C_2 = e^{i\frac{z_k}{2}\cos\phi} \tag{3.81}$$

$$\frac{C_1}{2F^*}i\,(g-q) + \frac{C_2}{F^*}i\,(q+g) = 0. \tag{3.82}$$

The constants are solved out

$$C_1 = e^{i\frac{z_k}{2}\cos\phi}\frac{q+g}{2q}, \tag{3.83}$$

$$C_2 = e^{i\frac{z_k}{2}\cos\phi}\frac{q-g}{2q}. \tag{3.84}$$

where $F$ is defined in 3.72 and $l$ and $g$ are defined in 3.78. The second element of wave function becomes

$$\psi_{b2}(x) = \frac{-F}{q}e^{i\frac{z_k}{2}\cos\phi}e^{-\frac{i}{2}gx}\sin\left(\frac{1}{2}qx\right). \tag{3.85}$$

The transition probability becomes

$$P_{1\to 2} = |\psi_{b2}|^2 = \frac{|F|^2}{q^2}\sin^2\left(\frac{q}{2}x\right), \tag{3.86}$$

where $q$ is the oscillation wavenumber. Period of this oscillation is given by $T = \frac{2\pi}{q}$.

Compared to the results by Kneller et al [35], where the transition probability is

$$P_{12} = \frac{\kappa_n^2}{q_n^2}\sin^2(q_n x), \tag{3.87}$$

where $q_n^2 = k_n^2 + \kappa_n^2$ and $2k_n = \delta\tilde{k}_{12} + nk_\star$.

In my notation, $k$ is the same as their $k_\star$. After the first step of translation, we have $g = 2k_n$.

The definition of $\kappa_n$ is given by

$$\kappa_{ij,n} = (-i)^{n-1}\frac{nC_\star V_\star}{z_{ij}}J_n(z_{ij})\tilde{U}_{ei}^*\tilde{U}_{ej}e^{i(n\eta + z_{ij}\cos\eta)}, \tag{3.88}$$

in Kneller et al's notation and

$$\delta V_{ee}(x) = C_\star V_\star \sin(k_\star x + \eta). \tag{3.89}$$

So we conclude that my $|F|^2$ is related to Kneller et al's $|\kappa_n|^2$ through

$$|F|^2 = 4|\kappa_n|^2. \tag{3.90}$$

We also have

$$q^2 = |F|^2 + g^2 = 4q_n^2, \tag{3.91}$$

i.e., $q_n = \frac{q}{2}$. Now we see the method we have used gives exactly the same transition probability as Kneller et al's.

To make the numerical calculations easier, we rewrite the result by defining the

scaled variables

$$\hat{x} = \omega_m x, \tag{3.92}$$

$$\hat{k} = \frac{k}{\omega_m}, \tag{3.93}$$

$$\hat{A} = \frac{A}{\omega_m}, \tag{3.94}$$

$$\hat{g} = \frac{g}{\omega_m} = n_0 \hat{k} - 1, \tag{3.95}$$

$$\hat{q} = \sqrt{|\hat{F}|^2 + \hat{g}^2} = \sqrt{|\hat{k} \tan 2\theta_m n_0 J_{n_0}(z_k)| + \hat{g}^2}, \tag{3.96}$$

so that $n_0 = \text{Round}\left(1/\hat{k}\right)$, $z_k = \frac{\hat{A}}{\hat{k}} \cos 2\theta_m$ and

$$P_{1\to 2} = \frac{\left|\hat{k} \tan 2\theta_m n_0 J_{n_0}(z_k)\right|^2}{\left|\hat{k} \tan 2\theta_m n_0 J_{n_0}(z_k)\right|^2 + \hat{g}^2} \sin^2\left(\frac{\hat{q}}{2}\hat{x}\right). \tag{3.97}$$

**Mathematical Analysis of The Result**

There are several question to answer before we can understand the picture of the math.

- What does each term mean in the Hamiltonian?
- What exactly is the unitary transformation we used to rotate the wave function?
- What is the physical meaning of Jacobi-Anger expansion in our calculation?

To answer the first question, we need to write down the solution to Schrodinger equation assuming the Hamiltonian has only one term. The results are listed below in Table 3.3.

The unitary transformation used is to move our reference frame to a co-rotating one. $-\frac{\omega_m}{2}\sigma_3$ is indeed causing the wave function to rotate and removing this term

| Hamiltonian | Solution to The First Element of Wave Function |
|---|---|
| $-\frac{\omega_m}{2}\sigma_3$ | $\psi_1 \sim e^{i\omega_m x/2}$ |
| $\frac{\delta\lambda}{2}\cos 2\theta_m\sigma_3$ | $\psi_1 \sim e^{i\frac{A\cos 2\theta_m}{2k}\cos(kx+\phi)}$ |
| $\frac{\delta\lambda}{2}\cos 2\theta_m\sigma_3$ | $\psi_1 = C_1 e^{i\frac{A\sin 2\theta_m}{2k}\cos(kx+\phi)} + C_2 e^{-i\frac{A\sin 2\theta_m}{2k}\cos(kx+\phi)}$ |

Table 3.3: Each terms in Hamiltonian and the corresponding solutions to the specific term.

using a transformation means we are co-rotating with it. $\frac{\delta\lambda}{2}\cos 2\theta_m\sigma_3$ causes a more complicated rotation however it is still a rotation.

As for Jacobi-Anger expansion, it expands an oscillating matter profile to infinite constant matter potentials. To see it more clearly, we assume that $\delta\lambda = \lambda_c$ is constant. After the unitary transformation, the effective Hamiltonian is

$$H' = \frac{\sin 2\theta_m}{2}\lambda_c \begin{pmatrix} 0 & e^{2i\eta(x)} \\ e^{-2i\eta(x)} & 0 \end{pmatrix}, \tag{3.98}$$

where $\eta(x) = -\frac{\omega_m}{2}x + \frac{\cos 2\theta_m}{2}\lambda_c x$ and we have chosen $\eta(0) = 0$. The 12 element of the Hamiltonian becomes

$$\frac{\sin 2\theta_m}{2}\lambda_c e^{2i\eta(x)} = \frac{\sin 2\theta_m}{2}\lambda_c e^{2i\left(\frac{\omega_m}{2} + \frac{\cos 2\theta_m}{2}\lambda_c\right)x}. \tag{3.99}$$

The significance of it is to show that a constant matter profile will result in a simple exponential term. However, as we move on to periodic matter profile, we have a Hamiltonian element of the form

$$h = \frac{\sin 2\theta_m}{2}A\sin(kx+\phi)e^{2i\left(-\frac{\omega_m}{2}x + \frac{A\cos 2\theta_m}{2k}\cos(kx+\phi)\right)}, \tag{3.100}$$

as derived in Eqn. 3.57. To compare with the constant matter case, we make a table of relevant terms in Hamiltonian, Table 3.4.

The periodic profile comes into the exponential. Jacobi-Anger expansion (Eqn. A.27) expands the periodic matter profile into infinite constant matter profiles. By comparing the two cases, we conclude that $\cos 2\theta_m\lambda_c$ corresponds to $nk$. The RWA

| Constant Matter Profile $\delta\lambda = \lambda_c$ | Periodic Matter Profile $\delta\lambda = A\sin(kx+\phi)$ |
|---|---|
| $\frac{\sin 2\theta_m}{2}\lambda_c e^{i\cos 2\theta_m \lambda_c x}$ | $\frac{A\sin 2\theta_m}{4}\sum_{n=-\infty}^{\infty} e^{in\phi}\left(-i^n\right)\frac{2n+1}{z_k}J_n(z_k)e^{i(nk-\omega_m)x}$ |

Table 3.4: Comparison of the off diagonal element of Hamiltonian for constant matter density profile and the periodic matter density profile.

approximation we used to drop fast oscillatory terms in the summation is to find the most relevant constant matter profile per se.

The big question is which constant matter profiles are the most important ones? Mathematically, we require the phase to be almost zero, i.e. Eqn. 3.66 or

$$n_0 k - \omega_m \sim 0, \tag{3.101}$$

where $n_0 = \text{Round}\left(\frac{\omega_m}{k}\right)$.

We define an effective matter density out of the Jacobi-Anger expanded series

$$\lambda_c' = \frac{n_0 k}{\cos 2\theta_m}. \tag{3.102}$$

Then we can rewrite the RWA requirement as

$$\lambda_c' - \cos 2\theta_m \omega_m = 0. \tag{3.103}$$

**The Resonances**

Now we check the Hamiltonian again to see if we could locate some physics. In the newly defined basis and using scaled quantities

$$\hat{\mathbf{H}} = \begin{pmatrix} 0 & \hat{h} \\ \hat{h}^* & 0 \end{pmatrix}, \tag{3.104}$$

where

$$\hat{h} = \frac{1}{2}\hat{B}_n e^{i(n\hat{k}-1)\hat{x}}, \tag{3.105}$$

and

$$\hat{B}_n = (-i)^n \hat{k} \tan 2\theta_{\rm m} n J_n(\frac{\hat{A}}{\hat{k}} \cos 2\theta_{\rm m}). \tag{3.106}$$

It becomes much more clearer if we plug $\hat{h}$ back into Hamiltonian. What we find is that

$$\hat{\mathbf{H}} = \sum_{n=-\infty}^{\infty} \begin{pmatrix} 0 & -\frac{1}{2}\hat{B}_n e^{i(n\hat{k}-1)\hat{x}} \\ -\frac{1}{2}\hat{B}_n^* e^{-i(n\hat{k}-1)\hat{x}} & 0 \end{pmatrix}. \tag{3.107}$$

With some effort, we find that the solution to the second amplitude of the wave function is

$$\psi_2 = \frac{i}{\hat{B}_n \hat{W}} e^{-i(n\hat{k}-1)\hat{x}} \left|\hat{B}_n\right|^2 \sin\left(\frac{1}{2}(n\hat{k}-1-\hat{W})\hat{x}\right), \tag{3.108}$$

where

$$\hat{W} = \sqrt{(n\hat{k}-1)^2 + \left|\hat{B}_n\right|^2}. \tag{3.109}$$

At this stage, it is quite obvious that our system is a composite Rabi oscillation system. For each specific $n$ term we write down the hopping probability from light state to the heavy state,

$$P_{\rm L\to H}^{(n)} = \frac{\left|\hat{B}_n\right|^2}{\left|\hat{B}_n\right|^2 + (n\hat{k}-1)^2} \sin^2\left(\frac{\hat{q}^{(n)}}{2}\hat{x}\right), \tag{3.110}$$

where

$$\Gamma^{(n)} = \left|\hat{B}_n\right|, \quad \text{width of resonance } (n\hat{k} \text{ as parameter}) \tag{3.111}$$

$$\hat{q}^{(n)} = \sqrt{|\Gamma^{(n)}|^2 + (n\hat{k}-1)^2}, \quad \text{frequency of oscillations} \tag{3.112}$$

We define the scaled quantities,

$$\hat{x} = \omega_{\rm m} x, \tag{3.113}$$

$$\hat{h} = h/\omega_{\rm m}, \tag{3.114}$$

$$\hat{B}_n = B_n/\omega_{\rm m}, \tag{3.115}$$

$$\hat{k} = k/\omega_{\rm m}, \tag{3.116}$$

$$\hat{A} = A/\omega_{\rm m}, \tag{3.117}$$

$$\hat{q} = q/\omega_{\rm m}. \tag{3.118}$$

Just a comment. $B_n$ is used here because I actually want to use it for multi-frequency case and I just think $B_n$ is better than $F$.

Resonance width of each order of resonance (each $n$) should be calculated analytically.

To find the exact width is hopeless since we need to inverse Bessel functions. Nonetheless, we can assume that the resonance is very narrow so that $|F|^2$ doesn't change a lot. With the assumption, the FWHM (Full Width at Half Maximum) is found be setting the amplitude to half, which is

$$\Gamma = \left|\frac{\hat{F}}{n_0}\right| = \left|\hat{k}\tan 2\theta_m \frac{J_{n_0}(n_0\hat{A}\cos 2\theta_m/\hat{k})}{n_0}\right|. \tag{3.119}$$

To verify this result, we compare it with the width found numerically from the exact amplitude.

Given this result, and equation 3.74, we infer that the coefficient in front of the phase term of 12 element in Hamiltonian is related to the width, while the the deviation from the exact resonance is given by $\hat{g} = n_0\hat{k} - 1$.

the width of the resonance is

$$\Gamma = \left|\frac{F}{n_0}\right|. \tag{3.120}$$

### 3.10.2 Multiple Matter Density Frequencies

However, as we proceed to the more realistic matter profile, multi-frequency matter profiles are necessary. Generally, we choose the perturbation matter profile upon a constant background to be

$$\delta\lambda(x) = \sum_n A_n \sin(k_n x + \phi_n). \tag{3.121}$$

Applying the Rabi basis and solving for $\eta$ we conclude that

$$\eta(x) = -\frac{\omega_m}{2}x - \frac{\cos 2\theta_m}{2}\sum_n \frac{A_n}{k_n}\cos(k_n x + \phi_n). \tag{3.122}$$

We formulate the Hamiltonian in Rabi basis to be the form

$$H^{(R)} = -\frac{1}{2}\sigma_3 + \begin{pmatrix} 0 & h \\ h^* & 0 \end{pmatrix}, \tag{3.123}$$

We write down the off diagonal element $h$ for the multi-frequency matter density profile

$$h = \frac{\sin 2\theta_m}{2}\sum_a A_a \sin(k_a x + \phi_a)e^{-i\omega_m x}\prod_a \sum_{n=-\infty}^{\infty}(-i)^n J_n(z_{k_a})e^{in(k_a x+\phi_a)} \tag{3.124}$$

To demonstrate the procedure of Jacobi-Anger expansion as well as the technique to decompose the problem into simple Rabi oscillations, we adopt a two frequencies matter density scenario.

To work out the equation of motion that we could solve, we deal with two frequencies first,

$$\delta\lambda(x) = A_1 \sin(k_1 x + \phi_1) + A_2 \sin(k_2 x + \phi_2), \tag{3.125}$$

while

$$h = \frac{\sin 2\theta_m}{2}\sum_{a=1}^{2} A_a \sin(k_a x + \phi_a)e^{-i\omega_m x}\prod_{a=1}^{2}\sum_{n=-\infty}^{\infty}(-i)^n J_n(z_{k_a})e^{in(k_a x+\phi_a)}. \tag{3.126}$$

A useful trick for multiplication of two summations is

$$\sum_n a_n \sum_m b_m = \sum_{N=-\infty}^{\infty} \sum_{m+n=N} a_n b_m = \sum_{N=-\infty}^{\infty} \sum_{n=-\infty}^{N} a_n b_{N-n}. \tag{3.127}$$

For further simplifications of the problem, we follow a rule to sum over a line $m+n = N$ then sum over $N$, which is illustrated in Fig. 3.15.

The multiplication in Eqn. 3.126 becomes

$$\begin{aligned} h =& \frac{\sin 2\theta_m}{2} \sum_{a=1}^{2} A_a \sin(k_a x + \phi_a) e^{-i\omega_m x} \\ & \sum_{N=-\infty}^{\infty} \sum_{n=-\infty}^{N} (-i)^n J_n(z_{k_1}) e^{in(k_1 x+\phi_1)} (-i)^{N-n} J_{N-n}(z_{k_2}) e^{i(N-n)(k_2 x+\phi_2)} \\ =& \frac{\sin 2\theta_m}{2} \sum_{a=1}^{2} A_a \sin(k_a x + \phi_a) e^{-i\omega_m x} \\ & \sum_{N=-\infty}^{\infty} \sum_{n=-\infty}^{N} (-i)^N J_n(z_{k_1}) J_{N-n}(z_{k_2}) e^{in((k_1-k_2)x+\phi_1-\phi_2)+iN(k_2 x+\phi_2)} \end{aligned} \tag{3.128}$$

To proceed on, we rewrite $\sum_{a=1}^{2} A_a \sin(k_a x + \phi_a)$,

$$\begin{aligned} & A_1 \sin(k_1 x + \phi_1) + A_2 \sin(k_2 x + \phi_2) \\ =& \frac{A_1}{2i} \left( e^{i(k_1 x+\phi_1)} + e^{-i(k_1 x+\phi_1)} \right) + \frac{A_2}{2i} \left( e^{i(k_2 x+\phi_2)} + e^{-i(k_2 x+\phi_2)} \right). \end{aligned} \tag{3.129}$$

We define

$$h = h_1 + h_2, \tag{3.130}$$

where

$$\begin{aligned} h_1 =& \frac{A_1 \sin 2\theta_m}{4i} \Bigg( \sum_{N=-\infty}^{\infty} \sum_{n=-\infty}^{N} (-i)^N J_n(z_{k_1}) J_{N-n}(z_{k_2}) e^{i((n+1)(k_1 x+\phi_1)+(N-n)(k_2 x+\phi_2)-\omega_m x)} \\ & \sum_{N=-\infty}^{\infty} \sum_{n=-\infty}^{N} (-i)^N J_n(z_{k_1}) J_{N-n}(z_{k_2}) e^{i((n-1)(k_1 x+\phi_1)+(N-n)(k_2 x+\phi_2)-\omega_m x)} \Bigg), \end{aligned} \tag{3.131}$$

and

$$h_2 = \frac{A_2 \sin 2\theta_m}{4i}\Bigg( \sum_{N=-\infty}^{\infty} \sum_{n=-\infty}^{N} (-i)^N J_n(z_{k_1}) J_{N-n}(z_{k_2}) e^{i(n(k_1 x+\phi_1)+(N-n+1)(k_2 x+\phi_2)-\omega_m x)} \\ \sum_{N=-\infty}^{\infty} \sum_{n=-\infty}^{N} (-i)^N J_n(z_{k_1}) J_{N-n}(z_{k_2}) e^{i(n(k_1 x+\phi_1)+(N-n-1)(k_2 x+\phi_2)-\omega_m x)} \Bigg). \quad (3.132)$$

We keep only terms that are integers for each summation to satisfy the relations

$$(n_{11,N}+1)k_1 + (N-n_{11,N})k_2 - \omega_m \sim 0 \quad (3.133)$$

$$(n_{12,N}-1)k_1 + (N-n_{12,N})k_2 - \omega_m \sim 0 \quad (3.134)$$

$$n_{21,N}k_1 + (N-n_{21,N}+1)k_2 - \omega_m \sim 0 \quad (3.135)$$

$$n_{22,N}k_1 + (N-n_{22,N}-1)k_2 - \omega_m \sim 0. \quad (3.136)$$

so that the $x$ dependent exponential almost vanishes (obtain the largest wavelength in fact). Notice that each $n_{ij,N}$ depends on the summation index $N$.

We solve each $n_{ij,N}$,

$$n_{11,N} \sim \text{Round}\left[\frac{\omega_m - Nk_2 - k_1}{k_1 - k_2}\right] \quad (3.137)$$

$$n_{12,N} \sim \text{Round}\left[\frac{\omega_m - Nk_2 + k_1}{k_1 - k_2}\right] \quad (3.138)$$

$$n_{21,N} \sim \text{Round}\left[\frac{\omega_m - (N+1)k_2}{k_1 - k_2}\right] \quad (3.139)$$

$$n_{22,N} \sim \text{Round}\left[\frac{\omega_m - (N-1)k_2}{k_1 - k_2}\right]. \quad (3.140)$$

Another important constrain is that $n \leq N$, thus we have

$$N_{11} \sim \text{Round}\left[\frac{\omega_m - k_1}{k_1}\right] \quad (3.141)$$

$$N_{12} \sim \text{Round}\left[\frac{\omega_m + k_1}{k_1}\right] \quad (3.142)$$

$$N_{21} \sim \text{Round}\left[\frac{\omega_m - k_2}{k_1}\right] \quad (3.143)$$

$$N_{22} \sim \text{Round}\left[\frac{\omega_m + k_2}{k_1}\right], \quad (3.144)$$

for each summation over $N$ and we require $N \geq N_{ij}$ for each summation. We also assumed $k_1 > k_2$. In other words, $N_{ij}$ are the lower limits of the summations over $N$'s.

We keep only the resonance terms for the summation over $n$'s,

$$h_1 \approx \frac{A_1 \sin 2\theta_m}{4i} \Bigg( \sum_{N=N_{11}}^{\infty} (-i)^N J_{n_{11}}(z_{k_1}) J_{N-n_{11}}(z_{k_2}) e^{i((n_{11}+1)(k_1 x+\phi_1)+(N-n_{11})(k_2 x+\phi_2)-\omega_m x)}$$
$$\sum_{N=N_{12}}^{\infty} (-i)^N J_{n_{12}}(z_{k_1}) J_{N-n_{12}}(z_{k_2}) e^{i((n_{12}-1)(k_1 x+\phi_1)+(N-n_{12})(k_2 x+\phi_2)-\omega_m x)} \Bigg), \quad (3.145)$$

and

$$h_2 \approx \frac{A_2 \sin 2\theta_m}{4i} \Bigg( \sum_{N=N_{21}}^{\infty} (-i)^N J_{n_{21}}(z_{k_1}) J_{N-n_{21}}(z_{k_2}) e^{i(n_{21}(k_1 x+\phi_1)+(N-n_{21}+1)(k_2 x+\phi_2)-\omega_m x)}$$
$$\sum_{N=N_{22}}^{\infty} (-i)^N J_{n_{22}}(z_{k_1}) J_{N-n_{22}}(z_{k_2}) e^{i(n_{22}(k_1 x+\phi_1)+(N-n_{22}-1)(k_2 x+\phi_2)-\omega_m x)} \Bigg). \quad (3.146)$$

One can imagine how hard it is to solve the equation of motion with this $h$. More approximations are required. We will use the approximations that Kelly Patton et al used [40].

By looking at the Hamiltonian, we can identify terms like this

$$h_a = \left( \frac{\sin 2\theta_m}{2} A_a \sin(k_a x + \phi_a) e^{-i\omega_m x} \sum_{n=-\infty}^{\infty} (-i)^n J_n(z_{k_a}) e^{in(k_a x+\phi_a)} \right)$$
$$\prod_{b \neq a} \sum_{n=-\infty}^{\infty} (-i)^n J_n(z_{k_b}) e^{in(k_b x+\phi_b)}, \quad (3.147)$$

where the parenthesis part is what we would have if only one frequency is used and we also have

$$h = \sum_a h_a, \quad (3.148)$$

for all frequencies. This reminds us that each of these terms means the interference due to other frequencies. As a simple example, we demonstrate two-frequency case.

The two-frequency matter perturbation system has a Hamiltonian element $H_{12}$

$$h = h_1 + h_2, \tag{3.149}$$

where

$$\begin{aligned} h_1 =& -\frac{k_1 \tan 2\theta_m}{2} \sum_{n_1=-\infty}^{\infty} (-i)^{n_1} n_1 J_{n_1}(z_{k_1}) e^{i(n_1 k_1 - \omega_m)x} e^{in_1\phi_1} \\ & \sum_{n_2=-\infty}^{\infty} (-i)^{n_2} J_{n_2}(z_{k_2}) e^{i(n_2 k_2)x} e^{in_2\phi_2}, \end{aligned} \tag{3.150}$$

$$\begin{aligned} h_2 =& -\frac{k_2 \tan 2\theta_m}{2} \sum_{n_2=-\infty}^{\infty} (-i)^{n_2} n_2 J_{n_2}(z_{k_2}) e^{i(n_2 k_2 - \omega_m)x} e^{in_2\phi_2} \\ & \sum_{n_1=-\infty}^{\infty} (-i)^{n_1} J_{n_1}(z_{k_1}) e^{in_1 k_1 x} e^{in_1\phi_1} \end{aligned} \tag{3.151}$$

with red color coding the second frequency and blue coding the first frequency. $h$ is symmetric under exchange of index 1, 2 since the exchange simply switches $h_1$ and $h_2$.

The next question to ask is which term dominates. To grasp a clue, we need to identify which term in the summation dominates. Without a good analytical analysis, the only way to do is to numerically calculate the effect of each order.

By order, we are already thinking of a dominating term which is not true. Nonetheless, we assume RWA can be applied to the part that looks like one frequency only. In our two-frequency example, first RWA leads to

$$\begin{aligned} h_1 \approx& -\frac{k_1 \tan 2\theta_m}{2} (-i)^{n_{1,0}} n_{1,0} J_{n_{1,0}}(z_{k_1}) e^{i(n_{1,0} k_1 - \omega_m)x} e^{in_{1,0}\phi_1} \\ & \sum_{n_2=-\infty}^{\infty} (-i)^{n_2} J_{n_2}(z_{k_2}) e^{i(n_2 k_2)x} e^{in_2\phi_2}, \end{aligned} \tag{3.152}$$

$$\begin{aligned} h_2 \approx& -\frac{k_2 \tan 2\theta_m}{2} (-i)^{n_{2,0}} n_{2,0} J_{n_{2,0}}(z_{k_2}) e^{i(n_{2,0} k_2 - \omega_m)x} e^{in_{2,0}\phi_2} \\ & \sum_{n_1=-\infty}^{\infty} (-i)^{n_1} J_{n_1}(z_{k_1}) e^{in_1 k_1 x} e^{in_1\phi_1}, \end{aligned} \tag{3.153}$$

where

$$n_{1,0} = \text{Round}\left[\frac{\omega_m}{k_1}\right], \tag{3.154}$$

$$n_{2,0} = \text{Round}\left[\frac{\omega_m}{k_2}\right]. \tag{3.155}$$

With this approximation, we can use RWA again by requiring

$$(n_{1,0}k_1 - \omega_m + n_2 k_2)x \sim 0, \tag{3.156}$$

$$(n_1 k_1 - \omega_m + n_{2,0}k_2)x \sim 0, \tag{3.157}$$

where the integer solutions are

$$n'_{2,0} = \text{Round}\left[\frac{n_{1,0}k_1 - \omega_m}{k_2}\right], \tag{3.158}$$

$$n'_{1,0} = \text{Round}\left[\frac{n_{2,0}k_1 - \omega_m}{k_1}\right]. \tag{3.159}$$

Now we can remove all the summations using another RWA approximation. However, whether it holds is up to investigation.

The final result is

$$\begin{aligned} h_1 \approx & -\frac{k_1 \tan 2\theta_m}{2}(-i)^{n_{1,0}} n_{1,0} J_{n_{1,0}}(z_{k_1}) e^{i(n_{1,0}k_1 - \omega_m)x} e^{i n_{1,0}\phi_1} (-i)^{n'_{2,0}} J_{n'_{2,0}}(z_{k_2}) e^{i(n'_{2,0}k_2)x} e^{i n'_{2,0}\phi_2} \\ = & -\frac{k_1 \tan 2\theta_m}{2}(-i)^{n_{1,0}+n'_{2,0}} e^{i(n_{1,0}\phi_1 + n'_{2,0}\phi_2)} n_{1,0} \\ & J_{n_{1,0}}(z_{k_1}) J_{n'_{2,0}}(z_{k_2}) e^{i(n_{1,0}k_1 - \omega_m + n'_{2,0}k_2)x} \qquad (3.160) \\ \equiv & \frac{F_1}{2} e^{i(n_{1,0}k_1 - \omega_m + n'_{2,0}k_2)x}, \qquad (3.161) \end{aligned}$$

$$\begin{aligned} h_2 \approx & -\frac{k_2 \tan 2\theta_m}{2}(-i)^{n_{2,0}} n_{2,0} J_{n_{2,0}}(z_{k_2}) e^{i(n_{2,0}k_2 - \omega_m)x} e^{i n_{2,0}\phi_2} \sum_{n_1=-\infty}^{\infty} (-i)^{n_1} J_{n_1}(z_{k_1}) e^{i n_1 k_1 x} e^{i n_1 \phi_1} \\ = & -\frac{k_2 \tan 2\theta_m}{2}(-i)^{n_{2,0}+n'_{1,0}} e^{i(n_{2,0}\phi_2 + n'_{1,0}\phi_1)} n_{2,0} \\ & J_{n_{2,0}}(z_{k_2}) J_{n'_{1,0}}(z_{k_1}) e^{i(n_{2,0}k_2 - \omega_m + n'_{1,0}k_1)x} \qquad (3.162) \\ \equiv & \frac{F_2}{2} e^{i(n_{2,0}k_2 - \omega_m + n'_{1,0}k_1)x}. \qquad (3.163) \end{aligned}$$

Lowest order only works for very special cases where on of the wave vectors is very close to resonance. To fix this problem, we could add more higher orders, however, what does it mean to have higher orders needs a discussion.

We will develop a protocol to decide which order to include. The first thought of higher orders is to add more from the summation before the last RWA. However, it is highly suspicious that this is just like the one frequency case which has a very fast drop in the resonance width as we go to higher orders. This guess needs proof, numerically and analytically. When we mentioned higher orders, we actually mean higher orders in both $n_1$ and $n_2$. Notice that we can always write the 12 element of Hamiltonian as Eqn. 3.168, i.e.,

$$\begin{aligned} h =& h_1 + h_2 \qquad (3.164)\\ =& \sum_{n_1=-\infty}^{\infty}\sum_{n_2=-\infty}^{\infty} B_{n_1,n_2}(k_1,k_2)\Phi e^{i(n_1k_1+n_2k_2-\omega_m)x} \\ &+ \sum_{n_1=-\infty}^{\infty}\sum_{n_2=-\infty}^{\infty} B_{n_2,n_1}(k_2,k_1)\Phi e^{i(n_1k_1+n_2k_2-\omega_m)x} \\ =& \sum_{n_1=-\infty}^{\infty}\sum_{n_2=-\infty}^{\infty} \left(B_{n_1,n_2}(k_1,k_2) + B_{n_2,n_1}(k_2,k_1)\right)\Phi e^{i(n_1k_1+n_2k_2-\omega_m)x}, \qquad (3.165) \end{aligned}$$

without any approximations.

- One of the choices of adding higher orders is to use $n_1 = \text{Round}\left[\frac{\omega_m}{k_1}\right]$ and $n_2 = \text{Round}\left[\frac{n_1k_1-\omega_m}{k_2}\right]$ as the lowest order in $h_1$ and $n_2 = \text{Round}\left[\frac{\omega_m}{k_2}\right]$ and $n_1 = \text{Round}\left[\frac{n_2k_2-\omega_m}{k_1}\right]$ as the lowest order in $h_2$. Adding higher orders means we add or remove one from $n_1$ in $h_1$ and recalculate $n_2$, while add or remove one from $n_2$ in $h_2$ and recalculate $n_1$.

  That is to say, we always keep the RWA condition for the last RWA process. What can be changed is the first assumption that the most important term is when only one frequency is relevant which is not always true.

As an example, we now consider $n_{i,\pm1} = n_{i,0} \pm 1$ and $n'_{i,\pm1} = \text{Round}\left[\frac{n_{j,\pm1}k_j - \omega_m}{k_i}\right]$ with $j \neq i$, thus we replace $n_{i,0}$ with $n_{i,\pm1}$ to get higher order corrections, c.f. Fig. 3.16.

In realistic physical systems, it is more likely to have a matter profile so that we have the bottom left situation. In other words, RWA method breaks down in the most interesting case.

- Another choice is to add or remove one for both $n_1$ and $n_2$ for both terms in the Hamiltonian. The approach will define the order $n_{order}$ first, as will be applied to the n's. As an example, adding first order to $n_1$ will include all the possible combinations of $n_1, n_1 \pm 1$ for both terms without changing $n_2$. As an example, we compare the different orders of $n_1$ only with the numerical calculation without approximations in Fig. 3.17.

- Now according to the complete expression of the $_{12}$ element of Hamiltonian Eqn. 3.168, there is no difference between $n_1$ and $n_2$. Thus whenever we talk about different orders, we should not distinguish between the two integers. However, how to define zero order is not clear to me at this point. To find out, we need to know the resonance width of each pair of integers. The insight comes from the single frequency result. The width for single frequency $\Gamma = \left|\frac{\hat{F}}{n_0}\right| = \left|\hat{k}\tan 2\theta_m \frac{J_{n_0}(n_0\hat{A}\cos 2\theta_m/\hat{k})}{n_0}\right|$. depends on the coefficient in front of the phase in the Hamiltonian and the integer. The task is to derive or guess the resonance width for each pair of integers $n_1, n_2$.

As for a more systematic treatment of the two-frequency case, we geometrize the problem. The 12 element can be written as

$$h = h_1 + h_2, \tag{3.166}$$

where

$$h_1 = \sum_{n_1=-\infty}^{\infty}\sum_{n_2=-\infty}^{\infty}\left(-(-i)^{n_1+n_2}\frac{\tan 2\theta_m}{2}n_1k_1J_{n_1}(z_{k_1})J_{n_2}(z_{k_2})\right)e^{i(n_1\phi_1+n_2\phi_2)}e^{i(n_1k_1+n_2k_2-\omega_m)x},$$

$$h_2 = \sum_{n_1=-\infty}^{\infty}\sum_{n_2=-\infty}^{\infty}\left(-(-i)^{n_1+n_2}\frac{\tan 2\theta_m}{2}n_2k_2J_{n_1}(z_{k_1})J_{n_2}(z_{k_2})\right)e^{i(n_1\phi_1+n_2\phi_2)}e^{i(n_1k_1+n_2k_2-\omega_m)x}.$$

For simplicity, we define

$$\begin{aligned}B_{n_1,n_2}(k_1,k_2,A_1,A_2) &= -(-i)^{n_1+n_2}\tan 2\theta_m n_1k_1J_{n_1}(z_{k_1})J_{n_2}(z_{k_2})\\ &= -(-i)^{n_1+n_2}\tan 2\theta_m n_1k_1J_{n_1}(\frac{A_1}{k_1}\cos 2\theta_m)J_{n_2}(\frac{A_2}{k_2}\cos 2\theta_m),\\ \Phi &= e^{i(n_1\phi_1+n_2\phi_2)}.\end{aligned}$$

Notice that

$$B_{n_2,n_1}(k_2,k_1,A_2,A_1) = -(-i)^{n_1+n_2}\tan 2\theta_m n_2k_2J_{n_1}(\frac{A_1}{k_1}\cos 2\theta_m)J_{n_2}(\frac{A_2}{k_2}\cos 2\theta_m).$$

Using these definitions, we rewrite the Hamiltonian 12 element

$$\begin{aligned}h =& h_1+h_2 \qquad (3.167)\\ =&\frac{1}{2}\sum_{n_1=-\infty}^{\infty}\sum_{n_2=-\infty}^{\infty}B_{n_1,n_2}(k_1,k_2,A_1,A_2)\Phi e^{i(n_1k_1+n_2k_2-\omega_m)x}\\ &+\frac{1}{2}\sum_{n_1=-\infty}^{\infty}\sum_{n_2=-\infty}^{\infty}B_{n_2,n_1}(k_2,k_1,A_2,A_1)\Phi e^{i(n_1k_1+n_2k_2-\omega_m)x}\\ =&\frac{1}{2}\sum_{n_1=-\infty}^{\infty}\sum_{n_2=-\infty}^{\infty}\left(B_{n_1,n_2}(k_1,k_2,A_1,A_2)+B_{n_2,n_1}(k_2,k_1,A_2,A_1)\right)\Phi e^{i(n_1k_1+n_2k_2-\omega_m)x}\\ =&\frac{1}{2}\sum_{n_1=-\infty}^{\infty}\sum_{n_2=-\infty}^{\infty}B_2n_1,n_2(k_1,k_2,A_1,A_2)\Phi e^{i(n_1k_1+n_2k_2-\omega_m)x}, \qquad (3.168)\end{aligned}$$

where $B_2n_1,n_2(k_1,k_2,A_1,A_2) \equiv B_{n_1,n_2}(k_1,k_2,A_1,A_2)+B_{n_2,n_1}(k_2,k_1,A_2,A_1)$ is what we are interested in.

Comparing this expression with the single frequency one which is almost the same structure if we remove the two sums, and using the result 3.97, we can infer that the

transition probability,

$$P_{1\to 2}(x) = \frac{|\hat{B}_2|^2}{|\hat{B}_2|^2 + \hat{g}_2^2} \sin^2\left(\frac{q_2}{2}x\right), \tag{3.169}$$

where $\hat{B}_2 = \frac{B_2}{\omega_m} = \frac{B_{n_1,n_2}(k_1,k_2,A_1,A_2)+B_{n_2,n_1}(k_2,k_1,A_2,A_1)}{\omega_m}$ and $\hat{g}_2 = \frac{g}{\omega_m} = n_1\hat{k}_1 + n_2\hat{k}_2 - 1$ which tells us how far from resonance and $q_2 = \sqrt{|\hat{B}_2|^2 + \hat{g}^2}$.

The width then is similar to 3.120, except that we could not define the width as a function of single variables since two wave vector are used. However, it is still reasonable to give the FWHM condition,

$$n_1\hat{k}_1 + n_2\hat{k}_2 - 1 = \pm|\hat{B}_2| = \left|\frac{B_{n_1,n_2}(k_1,k_2,A_1,A_2) + B_{n_2,n_1}(k_2,k_1,A_2,A_1)}{\omega_m}\right|. \tag{3.170}$$

For a given pair of integers $n_1, n_2$, we could find the amplitude as a function of $k_1, k_2$.

A solution shows that this is correct. The solution to the second element of wave function is

$$\psi_{b2} = i\frac{|\hat{B}_2|^2 e^{-\frac{i}{2}\hat{g}_2\hat{x}}}{\hat{B}_2\sqrt{|\hat{B}_2|^2 + \hat{g}^2}} \sin\left(\frac{\sqrt{|\hat{B}_2|^2 + \hat{g}^2}}{2}x\right). \tag{3.171}$$

It is very confusing when we write down the requirement for width 3.170, since we need to assume $|\hat{F}_2|$ to be almost constant to arrive this result. What values of $\hat{k}_1, \hat{k}_2$ do we need to calculate $|\hat{F}_2|$? The idea is to find the FWHM (Full Width Half Maximum) when a point is deviating from the line. To be specific, we find the line that is the resonance using $n_1k_1 + n_2k_2 = 1$, which is plotted as dashed red line in 3.18. To characterize the distance, we need a line that is perpendicular to this red dashed resonance line, which also is passing through the values of $(k_10, k_2) = (k_{10}, k_{20})$ which is given in the system. Under this scheme, the resonance width is define as the distance from the resonance line when the amplitude reduces to half on this blue dotted perpendicular line.

In the language of algebra, we could derive the interception point of the two lines,

which is

$$k_{1,\text{intercept}} = \frac{n_2^2 k_{10} + n_2 k_{20} + n_1}{n_1^2 + n_2^2}, \tag{3.172}$$

$$k_{2,\text{intercept}} = \frac{n_1}{n_2} k_{1,\text{intercept}} - \frac{1}{n_2}, \tag{3.173}$$

where $k_{10}$ and $k_{20}$ are the values given in the matter perturbation of the system.

Using this method, we can define a reasonable width for two frequency matter perturbation case,

$$\Gamma_2 = \frac{B_2(k_{1,\text{intercept}}, k_{2,\text{intercept}})}{\sqrt{n_1^2 + n_2^2}}. \tag{3.174}$$

To apply the width in a problem, we need to calculate the distance between the given point $(k_{10}, k_{20})$ of the system to a certain resonance line which depends on $n_1, n_2, A_1, A_2, \theta_m$. This is as simple as point to line distance, which is calculated using

$$d = \frac{|n_1 k_{10} + n_2 k_{20} - 1|}{\sqrt{n_1^2 + n_2^2}}. \tag{3.175}$$

The requirement for a pair of $(n_1, n_2)$ to be important is determined by defining a quantity that compares the distance from a certain resonance line with the width of this resonance line,

$$Q_2 = \frac{d}{\Gamma_2}. \tag{3.176}$$

## 3.11 Conclusions

The solar neutrinos behave very differently from lab experiments since the Sun provides a high matter density lab which can not be built on the Earth. What's even more exotic, in a supernova explosion, $10^{58}$ neutrinos are released from the proto-neutron star, which is of radius 10km, in a few seconds. The huge number density of neutrinos and large density of matter both change the neutrino oscillations dramatically. The matter effect in supernova is also much more complicated than MSW

for solar neutrinos since the rich distribution of matter density and high speed motion. In addition to matter effect, neutrino neutrino interaction will be very efficient because of the high neutrino number density.

Apart from the emission of neutrinos from nuclear reactions of electron capture and positron emission in the solar interior, supernova environment also gives rise to Bremsstrahlung pair neutrino production, electron-positron neutrino pair production, which brings all three flavors and also anti-neutrinos into the spectra. However, even the with the presence of intensive interaction between neutrinos and the leptons and hardrons, which thermalize the neutrinos in the supernova core, the neutrino spectrum escaping from the supernova core is not completely Fermi-Dirac distribution. Nonetheless, it is possible to parametrize it using nominal Fermi-Dirac distribution,[21]

$$f(E) \propto \frac{E^2}{1 + \exp(E/kT - \mu)}. \tag{3.177}$$

Some numerical results show that there is a deviation from this Fermi-Dirac distribution [15, 20]. Meanwhile, Keil Mathias and Georg Raffelt showed that it is good enough to approximate the neutrino spectrum from supernova in Monte Carlo simulations using the so called "alpha fit",

$$f(E) \propto E^{\alpha} \exp\left(-(\alpha+1)\frac{E}{\langle E\rangle}\right), \tag{3.178}$$

where $\langle E\rangle$ is the average energy, or the first moment of energy. The values from Monte Carlo simulations falls into the range $\alpha = 2.5 \sim 5$, which clearly shows the spectra are pinched. It's a hint that the detection of deviation from nominal Fermi-Dirac distribution will show evidence of core-collapse information.

Even though we understand solar neutrinos well, the neutrino oscillations of supernova explosions are not so to our complete knowledge. The flavor content is subject to the solution to the neutrino oscillations. Phenomena such as spectral split due to neutrino-neutrino interaction and matter effect reshape the neutrino

spectra significantly. That being said, more research on supernova neutrinos, especially supernova neutrino oscillations is critical to understand supernova explosion mechanisms, as well as future observation of supernova neutrino data.

In conclusion, we have provided an interpretation for neutrino flavor conversion in fluctuating matter with the help of Rabi oscillations. The work provided two different points of view that is related to Rabi oscillations.

The first point of view was to interpret the neutrino flavor conversions in background matter basis. In this basis, matter density fluctuations will introduced a fluctuation part to the diagonal elements of the Hamiltonian, which means that the energy gap is fluctuating if we draw analogy between this Hamiltonian and the Hamiltonian of Rabi oscillations. For neutrino flavor conversions in a single frequency matter profile, the neutrino flavor oscillations becomes large when the matter fluctuation frequency is close to the energy gap, which is the resonance condition. We anticipated that the fluctuations of energy gap have limited effects on neutrino flavor conversions under this resonance condition. Thus the matter fluctuation only works as a pure flipping field that converts neutrinos from one flavor to another.

As we added more frequencies of matter density fluctuations, the neutrino flavor conversions becomes nontrivial due to the interferences between the difference matter profile frequencies. To quantify the interference between different Rabi oscillation modes, we defined relative detuning which describes how off-resonance a Rabi oscillation is. In the case of single frequency Rabi oscillations, the relative detuning becomes 0 under the resonance condition. As a second frequency is added to the oscillations, the energy gap is shifted due to this new frequency. A measure of the interference effect is to consider the relative detuning of the first frequency which is at resonance, under the shifted energy gap. Numerical results verified this conjecture. With the interference mechanism, we revisit the single frequency matter profile neutrino oscillations.

Another view is to switch to a basis where the neutrino oscillations Hamiltonian is decomposed into infinite Rabi oscillations. Equivalently speaking, the oscillations are consequences of superposition of Rabi oscillations, which we call modes of oscillations. This view was applied to emphasis the approximations that the change of energy gap due to matter fluctuation can be neglected under resonance condition in the previous background matter basis.

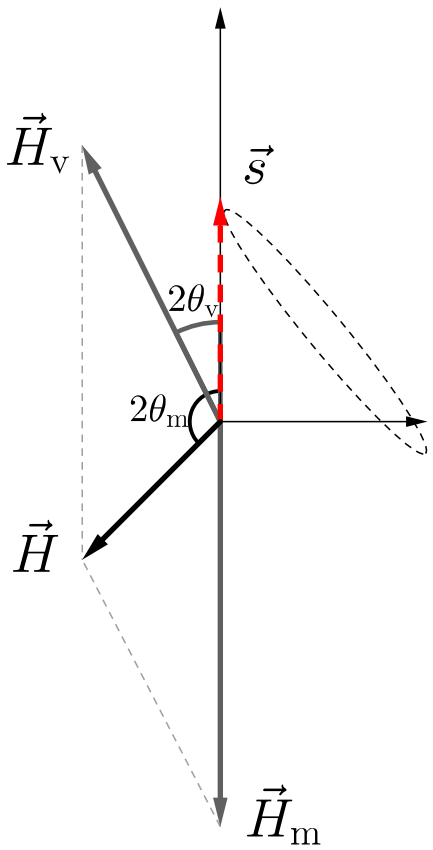


Figure 3.4: Neutrino oscillations in flavor isospin picture, with the presence of matter potential. The flavor isospin is denoted as red dashed arrow. It starts from electron flavor. The two gray vectors stand for the Hamiltonians of vacuum $\vec{H}_{\rm v}$ and matter $\vec{H}_{\rm m}$.

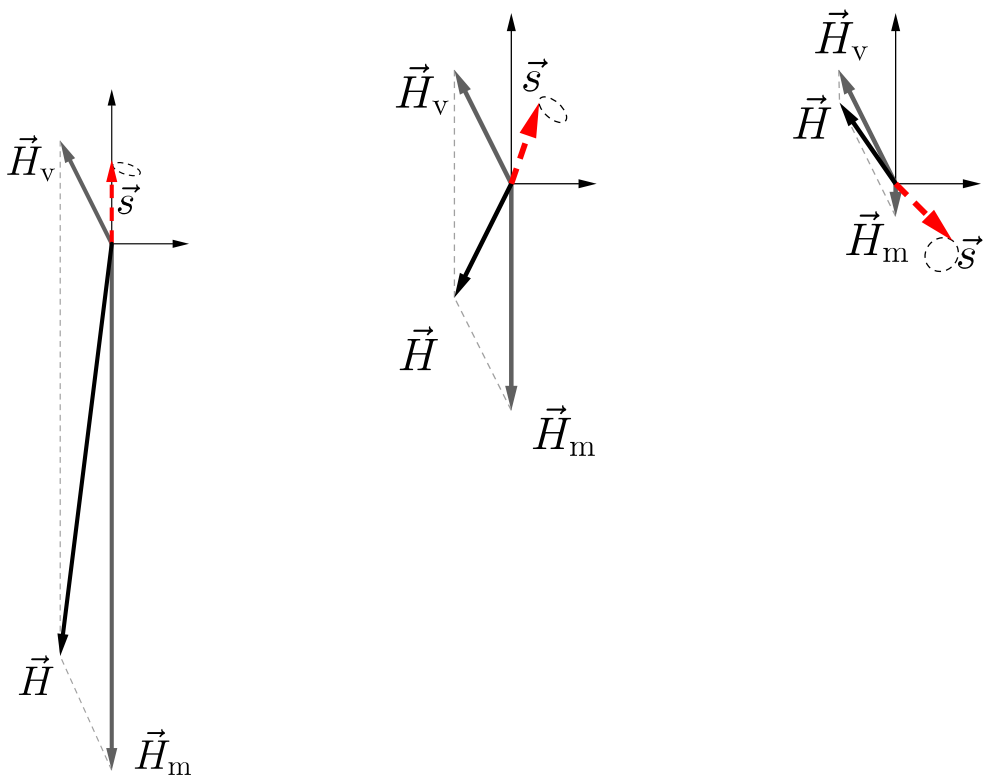


(a) High matter density (b) Medium matter density (c) Low matter density

Figure 3.5: Flavor isospin picture of neutrino oscillations in matter. $\vec{H}_{\rm v}$ is the vacuum contribution to Hamiltonian, and $\vec{H}_{\rm m}$ corresponds to the matter potential.

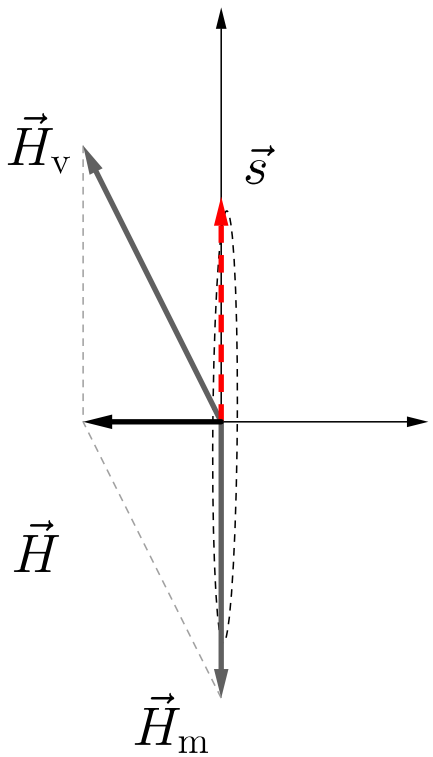


Figure 3.6: MSW resonance happens when electron neutrinos go through a critical matter density.

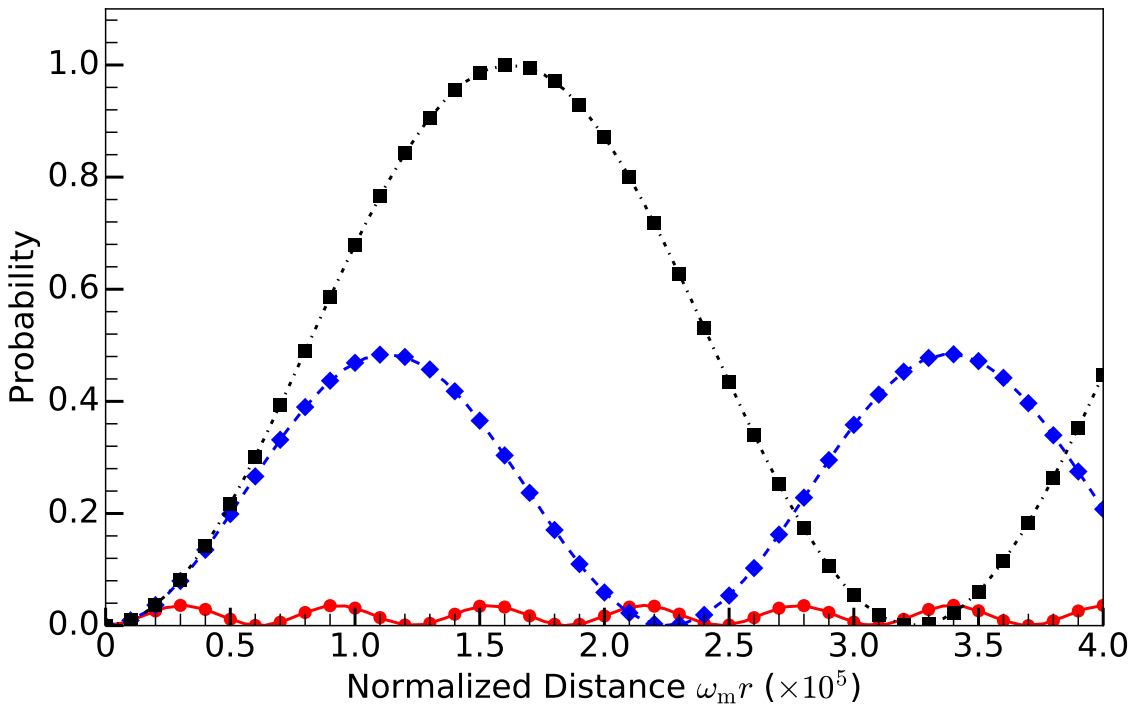


Figure 3.7: Single frequency matter profile and Rabi oscillation. The markers are numerical results for the transition probabilities between two background mass eigenstates for the neutrinos with matter perturbation $A_1 \sin(k_1 r)$. The dots, diamonds, and squares are for $k_1 = \omega_m$, $k_1 = (1 - 2 \times 10^{-5})\omega_m$, and $k_1 = (1 - 10^{-4})\omega_m$ respectively. The lines are the predictions using Rabi formula. During the calculation, $\lambda_0$ is set to 0.5 of the MSW resonance potential $\lambda_{MSW} = \omega_v \cos 2\theta_v$ and mixing angle is chosen so that $\sin^2(2\theta_v) = 0.093$.

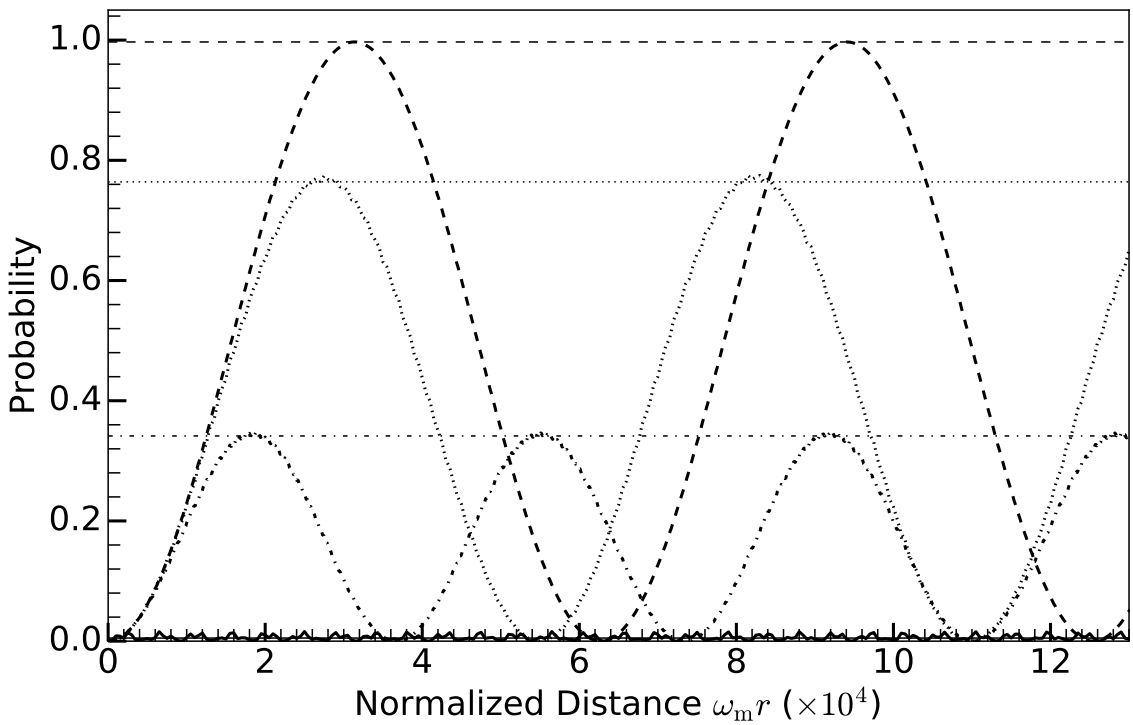


Figure 3.8: Reduction of transition amplitudes due to interference. Dashed line, dotted line, dash-dotted line, and solid line are for $A_2 = 10^{-2}\omega_{\rm m}$, $k_2 = 10\omega_{\rm m}$, $A_2 = 10^{-2}\omega_{\rm m}$, $k_2 = 10^{-1}\omega_{\rm m}$, $A_2 = 5.0 \times 10^{-2}\omega_{\rm m}$, $k_2 = 10\omega_{\rm m}$, and $A_2 = 5 \times 10^{-2}\omega_{\rm m}$, $k_2 = 10^{-1}\omega_{\rm m}$. In all the calculations, we choose $A_1 = 10^{-4}\omega_{\rm m}$, $k_1 = \omega_{\rm m}$. The grid lines are the transition amplitudes estimated using $D'$. During the calculation, $\Lambda_0$ is set to half of the MSW resonance potential, $\Lambda_0 = \frac{1}{2}\lambda_{\rm MSW} = \frac{1}{2}\omega_{\rm v} \cos 2\theta_{\rm v}$.

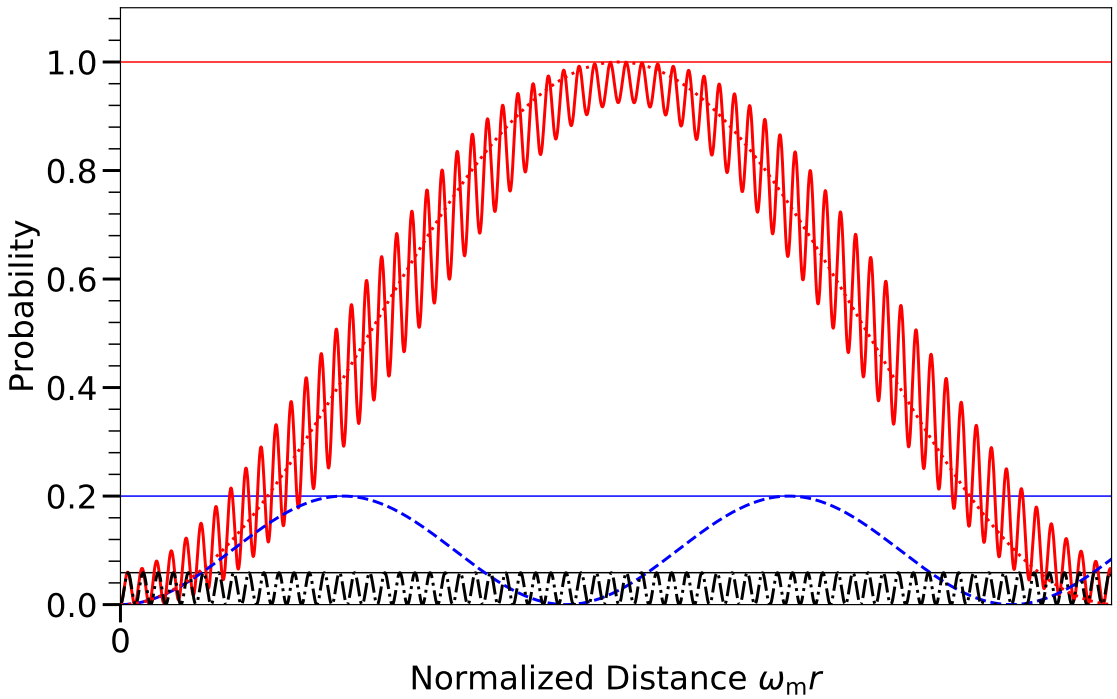


Figure 3.9: Constructive interference for two frequencies in matter density profile. The solid red line, dashed blue line, dash-dotted black line, are the transition probability for two frequencies combined, the first frequency $k_1$ only, the second frequency $k_2$ only. The amplitudes of each frequency are $A_1 = 0.4$, $A_2 = 2.6$ respectively. The grid lines are the oscillations amplitudes predicted by Rabi formula. The dotted red line is the oscillations predicted by Rabi formula for the two combined frequencies.

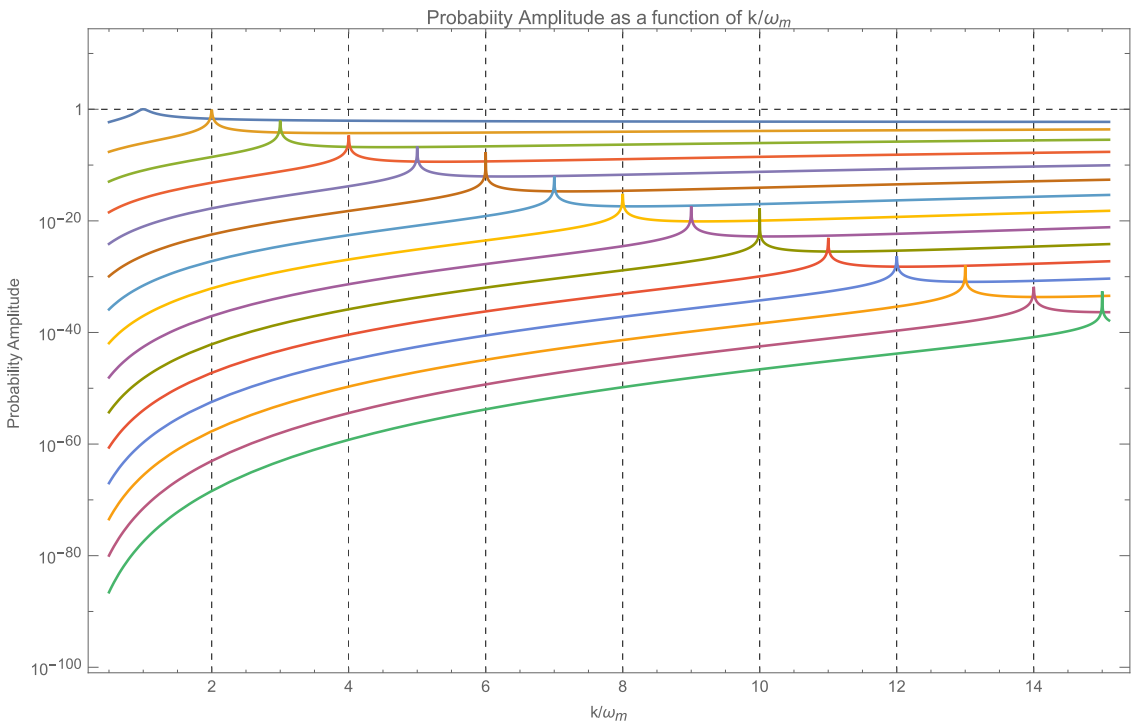


Figure 3.10: Probability amplitude as a function of $k/\omega_{\mathrm{m}}$ for each term in Jacobi-Anger expansion, with parameters $\lambda_1 = 0.1$,$\theta_{\mathrm{m}} = \pi/5$.

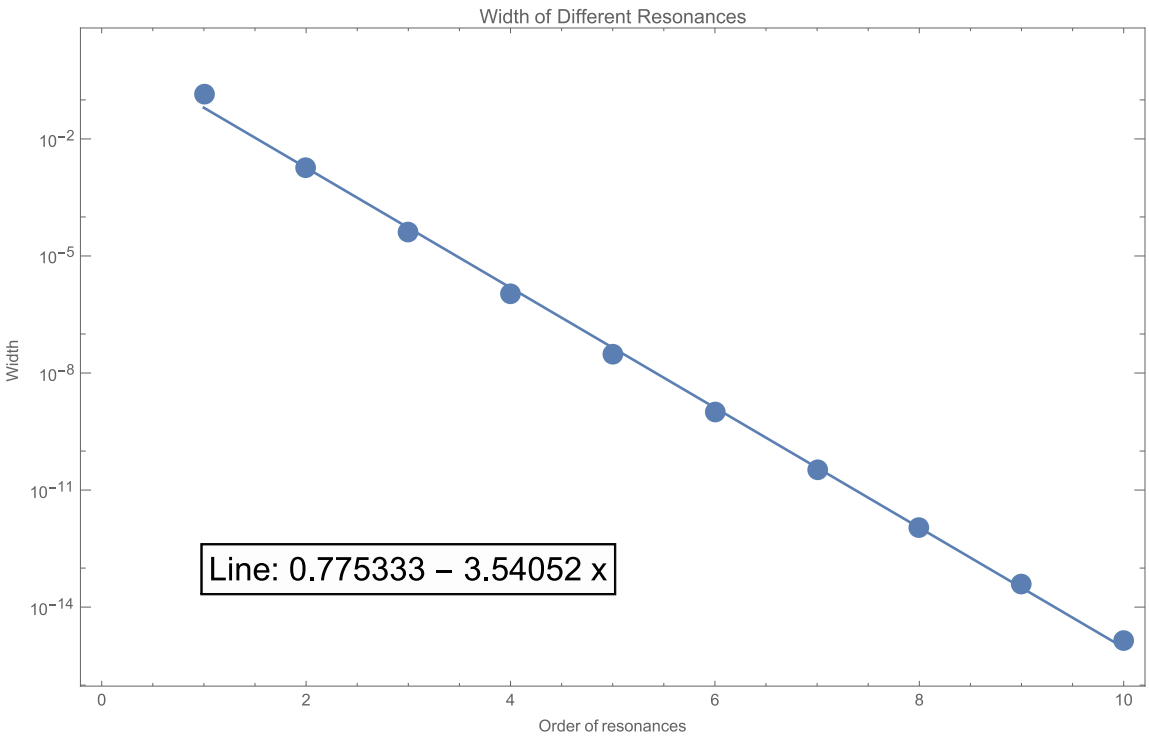


Figure 3.11: Resonance width as a function of mode order for each term in Jacobi-Anger expansion, with parameters $\lambda_1 = 0.1$,$\theta_{\rm m} = \pi/5$.

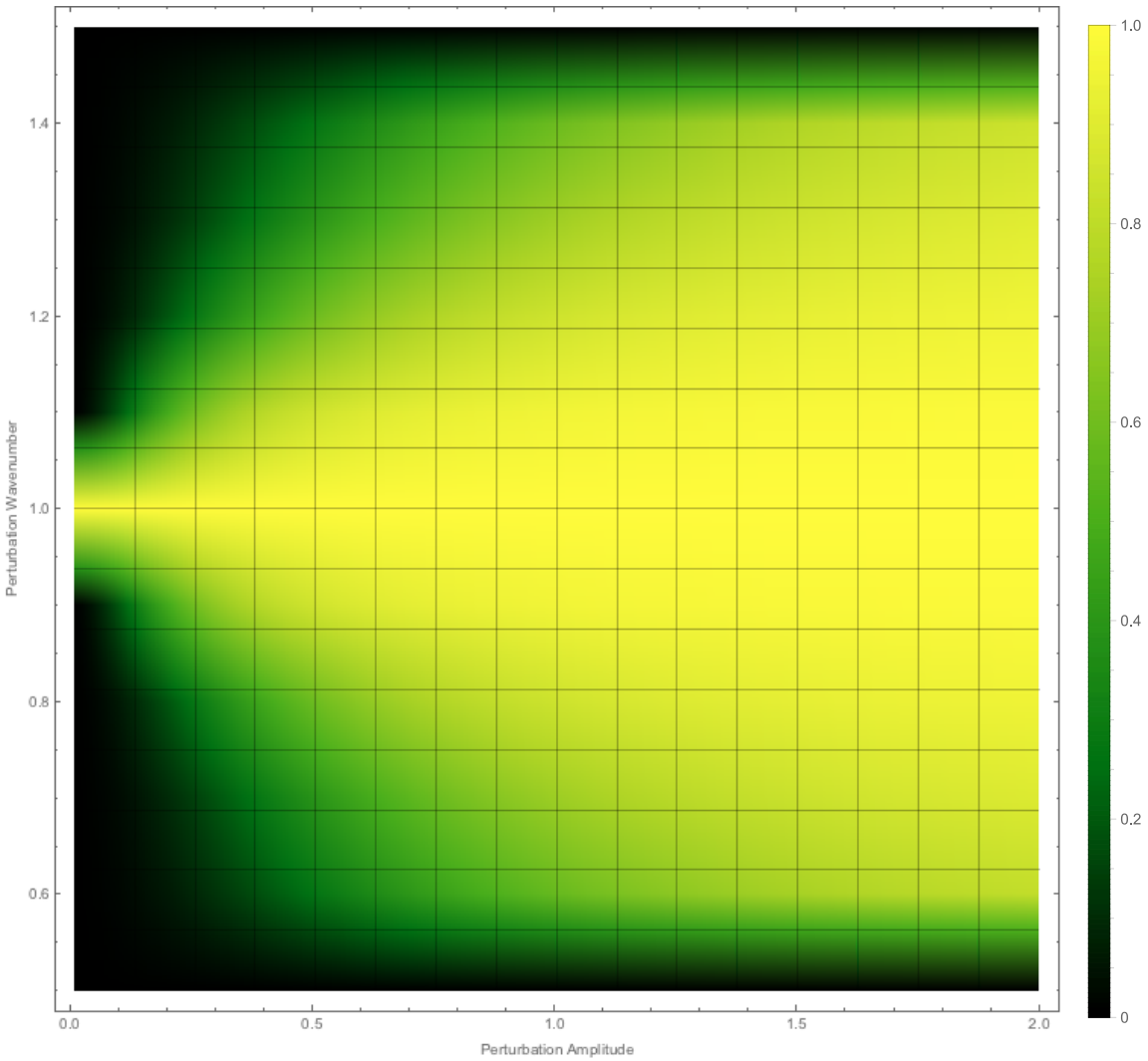


Figure 3.12: Transition probability amplitude at different perturbation amplitude and perturbation wavenumber. Larger amplitudes corresponds to larger resonance width, as another confirmation to Fig. 3.11.

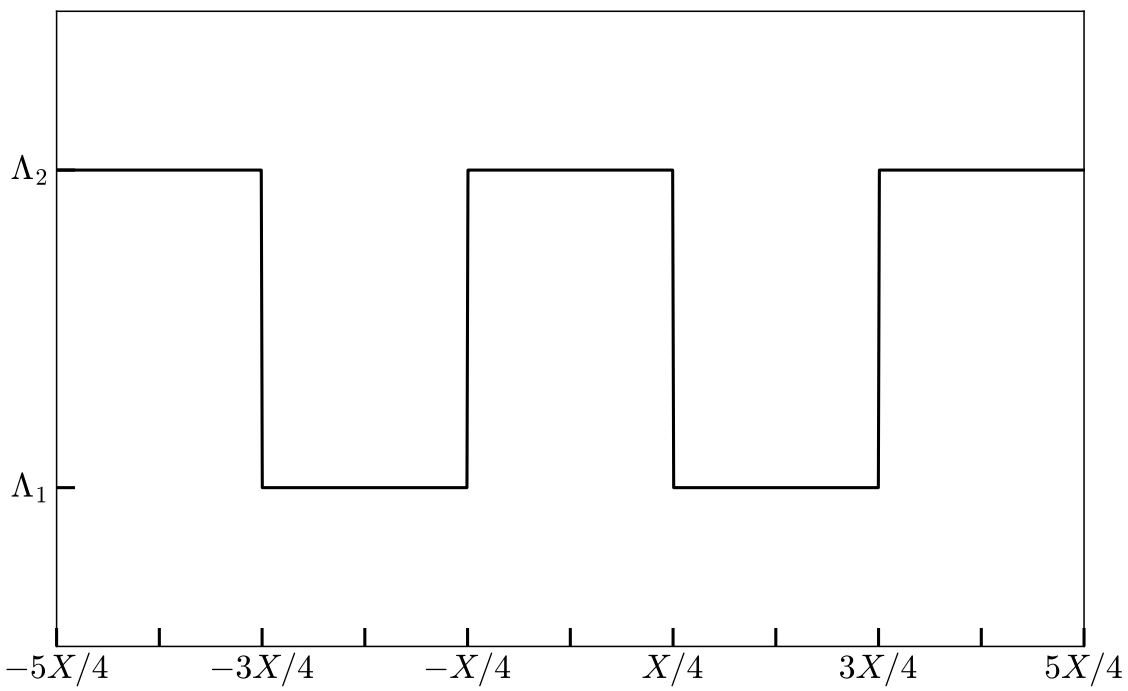


Figure 3.13: The castle wall matter potential profile with $X_1 = X_2 = X/2$.

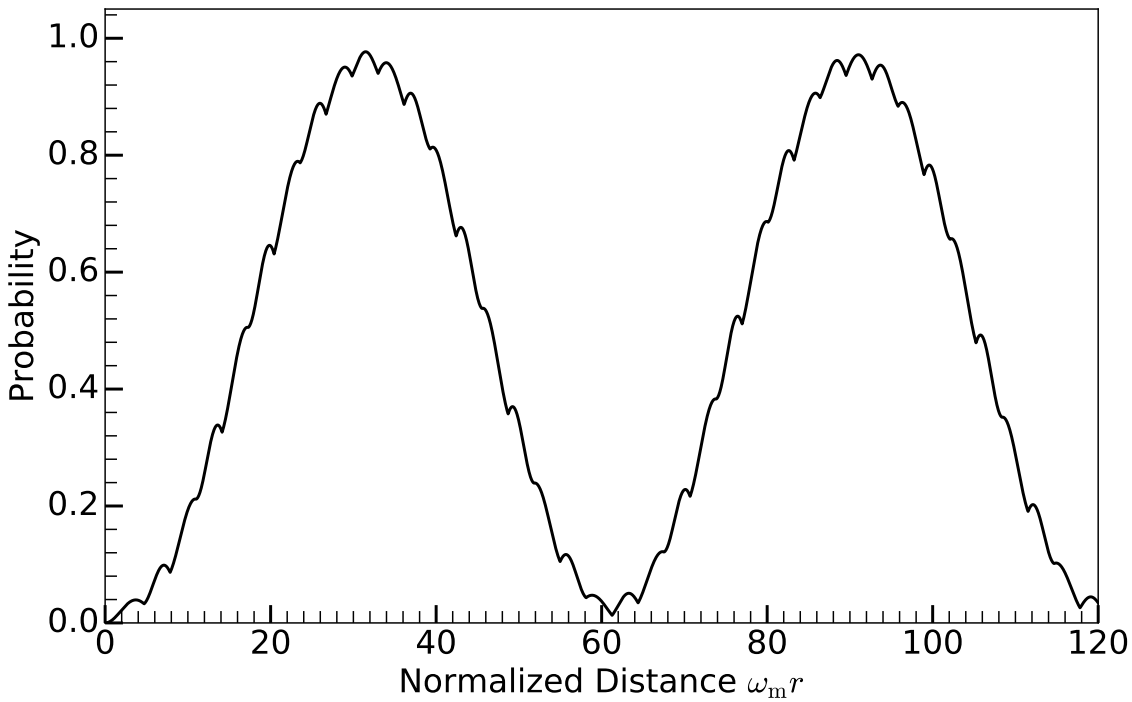


Figure 3.14: Transition probabilities for castle wall matter profile calculated numerically for $\Lambda_2 - \Lambda_1 = 0.4\Lambda_0$. During the calculation, the energy of neutrinos is 10 MeV, mass-squared difference is $\delta m^2 = 2.6 \times 10^{-3}\,\mathrm{eV}^2$, and the vacuum mixing angle chosen so that $\sin^2(2\theta_v) = 0.093$. The background potential $\Lambda_0$ is chosen so that it's half the MSW resonance potential, $\Lambda_0 = \frac{1}{2}\lambda_{\rm MSW} = \frac{1}{2}\omega_{\rm v}\cos 2\theta_{\rm v}$, and the base frequency is set to $k_0 = 2\pi/X = \omega_{\rm m}$.

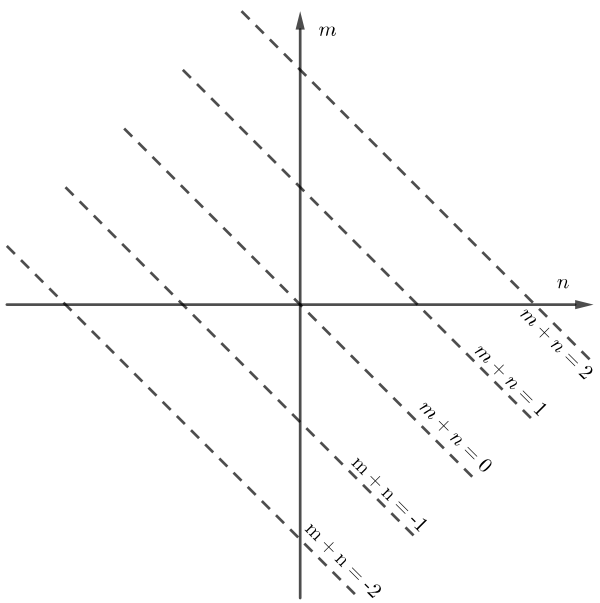


Figure 3.15: Rewrite multiplication of summations into summations only. The horizontal axis is for the summation index $n$ and the vertical axis is for the summation index $m$. The dashed lines are the lines of equal $m + n$.

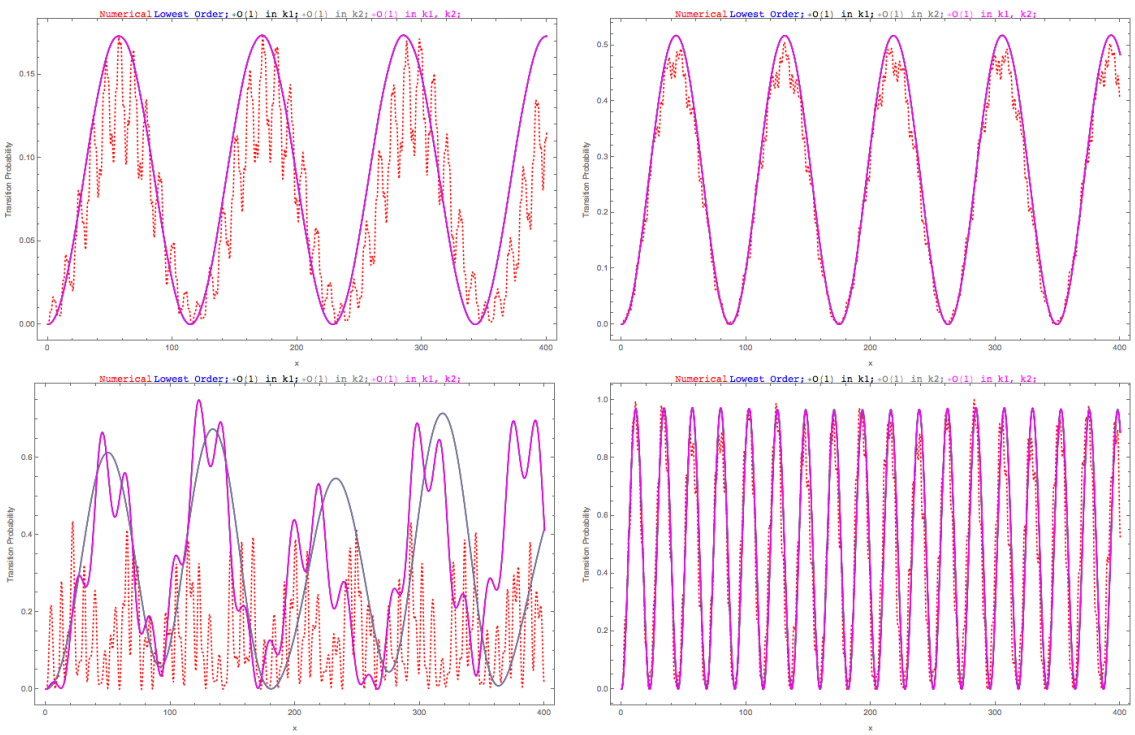


Figure 3.16: Top Left: Smaller wavenumber $k_1 = 0.95$ is at resonance and it has smaller perturbation amplitude ($k_2 = 1.55$); Top Right: Smaller wavenumber $k_1 = 0.95$ is at resonance and it has larger perturbation amplitude ($k_2 = 1.55$); Bottom Left: Larger wavenumber $k_2 = 0.95$ is at resonance and it has smaller perturbation amplitude ($k_1 = 0.35$); Bottom Right: Larger wavenumber $k_2 = 0.95$ is at resonance and it has larger perturbation amplitude ($k_1 = 0.35$). Red dotted line is numerical solution, black line is lowest approximation of $k_2$, magenta is higher order approximation of $k_2$.

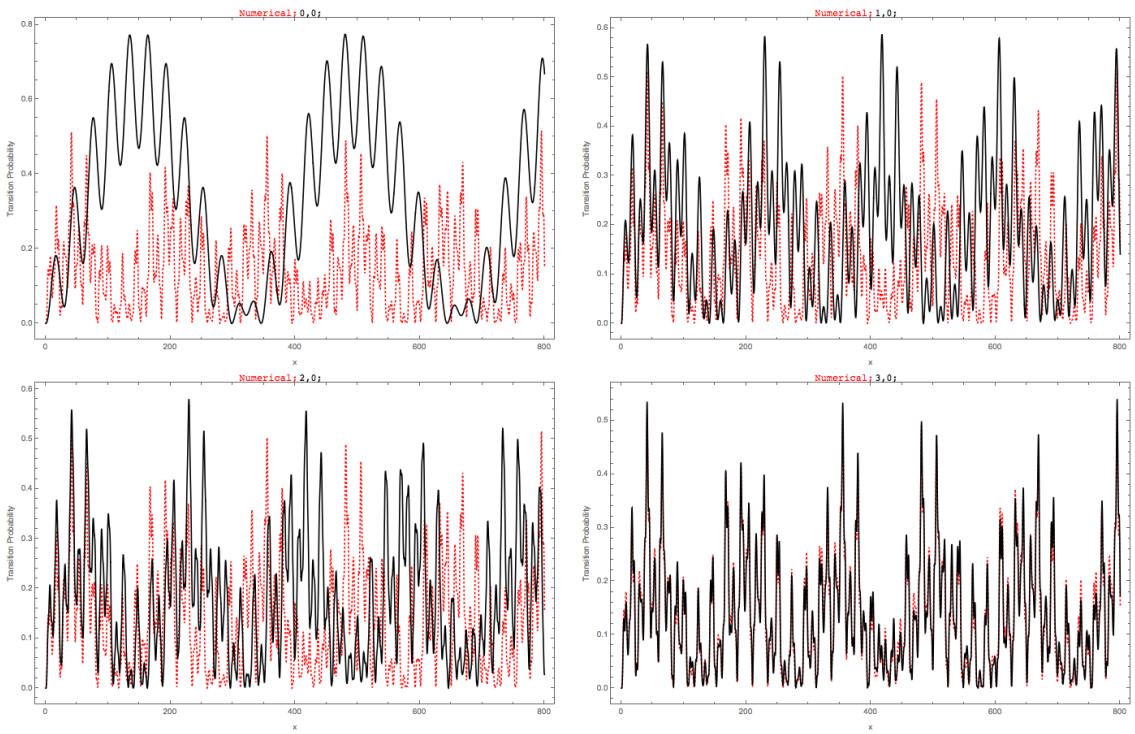


Figure 3.17: Compare the different orders with the numerical calculation without approximations, where red dotted line is the numerical calculation without approximation. As we could see from the figure, including up to third order in $n_1$ fixes the deviation from numerical calculation (red dotted line). The wave vectors are $k_1 = 0.5$, $k_2 = 0.8$, amplitudes are $A_1 = 0.1k_1^{-5/3}$, $A_2 = 0.1k_2^{-5/3}$, mixing angle in background matter is $\theta_m = \pi/5$.

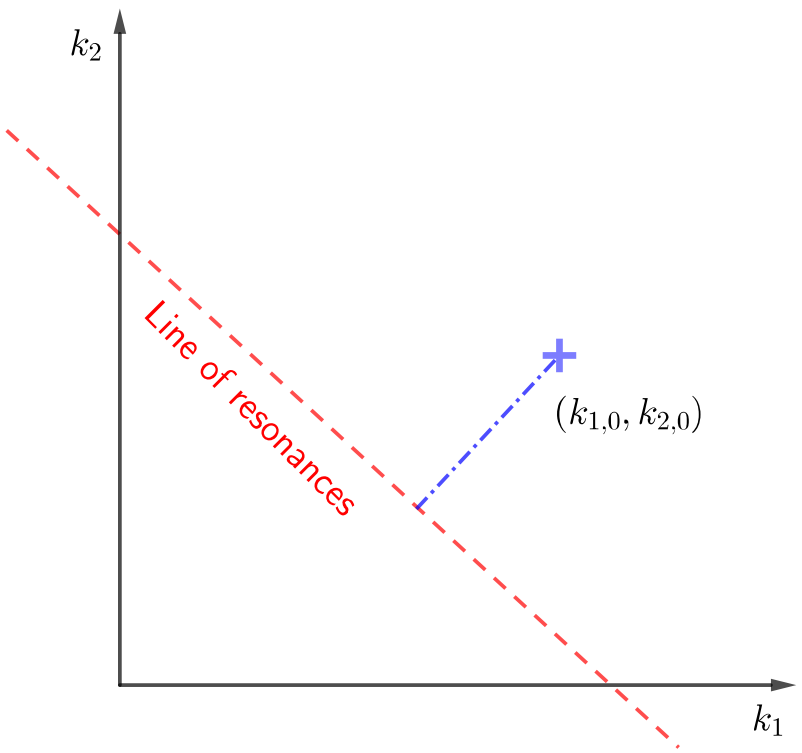


Figure 3.18: Diagram of Width for two frequencies in matter density profile. The red dashed line is the line when the resonances happen. The cross is the location for a system that with two frequencies in density profile, $k_{1,0}$ and $k_{2,0}$. The blue dash dotted line indicates the distance between the actual frequencies of the system and the resonances.

# Chapter 4

# Collective Neutrino Oscillations and Dispersion Relations

Neutrino oscillations in matter background is well defined linear dynamics as we discussed in the preceding chapters. However, the universe provides many other much more exciting labs for neutrino physics. One of such is early supernova explosions, where approximately $10^{58}$ neutrinos are released within seconds [8]. Such neutrino density would introduce new interaction terms into neutrino oscillations, the self-interaction potential $H_{\nu\nu}$ is comparable or even larger than the matter potential, depending on the region of interest in supernova explosions [4]. Thus self-interaction between neutrinos is not negligible. Meanwhile, unexpected rich dynamics has be proved to be present with the self-interactions [30, 24]. The fact that self-interaction introduces a new characteristic energy scale, new resonances such as matter-neutrino resonance is also possible [38, 43, 48].

In this chapter, I will review the fast modes in neutrino collective oscillations, and clarify the connection between fast modes and dispersion relation proposed by I. Izaguirre et al [50].

## 4.1 Collective Oscillations

### 4.1.1 Equation of Motion

The equation of motion for neutrino oscillations with self-interaction was first derived in [11]. For the purpose of the thesis, I will skip the quantum field theory derivations but write it down and clarify some conventions. Without much effort, we know that the equation of motion is the Liouville's equation

$$i\frac{d}{dt}\rho = [H, \rho]. \tag{4.1}$$

For the purpose of neutrino oscillations, we always assume they travel with speed of light thus

$$\frac{d}{dt} = \frac{d}{dr}, \tag{4.2}$$

where $r$ is the distance travelled by the neutrino. However, in general, what we should have is

$$\frac{d}{dt} = \partial_t + \mathbf{v}\cdot\boldsymbol{\nabla}. \tag{4.3}$$

The Hamiltonian is composed of three different terms,

$$H = H_{\rm v} + H_{\rm m} + H_{\nu\nu}, \tag{4.4}$$

where each term is explicitly written down

$$H_v = -\frac{1}{2}\beta\eta\omega_0\sigma_3 \tag{4.5}$$

$$H_m = \frac{1}{2}\sqrt{2}G_F n_e \sigma_3 \tag{4.6}$$

$$H_{\nu\nu} = \sqrt{2}G_F \int d\omega d\Omega_{\hat{v}'} n(\omega, \hat{v}')\beta(\hat{v}')\rho(\omega, \hat{v}')(1 - \hat{v}\cdot\hat{v}'). \tag{4.7}$$

I use $\eta = \pm 1$ for Normal Hierarchy and Inverted Hierarchy respectively, $\beta = 1$ for neutrinos and $\beta = -1$ for antineutrinos. In other words, the vacuum frequency is $\omega_v = \eta\omega_0$. $\beta(\hat{v}')$ indicates whether the density matrix $\rho(\omega, \hat{v}')$ is for neutrinos or

antineutrinos. If $\rho(\omega, \hat{v}')$ is for antineutrinos, $\beta(\hat{v}') = -1$, otherwise $\beta(\hat{v}') = 1$. More explicitly, the vacuum term is

$$H_v = \begin{cases} -\frac{1}{2}\eta\omega_0\sigma_3 & \text{for neutrinos} \\ \frac{1}{2}\eta\omega_0\sigma_3 & \text{for antineutrinos} \end{cases}$$

while the neutrino-neutrino interaction Hamiltonian is

$$H_{\nu\nu} = \begin{cases} \sqrt{2}G_F \int d\omega d\Omega_{\hat{v}'} n(\omega, \hat{v}')\rho(\omega, \hat{v}')(1 - \hat{v}\cdot\hat{v}') & \text{interacting with neutrinos} \\ -\sqrt{2}G_F \int d\omega d\Omega_{\hat{v}'} n(\omega, \hat{v}')\bar{\rho}(\omega, \hat{v}')(1 - \hat{v}\cdot\hat{v}') & \text{interacting with antineutrinos} \end{cases}$$

Please note that in this notion,

- $\omega_0$ is meant to be the absolute value of the frequency, since $\eta$ takes care of the signs;
- The integral in $H_{\nu\nu}$ must take care of both interactions with neutrinos and anti-neutrinos.

For simplicity, we define some new quantities.

- We define $\lambda$ to measure the matter interactions

$$\lambda = \sqrt{2}G_F n_e. \tag{4.8}$$

- Angle distribution of number density is defined as

$$f(\hat{v}) = \frac{n(\omega, \hat{v})}{n_{\mathrm{t}}}, \tag{4.9}$$

  where $n_{total}$ is the total number density of neutrinos for all energies. It can also be defined for anti-neutrinos

$$\bar{f}(\hat{v}) = \frac{\bar{n}(\omega, \hat{v})}{\bar{n}_{\mathrm{t}}}, \tag{4.10}$$

where $\bar{n}_{\rm t}$ is the total number density of antineutrinos. In models where neutrinos are emitted from a line, the direction of momentum $\hat{v}$ depends on one angle, hence $f(\theta)$. With this definition, we know that the number density of neutrinos within an angle $[\theta, \theta + d\theta]$ can be calculated

$$n_{\rm t} f(\theta) d\theta. \tag{4.11}$$

Similarly, the the number density of antineutrinos within angle $[\theta, \theta + d\theta]$ is

$$\bar{n}_{\rm t} \bar{f}(\theta) d\theta. \tag{4.12}$$

- An asymmetry parameter can be defined to connect the total number density of neutrinos and antineutrinos,

$$\alpha = \frac{\bar{n}_{\rm t}}{n_{\rm t}}. \tag{4.13}$$

With the three definitions we simplify the neutrino self-interactions with matter effect

$$\begin{aligned} H_m =& \frac{1}{2}\lambda\sigma_3 \\ H_{\nu\nu} =& \sqrt{2} G_F n_{\rm t} \int d\omega d\Omega_{\hat{v}'} f(\omega, \hat{v}) \rho(\omega, \hat{v}') (1 - \hat{v} \cdot \hat{v}') \\ & - \sqrt{2} G_F \bar{n}_{\rm t} \int d\omega d\Omega_{\hat{v}'} \bar{f}(\omega, \hat{v}) \bar{\rho}(\omega, \hat{v}') (1 - \hat{v} \cdot \hat{v}') \\ =& \frac{1}{2}\mu \int d\omega d\Omega_{\hat{v}'} f(\omega, \hat{v}) \rho(\omega, \hat{v}') (1 - \hat{v} \cdot \hat{v}') \\ & - \frac{1}{2}\alpha\mu \int d\omega d\Omega_{\hat{v}'} \bar{f}(\omega, \hat{v}) \bar{\rho}(\omega, \hat{v}') (1 - \hat{v} \cdot \hat{v}'), \end{aligned}$$

where

$$\mu = 2\sqrt{2} G_F n_{\rm t}. \tag{4.14}$$

### 4.1.2 Synchronization in Neutrino Oscillations

With the equation of motion, many aspects of such a system has been explored, such as neutrino bulb model, line model, etc. New dynamics, such as spectral split,

synchronizations, matter-neutrino resonances, have been identified [24, 38, 43]. Synchronization is one of the most astonishing results which might happen when neutrino number density is high. In this section, I will explain how this is possible.

To grab the flavor of this phenomenon, I use the flavor isospin picture. Flavor isospin was explained in Sec. 2.1. Here we explain another definition of it

$$\rho = 1 + \frac{1}{2}\vec{P}\cdot\vec{\sigma}. \tag{4.15}$$

For antineutrinos, the flavor isospin is defined as

$$\bar{\rho} = 1 - \frac{1}{2}\vec{P}\cdot\vec{\sigma}. \tag{4.16}$$

The reason for the negative sign is that we usually reformulate the formula for antineutrinos and define the anti-neutrinos to have negative frequency.

With flavor isospin defined, to derive an equation for flavor isospin, we need to decompose the Hamiltonian into vectors. The vacuum and matter part is easy. It's straight forward to write down the vacuum part and matter part of Hamiltonian using three dimensional vectors in flavor isospin space,

$$\vec{H}_{\rm v} = \omega_{\rm v}\begin{pmatrix} -\sin 2\theta_{\rm v} \\ 0 \\ \cos 2\theta_{\rm v} \end{pmatrix}$$

$$\vec{H}_{\rm m} = \begin{pmatrix} 0 \\ 0 \\ -\lambda \end{pmatrix}$$

But the neutrino coherent scattering term requires some simplifications. For the purpose of the physics picture, we consider isotropic and homogeneous model which leads to

$$\sqrt{2}G_{\rm F}n_\nu \int d\vec{p}'^3(1-\vec{p}\cdot\vec{p}')(\rho_{\vec{p}'}-\bar{\rho}_{\vec{p}'}) = \sqrt{2}G_{\rm F}n_\nu \int dE'\frac{1}{n_\nu}(\rho_{E'}-\bar{\rho}_{E'}). \tag{4.17}$$

We have to define a vector, which is an integral of polarization vector over all energies or frequencies,

$$\vec{D} = \int d\omega' \vec{P}(\omega'). \tag{4.18}$$

Expression 4.17 becomes $\mu\vec{D}$, where $\mu = \sqrt{2}G_{\rm F}n_{\nu}$.

For single energy or flavor isospins aligned in the same direction, this vector is in the direction of flavor isospin vector. If flavor isospins were initially prepared in completely random and uniformly distributed directions, $\vec{D} \sim 0$.

Synchronization occurs when the neutrino number density becomes large. $\vec{D}$ will wobble around very fast due to the precessions of flavor isospins, but almost stays in one direction. All the spins precess with the same frequency which is determined by $\mu$.

With vacuum contribution $\vec{H}_{\rm v}$ and matter contribution $\vec{H}_{\rm m}$ to the Hamiltonian, we expect $\vec{D}$ to precess around $\vec{H}_{\rm v} + H_{\rm v}$, if the precession frequency of flavor isospins around $\vec{D}$ is much larger than the precession frequency of $\vec{D}$ around $\vec{H}_{\rm v} + H_{\rm v}$.

## 4.2 Two Beams Model and Linear Stability Analysis

For nonlinear systems, linear stability analysis comes into play. I will go through the procedure and demonstrate the significance of instabilities and crossing in spectrum. For the sole purpose, I use a simple two-beam line model. The two beams model is simple mathematically, meanwhile reveals the key insights.

In this model, neutrinos are emitted in two different directions from a line which preserves translation symmetry on this line. The emission angles are shown in

Fig. 4.1. For convenience of notations, I define a number density distribution function

$$f(\hat{v},\omega) = \frac{n(\hat{v},\omega)}{n_t}, \tag{4.19}$$

where $n_t$ is the total number density of all neutrino emitted, $n(\hat{v},\omega)$ is the number density with momentum direction $\hat{v}$ and energy $\omega$. We also define

$$\mu = \sqrt{2}G_F n_t. \tag{4.20}$$

For two dimensional systems, we can calculate the neutrinos within an angle $[\theta, \theta+d\theta]$

$$n_t f(\hat{v},\omega)d\theta. \tag{4.21}$$

Similarly we can define the angular distribution for antineutrinos.

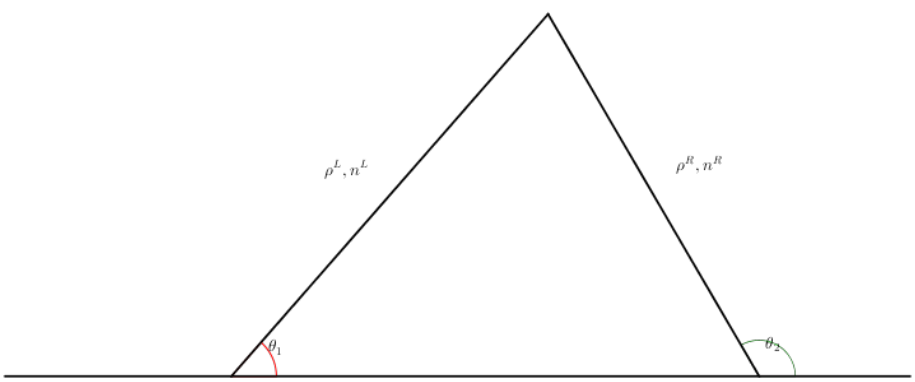


Figure 4.1: Geometry of two-beam model to be used in this section. Two neutrino beams are emitted, the states of which are denoted as $\rho^L$ and $\rho^R$, with number densities $n^L$ and $n^R$ respectively. The emission angles are shown in the figure as $\theta_2$ and $\theta_1$ respectively.

If all the beams are neutrinos, but with different energies for the left and right beams. The distribution function for beams is delta function. In fact, each beam is just half of the total neutrino number density $n_t$.

The Hamiltonian is a sum of vacuum terms, matter terms, and self-interaction terms,

$$H = H_v + H_m + H_{\nu\nu}, \tag{4.22}$$

where

$$H_v = -\eta\frac{1}{2}\omega\sigma_3 \tag{4.23}$$

$$H_m = \frac{1}{2}\lambda\sigma_3 \tag{4.24}$$

$$H^L_{\nu\nu} = \frac{1}{2}\mu^R\rho^R(1-\cos(\theta_1-\theta_2)) \tag{4.25}$$

$$H^R_{\nu\nu} = \frac{1}{2}\mu^L\rho^L(1-\cos(\theta_1-\theta_2)). \tag{4.26}$$

To linearize the equation of motion, we define the perturbed density matrix as

$$\rho = \frac{1}{2}\begin{pmatrix} 1 & \epsilon \\ \epsilon^* & -1 \end{pmatrix}, \tag{4.27}$$

where we have removed the trace part because it is alway time independent.

The linearized equation of motion becomes

$$i\partial_z\begin{pmatrix}\epsilon_1\\ \epsilon_2\end{pmatrix} = -i\begin{pmatrix}\cot\theta_1\partial_x & 0\\ 0 & \cot\theta_2\partial_x\end{pmatrix}\begin{pmatrix}\epsilon_1\\ \epsilon_2\end{pmatrix} + \frac{1}{2}\begin{pmatrix}(\lambda+\mu_2-\eta\omega_1-\mu_2\cos(\theta_1-\theta_2))/\sin\theta_1 & -\mu_2(1-\cos(\theta_1-\theta_2))/\sin\theta_1\\ -\mu_1(1-\cos(\theta_1-\theta_2))/\sin\theta_2 & (\lambda+\mu_1-\eta\omega_2-\mu_1\cos(\theta_1-\theta_2))/\sin\theta_2\end{pmatrix}\begin{pmatrix}\epsilon_1\\ \epsilon_2\end{pmatrix}, \tag{4.28}$$

where

$$\mu_1 = \sqrt{2}G_F n_{t,1}$$

$$\mu_2 = \sqrt{2}G_F n_{t,2}.$$

### 4.2.1 Left-right Symmetric Emission

We first consider a simple case, where $\theta_1 = \theta_2 \equiv \theta$, $\lambda = 0$, $\eta = 1$, and homogeneous in $x$ direction. For simplicity we define

$$\begin{aligned}\mu =& \sqrt{2} G_F (n_1 + n_2) \\ \mu_i =& \mu \frac{n_i}{n_1 + n_2} \equiv \mu f_i \\ \xi =& 1 - \cos(\theta_1 - \theta_2) \\ \omega_i' =& \lambda - \eta \omega_i .\end{aligned}$$

I am aware that this is not a self-consistent example since $\theta_1 = \theta_2$ indicates that $\xi = 0$. As we will see, no instability is present in this case. However, we keep the term $\xi$ because we need to analyze the effect of symmetry breaking. This example builds up a formalism.

The equation for perturbations becomes

$$i\partial_z \begin{pmatrix} \epsilon_1 \\ \epsilon_2 \end{pmatrix} = \frac{1}{2\sin\theta} \begin{pmatrix} \omega_1' + \mu f_2 \xi & -\mu f_2 \xi \\ -\mu f_1 \xi & \omega_2' + \mu f_1 \xi \end{pmatrix} \begin{pmatrix} \epsilon_1 \\ \epsilon_2 \end{pmatrix}. \tag{4.29}$$

Since $\mu$ is the most important energy scale in this problem, we scale all energies with it.

$$i\partial_{\hat{z}} \begin{pmatrix} \epsilon_1 \\ \epsilon_2 \end{pmatrix} = \frac{1}{2\sin\theta} \begin{pmatrix} \hat{\omega}_1' + f_2 \xi & -f_2 \xi \\ -f_1 \xi & \hat{\omega}_2' + f_1 \xi \end{pmatrix} \begin{pmatrix} \epsilon_1 \\ \epsilon_2 \end{pmatrix}, \tag{4.30}$$

where

$$\begin{aligned}\partial_{\hat{z}} =& \frac{d}{\mu dz} \\ \hat{\omega}_i' =& \frac{\omega_i'}{\mu}.\end{aligned}$$

The characteristic equation for this equation is

$$\left( (\Omega - \hat{\omega}_1' - f_2 \xi)(\Omega - \hat{\omega}_2' - f_1 \xi) - f_1 f_2 \xi^2 \right) = 0, \tag{4.31}$$

which is simplified to

$$(\Omega - \Omega_1)(\Omega - \Omega_2) - f_1 f_2 \xi^2 = 0,$$

where

$$\begin{aligned}\Omega_1 =& \hat{\omega}_1' + f_2 \xi \\ \Omega_2 =& \hat{\omega}_2' + f_1 \xi.\end{aligned}$$

Complete the square

$$(\Omega - (\Omega_1 + \Omega_2)/2)^2 = \frac{1}{4}(\Omega_1 - \Omega_2) + f_1 f_2 \xi^2.$$

The solution becomes

$$\Omega = \frac{1}{2}(\Omega_1 + \Omega_2) \pm \sqrt{(\Omega_1 - \Omega_2)^2/4 + f_1 f_2 \xi^2}. \tag{4.32}$$

The condition to have positive imaginary part is

$$(\Omega_1 - \Omega_2)^2 + 4 f_1 f_2 \xi^2 < 0,$$

or

$$-2\sqrt{-f_1 f_2 \xi^2} < \Omega_1 - \Omega_2 < 2\sqrt{-f_1 f_2 \xi^2},$$

and $f_1 f_2 \xi^2 < 0$. Recall the meaning of $f_i$,

$$f_i = \frac{n_i}{n_1 + n_2},$$

instability requires that we have a spectrum crossing, i.e., $n_1$ and $n_2$ have different signs. Plug in the definitions of $\Omega_i$,

$$-2\sqrt{-f_1 f_2 \xi^2} < \eta(-\omega_1 + \omega_2)/\mu + (f_2 - f_1)\xi < 2\sqrt{-f_1 f_2 \xi^2}.$$

From this we can infer

- $f_1 f_2$ has to be negative, which means we can NOT have instabilities with only neutrinos or antineutrinos with all the symmetries we assumed. This is crossing.

- $-\omega_1 + \omega_2 = 0$ will remove the instability. So we have to have both neutrinos and antineutrinos.
- $f_2 - f_1$, $\eta(\omega_2 - \omega_1)$, and $\mu$ set limit on each other.
- $\theta_1 = \theta_2 \equiv \theta$ removes the instability since it leads to $\xi = 0$. The emission has to be asymmetric in this simple two beams model. This is trivial since equal emission angle means the beams are not colliding.

Another way of understanding this equation is to think of it as the growth of the length of the vector $\vec{v} = (\epsilon_1, \epsilon_2)^T$. For an arbitrary matrix differential equation of the form

$$\partial_z \mathbf{v} = \mathbf{A}\mathbf{v},$$

we can always decompose the matrix $\mathbf{A}$ into symmetric part and skew-symmetric part

$$\mathbf{A} = \frac{1}{2}(\mathbf{A} + \mathbf{A}^T) + \frac{1}{2}(\mathbf{A} - \mathbf{A}^T) \equiv \mathbf{A}^+ + \mathbf{A}^-.$$

We can identify the effect of $f_1 - f_2$ but this is not particularly useful since we can not say anything about the eigenvalues of matrix $\mathbf{A}$ from the eigenvalues of matrix $\mathbf{A}^+$ and $\mathbf{A}^-$.

### 4.2.2 Breaking Symmetries

For a line model, the symmetries we have are

- Time translation symmetry;
- Translation symmetry along the line;
- Energy spectrum of the beams; One of particular interest is to have different neutrino spheres for different energies which can be investigated using two beam model.

- Number density of left and right beams;
- Angle of left and right beams;
- With and without matter.
- Similar to the discussion of varying matter potential, symmetries can be broken globally, i.e., distribution as a function of spacetime coordinates.

I will discuss some of the symmetries mentioned above.

**Emission Angle Parity Symmetry**

The emission angles change the value of $\xi = 1 - \cos(\theta_1 - \theta_2)$ as well as rescale the quantities by angle dependent factor $1/\sin\theta_i$.

To see the importance of angles, we can redefine some quantities

$$\begin{aligned}\omega_i'' =& \frac{\omega_i'}{\sin\theta_i} \\ f_1'' =& \frac{f_1}{\sin\theta_2} \\ f_2'' =& \frac{f_2}{\sin\theta_1}.\end{aligned}$$

The we will reach the same characteristic equation as Eqn. 4.31. So the angles serves as shift of energy gap and angular distribution.

The region of instability changes in a convoluted way. Given angles we can always write down the expression and find out.

- The criteria of existence of instability doesn't change.
- The region of instability changes.

### Matter Effect

Including matter will define vacuum frequencies, $\omega_i'$, which is effectively just a shift of vacuum frequencies. In the symmetric emission case, $\omega_1' - \omega_2'$ is independent of matter effect. But breaking the emission symmetry generates the degeneracy,

$$\hat{\omega}_1'' - \hat{\omega}_2'' = (\lambda/\sin\theta_1 - \lambda/\sin\theta_2 + \eta(-\omega_1/\sin\theta_1 + \omega_2/\sin\theta_2))/\mu`. \tag{4.33}$$

We notice that very large matter density shift the region to very small $\mu$.

However, matter effect is not always this simple. Suppose we have different matter potential for different beams, when they collide they would have built a different phase due to matter effect.

The inhomogeneous matter effect has been studied in [39]. It can excite high Fourier moments of polarization vector, which makes a lot of sense because it generates fine structure in the x direction. This might be integrated into LESA effect.

### Translation Symmetry

Translation symmetry is better explained by introducing Fourier transform in x direction.

For each mode, a term that is proportional to Fourier mode index $m$. It only appears in diagonal elements, thus is effectively a shift of vacuum frequencies, thus energies of neutrinos.

For each Fourier mode

$$\begin{pmatrix} \epsilon_1 \\ \epsilon_2 \end{pmatrix} = \mathbf{Q}(\Omega, k) e^{-i(\Omega t - kx)},$$

where we set $\Omega = 0$.

First term in RHS of Eqn. 4.28 becomes

$$-i \begin{pmatrix} \cot\theta_1 \partial_x & 0 \\ 0 & \cot\theta_2 \partial_x \end{pmatrix} \begin{pmatrix} \epsilon_1 \\ \epsilon_2 \end{pmatrix} = k \begin{pmatrix} \cot\theta_1 & 0 \\ 0 & \cot\theta_2 \end{pmatrix} \begin{pmatrix} Q_1 \\ Q_2 \end{pmatrix}.$$

We now define $\hat{\omega}_i''$, so that

$$\hat{\omega}_{k,i}'' = \hat{\omega}_i'' + 2\hat{k}\cot\theta_i,$$

where $\hat{k} = k/\mu$.

The $k$ term contributes to the difference between $\Omega_{k,i} \equiv \hat{\omega}_{k,i}'' + f_i''\xi$.

We notice that instability criteria doesn't change. However, the regime of instability changes. We also know that the instability region is determined by

$$|\Delta\hat{\omega}_{12}'' + 2\hat{k}(\cot\theta_1 - \cot\theta_2) + \Delta f_{12}''\xi| < \sqrt{-f_1 f_2 \xi^2}, \tag{4.34}$$

where $\Delta\hat{\omega}_{12}'' = \hat{\omega}_1'' - \hat{\omega}_2''$. The instability region shift from

$$-\sqrt{-f_1'' f_2'' \xi^2} - \Delta f_{12}''\xi < (\Delta\omega_{12}'' + 2k(\cot\theta_1 - \cot\theta_2))/\mu < \sqrt{-f_1'' f_2'' \xi^2} - \Delta f_{12}''\xi \tag{4.35}$$

If $|\Delta\omega_{12}'' + 2k(\cot\theta_1 - \cot\theta_2)|$ becomes larger, the region of instability is shifted to larger $\mu$, i.e., larger number density.

### Number Density of Emission

A crossing is required to have instability, i.e., $-f_1'' f_2'' > 0$. Meanwhile the number density on the left and right have little effects on the existence of instability. It shifts the region of instability for $\mu$.

### Energy of Emission

Different energy of two beams will make sure $-\omega_1 + \omega_2 \neq 0$. It has no effects on the criteria but changes the $\mu$ region of instability.

### General Solutions to Line Model

For completeness, we solve the general line model, c.f. Eqn. 4.28. We know that real symmetric matrix has only real eigenvalues, from which we infer that $\mu_1 = \mu_2$ and $\theta_1 = \theta_2$ removes the instability. For translation symmetric models, that is $\partial_x \to 0$, we have the eigenvalues

$$\Omega = \frac{1}{4}(A \pm B),$$

where

$$\begin{aligned}
A =& -\eta\omega_1/\sin\theta_1 - \mu_2/\sin\theta_1 + \eta\omega_2/\sin\theta_2 + \mu_1\xi/\sin\theta_2 + \lambda(1/\sin\theta_1 + 1/\sin\theta_2) \\
B =& (-4[(\lambda - \eta\omega_1)(\lambda + \eta\omega_2) + (\lambda(\mu_1 - \mu_2) - \eta(\mu_1\omega_1 + \mu_2\omega_2))\xi]\sin\theta_1\sin\theta_2 \\
&+[(\lambda + \eta\omega_2 + \mu_1\xi)\sin\theta_1 + (\lambda - \eta\omega_1 - \mu_2\xi)\sin\theta_2]^2\big)^{1/2}/(\sin\theta_1\sin\theta_2) \\
\xi =& 1 - \cos(\theta_1 - \theta_2).
\end{aligned}$$

For antineutrinos, I only need to change $\mu_i \to -\bar{\mu}_i$ and $\omega_i \to -\bar{\omega}_i$, where $\bar{\mu} = \sqrt{2}G_F\bar{n}_t$, so that the equation becomes

$$\begin{aligned}
i\partial_z \begin{pmatrix} \epsilon_1 \\ \epsilon_2 \end{pmatrix} =& -i \begin{pmatrix} \cot\theta_1\partial_x & 0 \\ 0 & \cot\theta_2\partial_x \end{pmatrix} \begin{pmatrix} \epsilon_1 \\ \epsilon_2 \end{pmatrix} \\
&+ \frac{1}{2} \begin{pmatrix} (\lambda - \bar{\mu}_2 + \eta\bar{\omega}_1 + \bar{\mu}_2\cos(\theta_1 - \theta_2))/\sin\theta_1 & \bar{\mu}_2(1 - \cos(\theta_1 - \theta_2))/\sin\theta_1 \\ \bar{\mu}_1(1 - \cos(\theta_1 - \theta_2))/\sin\theta_2 & (\lambda - \bar{\mu}_1 + \eta\bar{\omega}_2 + \bar{\mu}_1\cos(\theta_1 - \theta_2))/\sin\theta_2 \end{pmatrix} \begin{pmatrix} \epsilon_1 \\ \epsilon_2 \end{pmatrix}
\end{aligned}$$

Assume that the left beam is neutrino beam and the right beam is antineutrno beam. The linearized equation of motion becomes

$$\begin{aligned}
i\partial_z \begin{pmatrix} \epsilon_1 \\ \epsilon_2 \end{pmatrix} =& -i \begin{pmatrix} \cot\theta_1\partial_x & 0 \\ 0 & \cot\theta_2\partial_x \end{pmatrix} \begin{pmatrix} \epsilon_1 \\ \epsilon_2 \end{pmatrix} \\
&+ \frac{1}{2} \begin{pmatrix} (\lambda - \bar{\mu} - 2\eta\omega_1 + \bar{\mu}\cos(\theta_1 - \theta_2))/\sin\theta_1 & \bar{\mu}(1 - \cos(\theta_1 - \theta_2))/\sin\theta_1 \\ -\mu(1 - \cos(\theta_1 - \theta_2))/\sin\theta_2 & (\lambda + \mu + \eta\omega_2 - \mu\cos(\theta_1 - \theta_2))/\sin\theta_2 \end{pmatrix} \begin{pmatrix} \epsilon_1 \\ \epsilon_2 \end{pmatrix}
\end{aligned}$$

## 4.3 Fast Mode

In a paper by Chakraborty et al [44], they showed that neutrino flavor instabilities can grow with a rate that is proportional to the neutrino density, which has much faster oscillation frequencies than vacuum oscillations. For such a fast growth to happen, the author considered head on colliding neutrino beams. The derivation is much similar to what has been shown in the previous section.

As an estimation, the frequencies of vacuum oscillation is

$$\begin{aligned}\omega_{\mathrm{v}} =& \frac{\Delta m^2}{2E} \\ \sim& 6.3\times10^{-3}\mathrm{m}^{-1}\frac{\Delta m^2_{32}}{2.5\times10^{-3}\mathrm{eV}^2}\frac{1MeV}{E} \\ \sim& 1.90\times10^{-4}\mathrm{m}^{-1}\frac{\delta m^2}{7.5\times10^{-5}\mathrm{eV}^2}\frac{1\mathrm{MeV}}{E},\end{aligned}$$

where $E$ is the neutrino energy. The corresponding oscillation wavelength is simply give by

$$\begin{aligned}\lambda_{12} =& 2\pi/\omega_{12} \sim 1\mathrm{km} \\ \lambda_{32} =& 2\pi/\omega_{32} \sim 33.1\mathrm{km}.\end{aligned}$$

The fast modes instability grows with a rate proportional to the neutrino potential $\mu = \sqrt{2}G_F n_\nu$, which is very large in dense neutrino media. A large growth rate indicates a faster flavor transformation than vacuum oscillations.

### 4.3.1 Dispersion Relation of Neutrino Flavor Conversion

We consider two-flavor scenario ($\nu_{\mathrm{e}}$ and $\nu_{\mathrm{x}}$) of neutrino oscillations. We also assume that all neutrinos and antineutrinos are emitted as electron flavor. The flavor evolution of neutrino ensemble depends on flavor density matrices of neutrinos $\rho$ and

antineutrinos $\bar{\rho}$ with energy $E$, direction of velocity $\hat{\mathbf{v}}$,

$$\mathrm{i}(\partial_t + \mathbf{v}\cdot\nabla)\rho = [H, \rho_n]\,, \tag{4.36}$$

where $H$ is the Hamiltonian for neutrino oscillations. In the context, Hamiltonian depends on three different contributions from vacuum oscillations $H_{\mathrm{v}}$, interactions with matter $H_{\mathrm{m}}$, and interactions with neutrinos themselves $H_{\nu\nu}$. In this work, we ignore vacuum and matter terms since the concentration is on fast neutrino oscillations, which would occur even without neutrino mass differences [44, 49]. In order to calculate the neutrino self-interaction term $H_{\nu\nu}$, the distribution of neutrinos (antineutrinos) $f_{\nu_{\mathrm{e}}(\bar{\nu}_{\mathrm{e}})}(\hat{\mathbf{v}}, E)$ and $f_{\nu_{\mathrm{x}}(\bar{\nu}_{\mathrm{x}})}(\hat{\mathbf{v}}, E)$ is required, where $E$ is the energy of neutrinos (antineutrinos). We have

$$H_{\nu\nu} = \sqrt{2}G_{\mathrm{F}}\iint \frac{\mathrm{d}\cos\theta'\mathrm{d}\phi'}{4\pi}v^{\mu}v'_{\mu}\int\frac{E'^2\mathrm{d}E'}{2\pi^2}\left((f'_{\nu_{\mathrm{e}}} - f'_{\nu_{\mathrm{x}}})\rho' - (f'_{\bar{\nu}_{\mathrm{e}}} - f'_{\bar{\nu}_{\mathrm{x}}})\bar{\rho}'\right), \tag{4.37}$$

where $v^{\mu} = (1, \sin\theta\cos\phi, \sin\theta\sin\phi, \cos\theta)^{\mathrm{T}}$ is the four velocity of (anti)neutrinos in our spherical coordinate system. Without vacuum contribution, the equation of motion for antineutrinos has the same form [30].

We follow the same assumption in reference [50] that the the distribution of $\nu_x$ and $\bar{\nu}_x$ are the same, namely $f_{\nu_{\mathrm{x}}}(\hat{\mathbf{v}}, E) - f_{\bar{\nu}_{\mathrm{x}}}(\hat{\mathbf{v}}, E) = 0$. In addition, we have the same definition of electron lepton number (ELN) of neutrinos travelling in direction $\hat{\mathbf{v}}$ [50],

$$G(\hat{\mathbf{v}}) = \sqrt{2}G_{\mathrm{F}}\int\frac{E'^2\mathrm{d}E'}{2\pi^2}(f_{\nu_{\mathrm{e}}}(\cos\theta', \phi', E') - f_{\bar{\nu}_{\mathrm{e}}}(\cos\theta', \phi', E')). \tag{4.38}$$

To perform linear stability analysis, we assume that the density matrix has the form

$$\rho = \bar{\rho} = \begin{pmatrix} 1 & \epsilon \\ \epsilon^* & 0 \end{pmatrix}, \tag{4.39}$$

where $|\epsilon| \ll 1$. As a result, the linearized equations of motion depends only on $G(\hat{\mathbf{v}})$ and $\hat{\mathbf{v}}$. We also assume that all neutrinos and antineutrinos undergo the same

behavior in linear regime, $\epsilon = \tilde{\epsilon} e^{-\mathrm{i}(\Omega t - \mathbf{K}\cdot\mathbf{x})}$. Izaguirre, Raffelt, and Tamborra defined the polarization tensor [50],

$$\Pi^{\mu}{}_{\nu} = 1 + \int \frac{d\Omega}{4\pi} G(\theta,\phi) \frac{v^{\mu} v_{\nu}}{\omega - k\hat{\mathbf{k}}\cdot\hat{\mathbf{v}}}, \tag{4.40}$$

which defines the dispersion relation $\Pi^{\mu}{}_{\nu} a^{\nu} = 0$, with $a^{\nu} = \int \frac{d\cos\theta' d\phi'}{4\pi} G(\hat{\mathbf{v}}') v^{\nu} \tilde{\epsilon}$. We find the nontrivial solutions by setting [50],

$$\det\left(\Pi^{\mu}{}_{\nu}\right) = 0. \tag{4.41}$$

For simplicity, we consider axial symmetric neutrino emission so that Eq. (4.41) becomes

$$\begin{aligned} &\det\left(\omega \mathrm{I} + \frac{1}{2}\begin{pmatrix} I_0 & 0 & 0 & -I_1 \\ 0 & -\frac{1}{2}(I_0 - I_2) & 0 & 0 \\ 0 & 0 & -\frac{1}{2}(I_0 - I_2) & 0 \\ I_1 & 0 & 0 & -I_2 \end{pmatrix}\right) \\ &= 0, \end{aligned} \tag{4.42}$$

where $\mathbf{I}$ is the rank 4 identity matrix and

$$I_m = \int_{-1}^{1} du G(u) \frac{u^m}{1 - (|k|/\omega)\, u}. \tag{4.43}$$

where we define $u = \cos\theta$. Eq. (4.42) is equivalent to the result in reference [37]. $|k|/\omega$ is defined as the refractive index $n$ of the flavor wave. For spectrum $G(u)$ without zero values, the forbidden region is given by $1 - (|k|/\omega)\, u \leq 0$.

The dispersion relations can be categorized into two different types by symmetries. To incorporate azimuthal symmetry, we define solutions related to the first and second element of $a^{\nu}$ ($\nu = 1, 2$) to be multi-azimuthal angle (MAA) solutions since they are the only solutions that depend on azimuthal angle $\phi$. The other solutions which are related to $\nu = 0, 3$ are defined to be the multi-zenith angle (MZA)

solutions. The MAA solution is related to symmetry breaking in azimuthal angle only, which is determined by

$$\omega = \frac{1}{4}(I_0 - I_2). \tag{4.44}$$

Similarly, the MZA solution is related to symmetry breaking in both azimuthal angle and zenith angle, which is

$$\omega = -\frac{1}{4}\left(I_0 - I_2 \pm \sqrt{(I_0 + I_2 - 2I_1)(I_0 + I_2 + 2I_1)}\right). \tag{4.45}$$

We denote the solution associated with + sign in Eq. (4.45) as MZA+, while the solution assocated with − sign as MZA-. The two solutions are connected to each other in dispersion relations. In general, it doesn't provide physical insights to distingush the two branches of solutions since they are simply two branches of the solution.

The solutions to Eq. (4.44) and Eq. (4.45) are dispersion relations $D(\omega, \mathbf{k})$ for a chosen direction of $\hat{\mathbf{k}} = \hat{\mathbf{z}}$ with axial symmetric neutrino emission.

### 4.3.2 Instabilities and Gaps

In reference [50], the authors relate gaps in dispersion relation to instabilities of neutrino oscillations. In this section, we review the idea of correspondence between gaps and instabilities first. Then we show that this relation is not a solid theory that can be generalized to all cases.

We continue the discussion of axial symmetric neutrino emissions but with discretized zenith angles $\theta$ thus discretized $u$. Hence the ELN is independent of azimuth angle $\phi$. For neutrino emission with 2 zenith angles, the ELN spectrum is

$$G(u) = \sum_{i=1}^{2} g_i \delta(u - u_i). \tag{4.46}$$

The MAA solution becomes an equation of hypobola for $\omega$ and $k$, which has asymptotes $\omega = ku_i$ for $i = 1, 2$. Meanwhile, hyperbola equation has two solutions

of $\omega$ ($k$) for any given real $k$ ($\omega$). The solutions are either real which indicates stable solutions or complex which indicates exponential growth or decrease in linear regime. On the other hand, non-existence of real solutions of $\omega$ ($k$) for given real $k$ ($\omega$) is equivalent to gap in dispersion relation. Thus the equivalence of gap and instabilities is guaranteed in neutrino emission with two-zenith-angle emission. The numerical calculations is normalized using the maximium value in spectrum which is a convention we follow for all discrete emission calculations. Unit for $\omega$ and $k$ can be determined once the exact spectrum is determined. Upper panels of Fig. 4.2 is reproduction of left panels of Fig. 1 in reference [50]. The dispersion relation is shown as black lines. The real part $\omega_{\rm R}$ is shown as red solid lines. $\omega_{\rm R} \pm \omega_{\rm I}$ are shown are red dashed lines, where $\omega_{\rm I}$ is the imaginary part of $\omega$.

In core collapse supernova and neutron star mergers, neutrino emission is not in discrete zenith angles. More realistic models involve continuous zenith angle ELN spectra. In the case that the smooth and continuous ELN spectrum has no crossing, gap indeed indicates instabilities, as shown in reference [50]. In this section we prove that the instabilities in MAA, MZA+, or MZA- solution can only appear in either region $\omega \leq 0$ or region $\omega \geq 0$. As it suggests, the instability regions propagate only between the dispersion relation curves and the axis $\omega = 0$. We reproduced the calculation in reference [50] using the same Garching core-collapse supernova data set [52]. The spectrum shown in the left panel of Fig. 4.3 is polynomial fitting of the Garching 1D supernova simulation data. On the right of Fig. 4.3, the dispersion relation for MAA (MZA) solution is shown as red (green, blue) solid lines. Instabilities associated with MAA (MZA) solution is shown as light red (light green, light blue) blobs. The two branches of MZA solutions appear at the top half (MZA+) and lower half (MZA-). The result shows that instabilities occur either in region $\omega > 0$ or region $\omega < 0$ and with limits set the dispersion relation. We will prove that the instabilities appear between the dispersion relation and the axis $\omega = 0$.

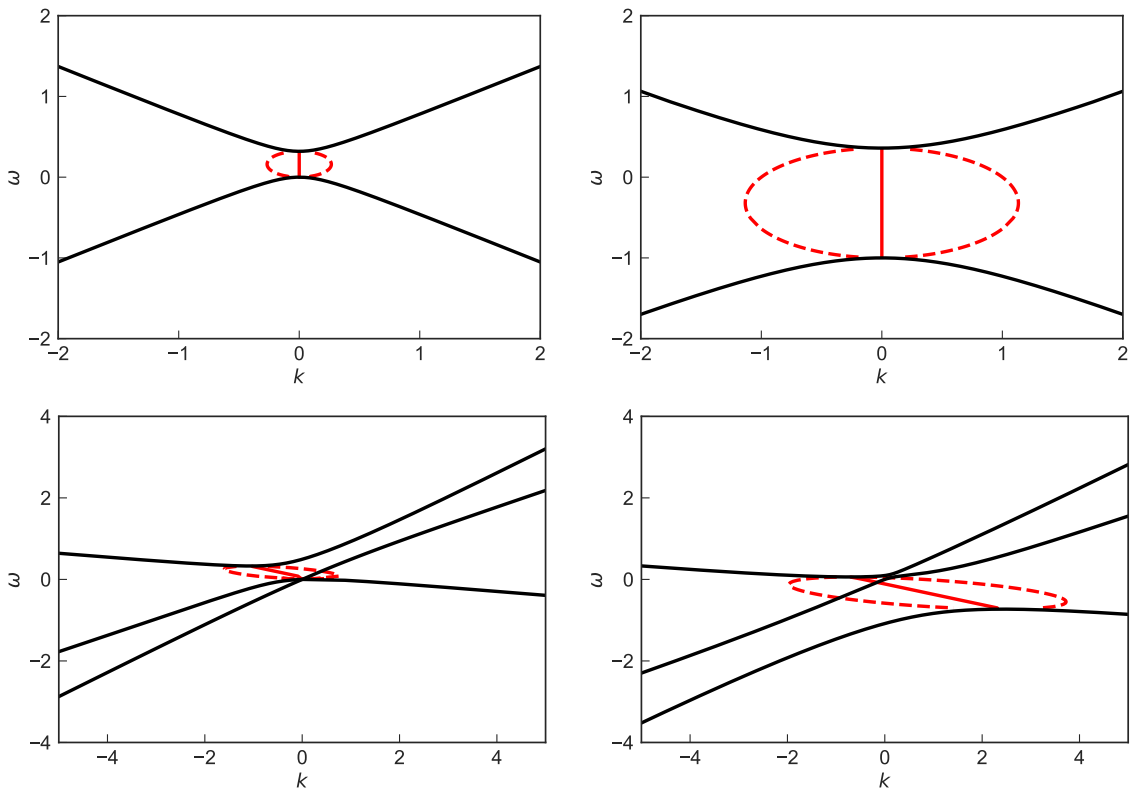


Figure 4.2: Dispersion relation and instabilities of two zenith angles spectrum (upper panels) and three zenith angles spectrum (lower panels). The black lines are the dispersion relations and the colored dots are examples of complex $\omega$ for real $k$. The left panels are the dispersion relation and linear stability analysis of MAA solutions while the right panels are for MZA solutions.

Suppose we are looking for complex solutions for given real omega as in Fig. 4.3, MAA solution Eq. (4.44) is rewritten as a function $k(\omega/k)$. More explicitly, we have to solve the integral function to find out $k$ for real $\omega$,

$$k = \frac{1}{4}\int \mathrm{d}u G(u)\frac{1-u^2}{\omega/k-u}. \tag{4.47}$$

To investigate how instabilities developed around the horizental axies, we solve Eq. (4.47) in the limit $\omega \to 0$. For complex $k$, the integral can be decomposed into the

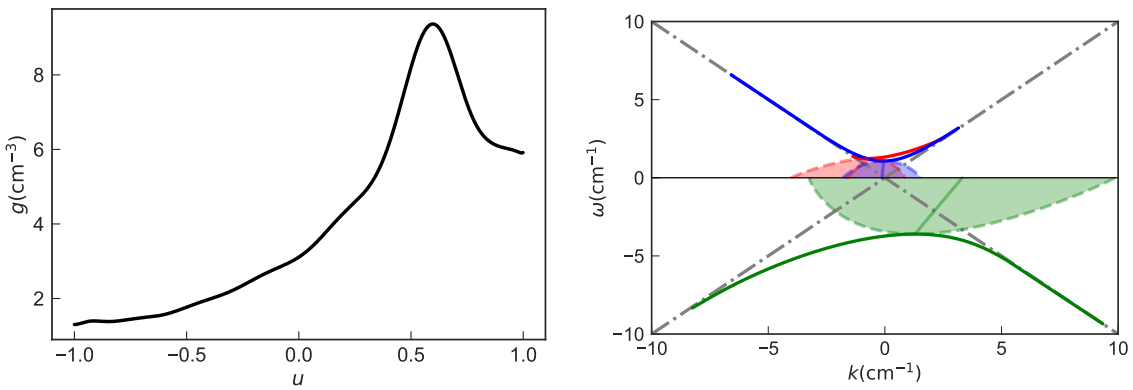


Figure 4.3: Dispersion relation and linear stability analysis (right panel) for a spectrum constructed from Garching 1D simulation data (left panel). Solid red line is dispersion relation for MAA solution while blue and green lines are for MZA solutions. Light red (green and green) blob is instability for MAA (MZA) solution.

principal value $\mathrm{Re}(k)$ and imaginary part $\mathrm{Im}(k)$ using SokhotskiPlemelj theorem,

$$\mathrm{Re}(k) = \frac{1}{4}\left(\mathcal{P}\int \mathrm{d}u G(u)\frac{1-u^2}{-u}\right) \tag{4.48a}$$

$$\mathrm{Im}(k) = \frac{\pi}{4}G(0)\,\mathrm{Sign}\,(\omega)\,\mathrm{Sign}\,(\mathrm{Im}(k))\,. \tag{4.48b}$$

Assuming no crossing is found in sepctrum $G(u)$ at $u = 0$, Eq. (4.48b) shows that $\omega$ must have the same sign as $G(0)$ if we find nonzero imaginary part in $k$. We conclude that instabilities can only grow either in the upper plane $\omega > 0$ or lower plane $\omega < 0$. What's more, the value of $k$ at limit $\omega \to 0$ can be solved out of Eq. (4.48a) and Eq. (4.48b). For instabilities the imaginary part of $k$ tells us the growth rate is,

$$|\mathrm{Im}(k)| = \frac{\pi}{4}|G(0)|. \tag{4.49}$$

Similar result is obtained for MZA solutions,

$$\left(4\,\mathrm{Re}(k) - \mathcal{P}\int \frac{G(u)}{u}\mathrm{d}u + U_1\right)^2 - \left(\mathrm{Sign}(\omega\,\mathrm{Im}(k))\pi G(0) + 4\,\mathrm{Im}(k)\right)^2 \tag{4.50}$$

$$= -\left(\mathcal{P}\int \frac{G(u)}{u}\mathrm{d}u + U_1\right)\pi\,\mathrm{Sign}(\omega\,\mathrm{Im}(k))G(0), \tag{4.51}$$

where $U_m = \int G(u)u^m \mathrm{d}u$ and all the integrals are over all the sepctrum. The equations are quadratic in both $\mathrm{Re}(k)$ and $\mathrm{Im}(k)$ so the real solutions can be calculated and verified with linear stability analysis. The imaginary part $\mathrm{Im}(k)$

$$\mathrm{Im}(k) = -\frac{1}{4}\pi G(0)\,\mathrm{Sign}(\omega\,\mathrm{Im}(k))\left(1 \pm \frac{\mathscr{P}\int \frac{G(u)}{u}du + \int G(u)udu}{4\,\mathrm{Re}(k) - \mathscr{P}\int \frac{G(u)}{u}du + \int G(u)udu}\right) \tag{4.52}$$

determines that the two different solutions are either in the region $\omega > 0$ or in the region $\omega < 0$ which corresponds to MZA+ and MZA- solutions. The instabilities in the two regions are not continuous at $\omega = 0$.

### 4.3.3 Instabilities Do Not Always Show Up as Gap

Even though the concept of gap leads to instabilities works well for the models in 4.3.2, it can not be generalized to arbitrary number of emission angles nor to continuous spectra with crossings. As an example, we perform linear stability analysis of the three zenith angles emission configuration which is determined by a cubic function both in $\omega$ and $k$. Three solutions of $k(\omega)$ for given real $\omega(k)$ are expected. As long as real solutions disappear, complex solutions emerge, which leads to instabilities occur even without an actual gap. Rather the decrease in the number of real solutions for fixed $\omega$ or $k$ corresponds to the instabilities. As an example, we plotted dispersion relation and instabilities for three zenith angles in lower panels of Fig. 4.2. For a given value of $\omega$ such as $\omega = 0.5$, the three MAA solutions (Fig. 4.2 lower left panel) of $k$ are $k = -4.6, 0.29, 1.2$. All three solutions are all real and indicate no spatial instabilities which is confirmed by calculation of instabilities shown as red blob. However, for another real $\omega = 0.2$, we find only one real solution $k = 0.4$ from dispersion relation. The other solutions are complex and proven to be $k = -0.557106 \pm 0.966535\mathrm{i}$ where the value with positive imaginary part leads to exponential growth. We conclude that instabilities doesn't require gap in dispersion

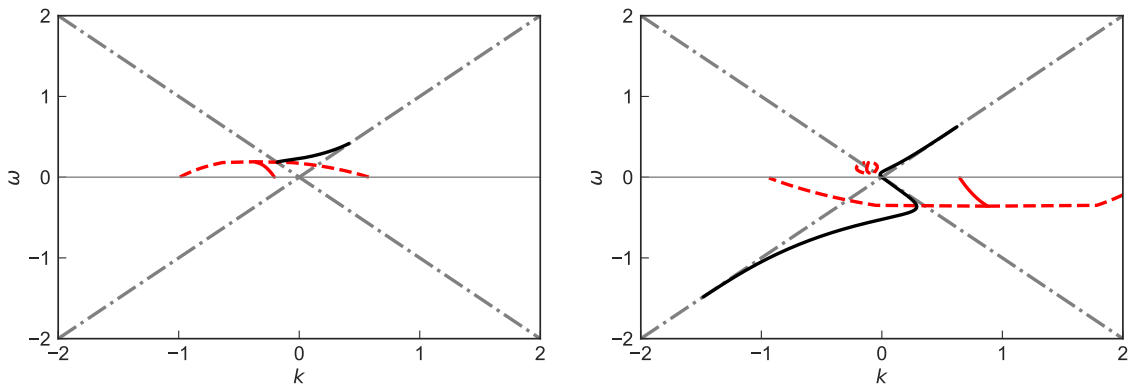


Figure 4.4: Dispersion relation and linear stability analysis for box spectrum. The box spectrum is defined to be $-0.1$ within range $u \in [-1, -0.3)$ and 1 within range $u \in [-0.3, 1]$. Left panel shows the dispersion relation and the complex $k$ for real $\omega$ for MAA solution. Right panel is the corresponding result for MZA solution. Dash-dotted gray lines are $\omega = \pm k$ which sets the boundaries of the forbidden region for dispersion relation.

relation except for two emission angles.

We will prove that instabilities for continuous emission angles do not necessarily correspond to gap in dispersion relation. In the earlier works of fast modes, Sawyer analyzed a box shaped angular distribution of neutrino emission [47]. To address the generality of our conclusion, we repeat the calculation for box spectrum with crossing.

We construct a box spectrum with value $-0.1$ within $u \in [-1, -0.3)$ and value 1 within $[-0.3, 1]$ as shown in the top left panel of Fig. 4.4. As in the discrete emission case, we normalize all quantities using the maximium value of the spectrum. With the spectrum defined, we calculate the dispersion relation and find out complex values of $k$ for real $\omega$. The result shows that the dispersion relation of both MAA solution and MZA solution contains only one curve. No gap is formed but we observe instabilities between this curve and $\omega = 0$ in MAA solution as well as two unstable regions of $k$ in MZA solution, which are plotted as red lines.

## 4.4 Conclusion

We have reviewed that dispersion relation gap and instabilities are the same thing for neutrino emission with two zenith angles for the quadratic nature of the problem. As for more realistic spectrum, we have proved that instabilities propagate in regions of either $\omega > 0$ or $\omega < 0$ and never cross $\omega = 0$. Hence the dispersion relation gaps should be defined as gaps between the dispersion relation curves and the axis $\omega = 0$ instead of the dispersion relation curves. We have also showed that instabilities is not necessarily shown as gap in dispersion relations for neutrino emission with more than two zenith angles and box spectrum with crossing. Through the discussions, we demonstrated that the relation between dispersion relation gaps and instabilities should be used with caution.

# Chapter 5

# Neutrino Halo Problem

One of the big questions about neutrino oscillations in supernovae is the so called halo problem. Cherry et al showed that neutrino flavor conversions are greatly affected by the back scattered neutrinos in supernovae [33]. Neutrinos around supernovae are scattered and some of them are scattered to move almost backward. On the other hand, neutrino self-interactions is proportional to the inner product of momenta of neutrinos, which leads to the dependence on $1 - \cos\theta$ where $\theta$ is the angles between momenta of two neutrinos. Most of the research has been concentrating on mostly forward scattering, with small values for $1-\cos\theta$. For back ward scattered neutrinos, the interaction potential can be much larger than the forward scattered neutrino contributions. Though the work by Sarikas et al showed that matter suppression is still significant within this region [34], it is not clear how exactly the neutrino halo alters neutrino oscillations. The halo problem itself is worth more calculations. In this chapter, I will present a relaxation method for this problem. The focus will be on the numerical method itself.

## 5.1 Line Model

We continue to use the simplified line model and build our intuitions out of it. The halo problem is simplified to have neutrinos emitted from a line $z = 0$ homogeneously, which are reflected from a certain distance $z = L$. In principle, the reflection angles doesnt have to be Snells law. The scattering can be in any angle with different amplitudes. Here I am using this very simple Snells law just to explore the effect of halo. It's crucial to keep an eye on the simplifications in this line model.

- Neutrinos are emitted from a line, which is not the case in a real supernova.
- Neutrinos are emitted with translation symmetry on the line. Breaking the symmetry might bring in other qualitatively different results.
- Neutrinos are reflected from a certain surface $z = L$, which is different from reality where neutrinos are scattered everywhere.
- Neutrinos are reflected according to Snell's law.
- Neutrinos are homogeneously reflected at $z = L$.

The algorithm that I used is relaxation method. The algorithm is meant to find the equilibrium state of neutrino oscillations with the presence of halo.

1. Calculate forward beam using 0 backward beam;
2. Calculate backward beam using forward beam calculated in 1;
3. Calculate forward beam using backward beam calculated in 2;
4. Repeat until the beams reach equilibrium.

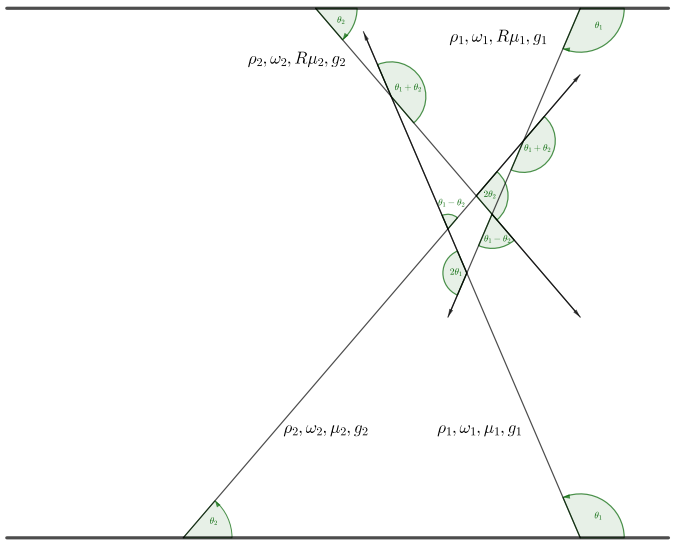


Figure 5.1: Line model used for halo problem. Neutrinos are emitted from the bottom line and reflected at the top line. Two neutrino beams are demonstrated in the figure. The beams are reflected from a surface at $z = L$.

## 5.2 Neutrino Beams Only

As a first step, I calculated neutrino oscillations with only neutrino beams. Before we rush to the numerical results, I linearized the equation of motion and worked out the linear stability analysis.

In linear regime, we define the density matrices for forward and backward beams to be

$$\rho_F = \frac{1}{2}\begin{pmatrix} 1 & \epsilon_F \\ \epsilon_B^* & -1 \end{pmatrix}$$
$$\rho_B = \frac{1}{2}\begin{pmatrix} 1 & \epsilon_B \\ \epsilon_B^* & -1 \end{pmatrix}.$$

The Hamiltonian for forward and back ward beams are

$$H_F = H_v + R\mu\rho_B$$
$$H_B = H_v + \mu\rho_F.$$

We will investigate the instability for zero mixing angle for new instabilities. The linearized equation of motion can be simplified to

$$i\partial_z \begin{pmatrix} \epsilon_F \\ \epsilon_B \end{pmatrix} = \begin{pmatrix} -\omega_v + R\xi\mu & -R\xi\mu \\ \xi\mu & \omega_v - \xi\mu \end{pmatrix} \begin{pmatrix} \epsilon_F \\ \epsilon_B \end{pmatrix}.$$

This equation can be easily solved. The eigenvalues are

$$\Omega_+ = \frac{1}{2}((R-1)\xi\mu + \sqrt{\Delta})$$
$$\Omega_- = \frac{1}{2}((R-1)\xi\mu - \sqrt{\Delta}),$$

where

$$\Delta = (1-R)^2\mu^2\xi^2 - 4\mu\xi\omega_v(1+R) + 4\omega_v^2. \tag{5.1}$$

The corresponding eigenvectors are

$$V_+ = \begin{pmatrix} \frac{-2\omega_v + \xi\mu(1+R) + \sqrt{\Delta}}{2\xi\mu} \\ 1 \end{pmatrix}$$
$$V_- = \begin{pmatrix} \frac{-2\omega_v + \xi\mu(1+R) - \sqrt{\Delta}}{2\xi\mu} \\ 1 \end{pmatrix}.$$

The general solution to the equation is

$$\begin{pmatrix} \epsilon_F(z) \\ \epsilon_B(z) \end{pmatrix} = C_+V_+e^{-i\Omega_+z} + C_-V_-e^{-i\Omega_-z}.$$

The special property about this reflection problem is that the density matrices for the forward and backward beams should be the same at the reflection point, say

$z = L$. With such a simple relation, we can find the relations between $C_\pm$ by setting $\epsilon_F(L) = \epsilon_B(L)$,

$$\frac{C_+}{C_-} = e^{-i(\Omega_- - \Omega_+)L} \frac{\sqrt{\Delta} + 2\omega_v + \mu\xi(1-R)}{\sqrt{\Delta} - 2\omega_v - \mu\xi(1-R)}. \tag{5.2}$$

The solution to be problem can be simplified,

$$\begin{pmatrix} \epsilon_F(z) \\ \epsilon_B(z) \end{pmatrix} = C_- e^{-i\Omega_- L} \left( \frac{\sqrt{\Delta} + 2\omega_v + \mu\xi(1-R)}{\sqrt{\Delta} - 2\omega_v - \mu\xi(1-R)} V_+ e^{-i\Omega_+(z-L)} + V_- e^{-i\Omega_-(z-L)} \right). \tag{5.3}$$

We are interested in the absolute values of each elements so that the overall factors can be neglected. The forward beam evolution is obtained by taking the absolute value of $\epsilon_F$,

$$\begin{aligned} |\epsilon_F| \propto & |(2\omega_v + \xi\mu(1-R) + i\delta)(-2\omega_v + \xi\mu(1+R) + i\delta)e^{\delta(z-L)} \\ & + (-2\omega_v - \xi\mu(1-R) + i\delta)(-2\omega_v + \xi\mu(1+R) - i\delta)e^{-\delta(z-L)}|, \end{aligned}$$

in which $\sqrt{\Delta}$ is replaced by $i\delta$. We collecting terms and verify that it has the form

$$|\epsilon_F| \propto A + B\cosh(2\delta(L-z)), \tag{5.4}$$

where $B \leq 0$. The only $z$ dependent term is $\cosh(2\delta(L-z))$, which is decreasing within $[0, L]$ and is increasing in $[L, 2L]$. The slope at $z = L$ is 0. An example is plotted in Fig. 5.2.

We expect the numerical calculations bare the same behavior that the instability leads to no growth but decrease in flavor conversion, assuming the neutrinos start from electron flavor. The result indeed confirms it. Fig. 5.3 is an example of it.

For linear stability analysis, we usually identify real characteristic values of the linearized equation of motion. In bipolar model as explained in Sec. C.3, real characteristic values of the equation of motion indicates exponential growth, while it always indicates exponential decrease in this simplified halo problem.

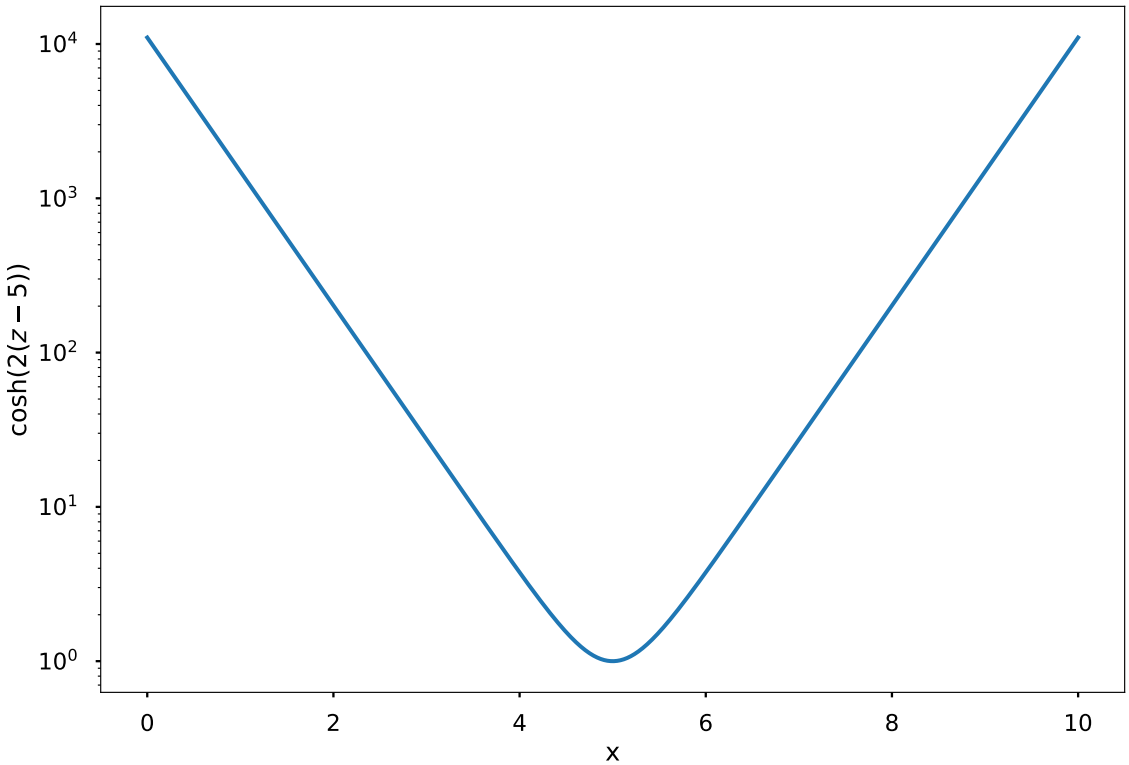


Figure 5.2: An example of $\cosh(2\delta(z-L))$ with $\delta = 1$, and $L = 5$. This function always reach the minimium at $z = L$.

We expect that only normal hierarchy has an instability region which is trivial since we noticed that the backward beam is acting like antineutrino beams but with different hierarchies.

$$i\partial_t \mathbf{s}_F = \mathbf{s}_F \times (\mathbf{H}_v + R\mu\mathbf{s}_B) \tag{5.5}$$

$$i\partial_t \mathbf{s}_B = \mathbf{s}_B \times (-\mathbf{H}_v - \mu\mathbf{s}_F). \tag{5.6}$$

Compare to Eq. C.25, we notice that the reflected beam works as an antineutrino beam but the system becomes the opposite hierarchy compared to bipolar model. We find the instability regions in Fig. 5.4.

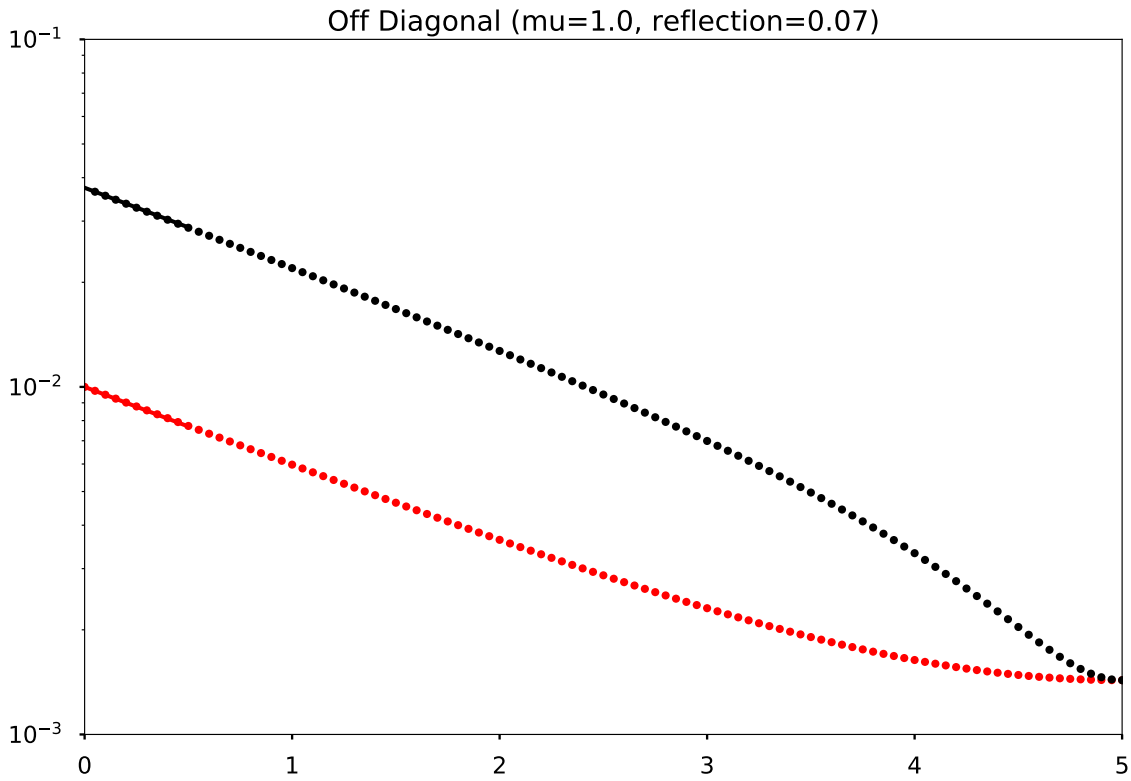


Figure 5.3: Absolute value of off diagonal element for $\mu = 1.0$, $R = 0.07$, $L = 5$, with normal hierarchy. The red dots are for the forward beam and the black dots are for the backward beams. The lines are indicating the predictions of linear stability analysis.

## 5.3 Two Beams Model with Reflection

The model is naturally extended to a two beams model including both neutrinos and antineutrinos. The configuration is exactly the same as shown in Fig. 5.1.

As the first step we work out the linear stability analysis. The four equations of

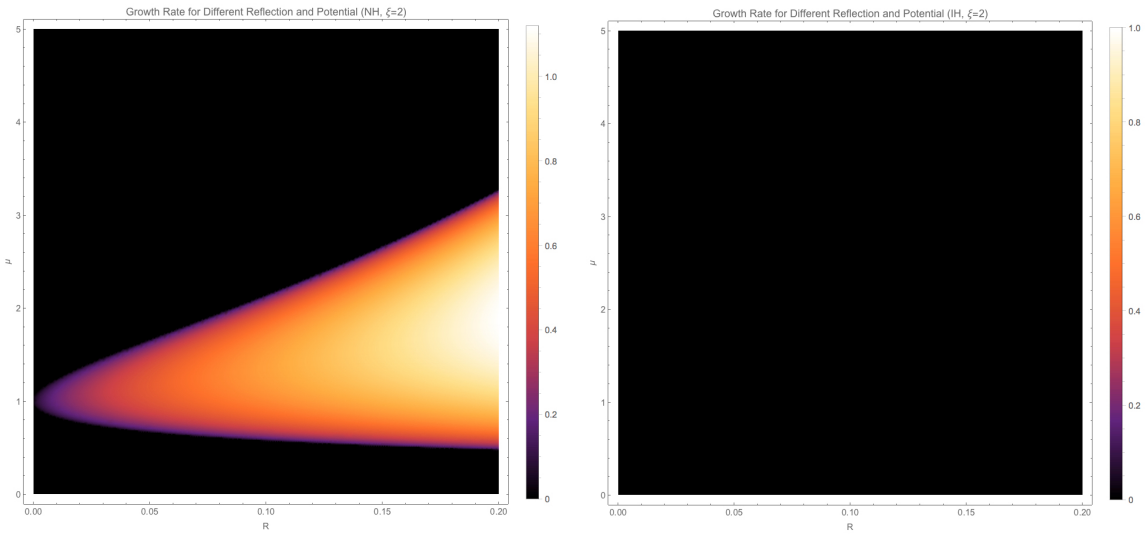


Figure 5.4: Instability regions for normal hierarchy (left) and inverted hierarchy (right) as a function of neutrino potential $\mu$ and reflection coefficient $R$, with vacuum mixing angle set to 0. No instabilities is found in inverted hierarchy.

motion are

$$i\partial_z\rho_1 = [H_1, \rho_1], \tag{5.7}$$

$$i\partial_z\rho_2 = [H_2, \rho_2], \tag{5.8}$$

$$-i\partial_z\rho_3 = [H_3, \rho_3], \tag{5.9}$$

$$-i\partial_z\rho_4 = [H_4, \rho_4], \tag{5.10}$$

where $_1$ and $_2$ are the quantities for two forward beams while $_3$ and $_4$ are the quantities for the corresponding backward going beams. For the purpose of this analysis we set $\theta_v = 0$. The Hamiltonians are

$$H_1 = -\eta\omega_v\sigma_3 + g_2\chi_-\mu_2\rho_2 + g_2\chi_+R\mu_2\rho_4 + g_1\chi_1R\mu_1\rho_3, \tag{5.11}$$

$$H_2 = \eta\omega_v\sigma_3 + g_1\chi_-\mu_1\rho_1 + g_2\chi_2R\mu_2\rho_4 + g_1\chi_+R\mu_1\rho_3, \tag{5.12}$$

$$H_3 = -\eta\omega_v\sigma_3 + Rg_2\chi_-\mu_2\rho_4 + g_2\chi_+\mu_2\rho_2 + g_1\chi_1\mu_1\rho_1, \tag{5.13}$$

$$H_4 = \eta\omega_v\sigma_3 + Rg_1\mu_1\chi_-\rho_3 + g_1\chi_+\mu_1\rho_1 + g_2\chi_2\mu_2\rho_2. \tag{5.14}$$

I have defined

$$\begin{aligned}\chi_+ =& 1 - \cos(\theta_1 + \theta_2),\\ \chi_- =& 1 - \cos(\theta_1 - \theta_2),\\ \chi_1 =& 1 - \cos(2\theta_1),\\ \chi_2 =& 1 - \cos(2\theta_2),\end{aligned}$$

and $g_i$ represents the energy spectrum of the neutrinos and $\eta$ stands for the hierarchy.

## 5.4 Relaxation Method for Numerical Solutions

We choose a relaxation method scheme to solve this non-local boundary value problem numerically. To begin with, we write down the discretization scheme.

$$\rho(t + \Delta t) = \left[\cos(2h\Delta t)\rho_n - 2u_i\rho_i u_n\right]\sigma_n \tag{5.15}$$

$$= \left[\cos(2h\Delta t)\rho_n + 2\sin^2(h\Delta t)u_i'\rho_i u_n'\right]\sigma_n \tag{5.16}$$

The reason that we use fixed step size for this problem is that it's easier to calculate the neutrino self-interactions on such fixed grids. The algorithm is described as

1. Calculate forward beam using 0 backward beam;
2. Calculate backward beam and forward beam together using the state of beams from the previous step current counter beams;
3. Repeat the previous step until the state of the beams reach equilibrium.

To speed up the calculations, I also implemented OpenMP for parallel computing. The code is tested using vacuum oscillations (shown in Fig. 5.5) and bipolar models. The reason that we still have conversions is because of the vacuum term, which is additional to linear stability analysis. It is also proven to reach equilibrium quickly as shown in Fig. 5.6.

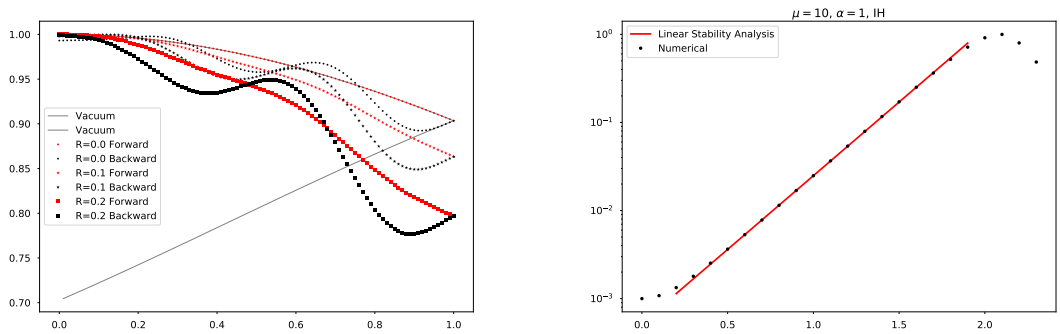


Figure 5.5: The left panel validates code by setting reflection to zero and approach vacuum for single forward beam. Meanwhile, we notice that for nonzero reflections, more conversion is done, which makes sense due to the similarity between $R$ and the asymmetry parameter $\alpha$ in bipolar model. The right panel validates the code by setting reflection to zero and compare with bipolar model for two beams case, where the slope matching the theoretical value 3.85.

## 5.5 Conclusion

Halo problem brings in more parameters to neutrino oscillations. In the spirit of numerical methods, we developed a parallelable relaxation method, using C++ and OpenMP. Both the analytical and numerical results showed that for the two realms, either single forward beam or two forward beams, we spot trivial results by drawing analogy with bipolar model, alas no new types of instabilities was found in these situations. On the other hand, reflection indeed may enhance the flavor conversions. Future work should be done to explore the effect of symmetry breaking and multiple emission beams.

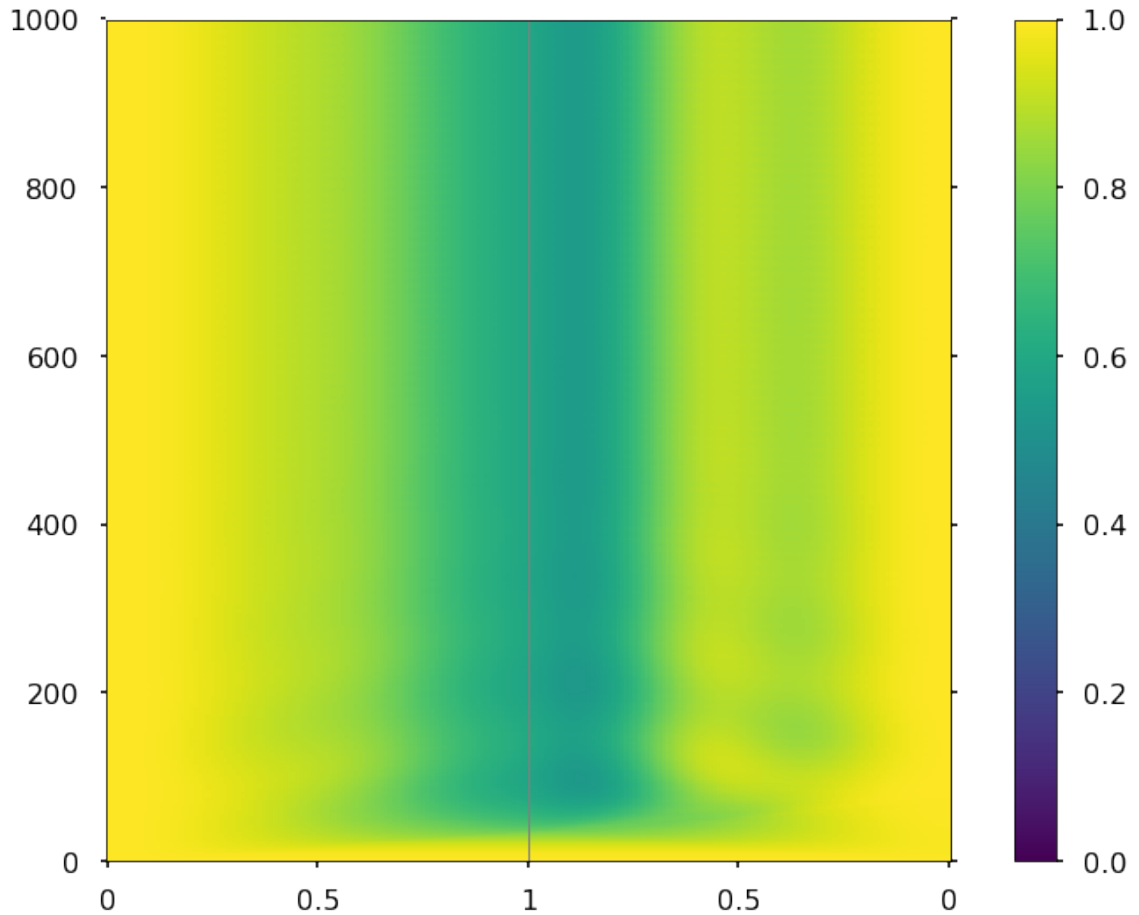


Figure 5.6: Relaxation method reaches equilibrium after some steps. The horizontal axis is the $z$ direction while the vertical axis is the number of iteration steps. The color indicates the survival probability for electron flavor. This calculation sets $\mu = 4$, $R = 0.2$, and is done within range $[0, 1]$. Equilibrium is reached around step 400 and the neutrino states stays in equilibrium.

# Appendices

# A Conventions

# B Rabi Oscillations

# C MSW Effect Revisited

# Appendix A

# Conventions

## A.1 Terms

- Normal hierarchy for two-flavor scenario is always defined as $m_2^2 - m_1^2 > 0$, i.e., $\omega_{\rm v} > 0$.

- Inverted hierarchy for two-flavor scenario is defined as $m_2^2 - m_1^2 < 0$, i.e., $\omega_{\rm v} < 0$.

- Solar neutrino mass splitting is $\delta m_{12}$, while atmospheric neutrino mass splitting refers to $\delta m_{23}$.

## A.2 Units

Natural units system makes the calculations of neutrinos convenient. By definition, we set reduced Planck constant and speed of light to be 1, $\hbar = 1 = c$. The conversion

between natural units and SI can be down by using the following relations,

$$1\text{GeV} = 5.08 \times 10^{15}\text{m}^{-1} \tag{A.1}$$

$$1\text{GeV} = 1.8 \times 10^{-27}\text{kg} \tag{A.2}$$

To convert between different physical quantities in this thesis, I always use the following tips.

- The energy-mass-momentum relations becomes $E^2 = p^2 + m^2c^2 = p^2 + m^2$. Thus mass $m$, momentum $\mathbf{p}$ and energy $E$ have the same dimension.
- An example of angular momentum in quantum mechanics is $L_z = m\hbar = m$ where $m$ is a quantum number. $\hbar$ is of dimension angular momentum.
- A plane wave in quantum mechanics is $\Psi = Ae^{\frac{Et-px}{\hbar}}$. $\frac{Et-px}{\hbar}$ should be dimensionless, which means $px$ has dimension angular momentum, which is obvious, meanwhile we notice that $Et$ also has the dimension of angular momentum. Previously we noticed momentum has the same dimension with energy, we should have time $t$ with the same dimension of length $x$. Also we can conclude that length and time have the same dimension as $1/E$.

## A.3 Pauli Matrices and Rotations

Given a rotation

$$U = \begin{pmatrix} \cos\theta & \sin\theta \\ -\sin\theta & \cos\theta \end{pmatrix}, \tag{A.3}$$

its effect on Pauli matrices are

$$U^\dagger \sigma_3 U = \cos 2\theta \sigma_3 + \sin 2\theta \sigma_1 \tag{A.4}$$

$$U^\dagger \sigma_1 U = -\sin 2\theta \sigma_3 + \cos 2\theta \sigma_1. \tag{A.5}$$

## A.4 Lorentzian Distribution

Three-parameter Lorentzian function is

$$f_{x_0,\sigma,A}(x) = \frac{1}{\pi}\frac{\sigma}{\sigma^2 + (x - x_0)^2}, \tag{A.6}$$

which has a width $2\gamma$.

## A.5 Fourier Series

The convention for the Fourier series used in this thesis is

$$\lambda(x) = \sum_{n=-\infty}^{\infty} \Lambda_n \exp\left(\frac{i2\pi nx}{X}\right) = \sum_{n=-\infty}^{\infty} \Lambda_n \exp\left(i\omega_0 nx\right), \tag{A.7}$$

where $\omega_0 = \frac{2\pi}{X}$. The coefficients are evaluated using the orthogonal relation of exponential functions for $n \neq 0$,

$$\begin{aligned}
\Lambda_n &= \frac{1}{X}\int_0^X \lambda(x) e^{-i\omega_0 nx} dx && \text{(A.8)}\\
&= \frac{1}{X}\left(\int_0^{X_1} \lambda_1 e^{-i\omega_0 nx} dx + \int_{X_1}^{X_1+X_2} \lambda_2 e^{-i\omega_0 nx} dx\right) && \text{(A.9)}\\
&= \frac{1}{X}\frac{X}{-i2\pi n}\left(\lambda_1 e^{-i\omega_0 nX_1} + \lambda_2\left(e^{-i\omega_0 nX} - e^{-i\omega_0 nX_1}\right)\right) && \text{(A.10)}\\
&= \frac{i}{2\pi n}\left(-\lambda_1 + (\lambda_1 - \lambda_2)e^{-i2\pi nX_1/X} + \lambda_2 e^{-i2\pi n}\right). && \text{(A.11)}
\end{aligned}$$

For $n = 0$, we have

$$\Lambda_0 = \frac{X_1\lambda_1 + X_2\lambda_2}{X}. \tag{A.12}$$

For functions with specific parity, the Fourier series is much more simpler. I'll list below the Fourier series for even functions, since no odd functions are used in this thesis. In general the Fourier series of a periodic function defined on $\left[-\frac{X}{2}, \frac{X}{2}\right]$ is

$$\lambda(x) = \frac{a_0}{2} + \sum_{n=1}^{\infty} a_n \cos(n2\pi x/X) + \sum_{n=1}^{\infty} b_n \sin(n2\pi x/X), \tag{A.13}$$

where

$$a_0 = \frac{2}{X}\int_{-X/2}^{X/2} \lambda(x)dx \tag{A.14}$$

$$a_n = \frac{2}{X}\int_{-X/2}^{X/2} \lambda(x)\cos(n2\pi x/X)dx \tag{A.15}$$

$$b_n = \frac{2}{X}\int_{-X/2}^{X/2} \lambda(x)\sin(n2\pi x/X)dx. \tag{A.16}$$

For even function $\lambda(x)$, we have

$$\lambda(x) = \frac{1}{2}a_0 + \sum_{n=1}^{\infty} a_n \cos(n2\pi x/X). \tag{A.17}$$

We shift the castle wall profile and make it always even, as shown in Fig. A.1, so that

$$\lambda(x) = \begin{cases} \lambda_2, & -\frac{X_2}{2} - \frac{X_1}{2} \leq x \leq -\frac{X_1}{2} \\ \lambda_1, & -\frac{X_1}{2} \leq x \leq \frac{X_1}{2} \\ \lambda_2, & \frac{X_1}{2} \leq x \leq \frac{X_1}{2} + \frac{X_2}{2} \end{cases} \tag{A.18}$$

Fourier series of the profile is

$$\lambda(x) = \frac{1}{2}\Lambda_0 + \sum_{q=1}^{\infty} \Lambda_q \cos\left(\frac{2\pi q x}{X}\right) = \frac{1}{2}\Lambda_0 + \sum_{q=1}^{\infty} \Lambda_q \cos\left(\omega_0 q x\right), \tag{A.19}$$

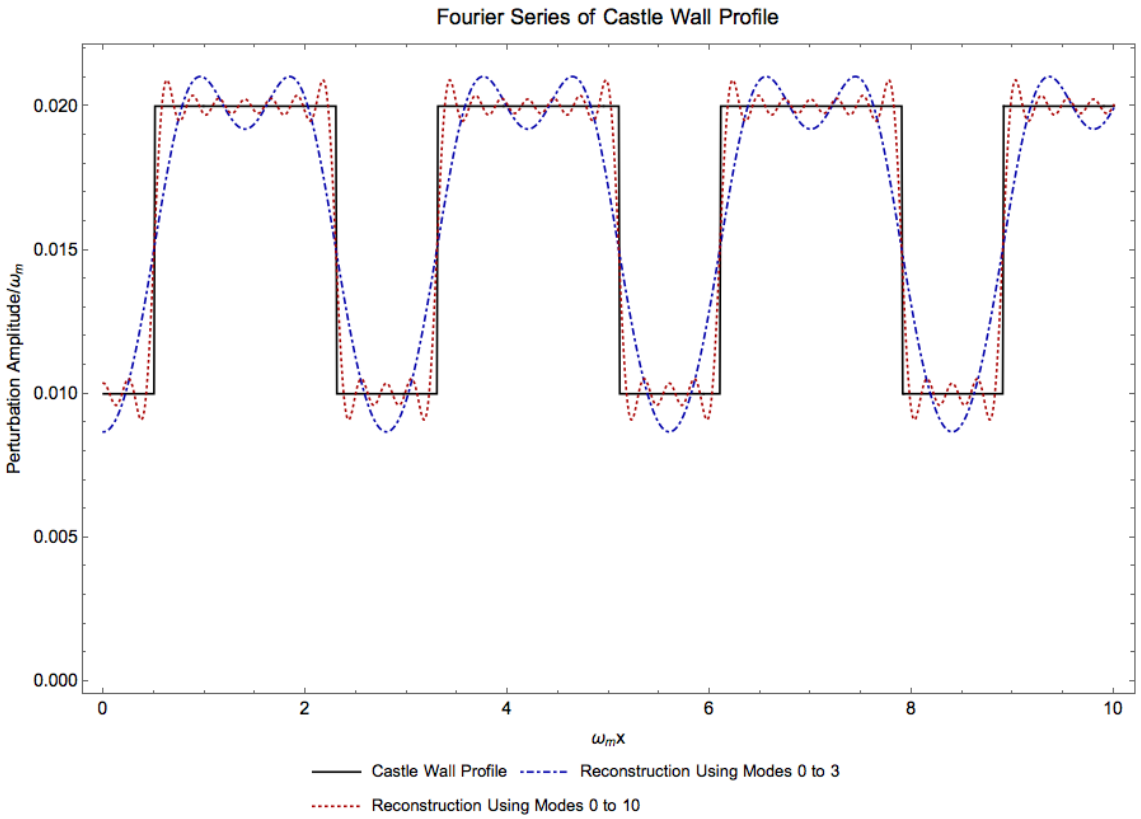


Figure A.1: Approaching an even function with Fourier series. The blue dash dotted line is the reconstruction of castle wall profile using 0 to 3 Fourier modes. The red dotted line is the reconstruction using 0 to 10 Fourier modes.

where

$$\Lambda_0 = \frac{2}{X}\int_{-X/2}^{X/2}\lambda(x)dx \tag{A.20}$$

$$= \frac{2}{X}\left(\lambda_2 X_2 + \lambda_1 X_1\right) \tag{A.21}$$

$$\Lambda_q = \frac{2}{X}\int_{-X/2}^{X/2}\lambda(x)\cos(n2\pi x/X)dx \tag{A.22}$$

$$= \frac{2}{X}\left(\lambda_2\int_{-X/2}^{-X_1/2}\cos(n2\pi x/X)dx + \lambda_1\int_{-X_1/2}^{X_1/2}\cos(n2\pi x/X)dx\right. \tag{A.23}$$

$$\left. + \lambda_2\int_{X_1/2}^{X/2}\cos(n2\pi x/X)dx\right) \tag{A.24}$$

$$= \frac{2}{q\pi}\left(\lambda_2\left(\sin(q\omega_0 X/2) - \sin(q\omega_0 X_1/2)\right) + \lambda_1\sin(q\omega_0 X_1/2)\right) \tag{A.25}$$

$$= \frac{2}{q\pi}\left(\lambda_2\left(\sin(q\pi) - \sin(q\pi X_1/X)\right) + \lambda_1\sin(q\pi X_1/X)\right) \tag{A.26}$$

## A.6 Jacobi-Anger expansion

One of the forms of Jacobi-Anger expansion is

$$e^{iz\cos(\Phi)} = \sum_{n=-\infty}^{\infty} i^n J_n(z) e^{in\Phi}. \tag{A.27}$$

## A.7 Bessel Functions

A special relation of Bessel function is that

$$J_n(n\mathrm{sech}\,\alpha) \sim \frac{e^{n(\tanh\alpha-\alpha)}}{\sqrt{2\pi n\tanh\alpha}} \tag{A.28}$$

for large $n$ [28]. As a matter of fact, for all positive $\alpha$, we always have $\tanh\alpha-\alpha<0$.

Using this relation and defining $\mathrm{sech}\,\alpha = A\cos 2\theta_m$, which renders

$$\alpha = 2n\pi i + \ln\left(\frac{1\pm\sqrt{-A^2\cos^2 2\theta_m+1}}{A\cos 2\theta_m}\right), \qquad n\in\text{Integers}, \tag{A.29}$$

where the Mathematica code to solve it is shown below,

```
In[1]:= Solve[Exp[z] + Exp[-z]
== 2/(A Cos[2 Subscript[\[Theta], m]]), z] // FullSimplify
```

we find out an more human readable analytical expression for the width

$$\Gamma = \left|2\hat{k}\tan 2\theta_m \frac{e^{n(\tanh\alpha-\alpha)}}{n_0\sqrt{2\pi n_0\tanh\alpha}}\right| \tag{A.30}$$

where $\alpha$ is solved out in A.29. For small $\alpha$, we have expansions for exponential functions and hyperbolic functions $\tanh\alpha\sim\alpha-\frac{\alpha^3}{3}$,

$$\Gamma \asymp 2\tan 2\theta_m \frac{e^{n\alpha^3/3}}{\sqrt{2\pi\alpha}n_0^{3/2}}. \tag{A.31}$$

However, it doesn't really help that much since $n$ is large and no expansion could be done except for significantly small $\alpha$.

## A.8 Conversions in Neutrino Physics

Using natural units, length = time = 1/energy, we could rescale almost all quantities in neutrino oscillations using energy, or whatever characteristic scale we have.

We use two flavor vacuum oscillations between the two masses $m_1$ and $m_2$ as an example. The characteristic energy scale is the oscillation frequency $\omega_{v,21}$. The equation of motion

$$i\frac{d}{dx}\Psi = \frac{\omega_v}{2}(-\cos 2\theta_v \boldsymbol{\sigma_3} + \sin 2\theta_v \boldsymbol{\sigma_1})\Psi, \tag{A.32}$$

can be rescaled using the characteristic energy scale $\omega_{v,21}$

$$i\frac{d}{d\hat{x}}\Psi = \frac{1}{2}(-\cos 2\theta_v \boldsymbol{\sigma_3} + \sin 2\theta_v \boldsymbol{\sigma_1})\Psi, \tag{A.33}$$

where $\hat{x} = \omega_{v,21}x$. It is convenient for numerical calculations to convert quantities into dimensionless ones.

However, we usually discuss oscillation length in SI units for a grip of the picture. To convert from natural units to SI units, we write down the conversion here. The oscillation angular frequency is given by

$$\begin{aligned}\omega_{v,21} &= \frac{\delta m^2}{2E} \\ &= \left(\frac{7.5\times 10^{-5}\mathrm{eV}^2}{2\times 1\mathrm{MeV}}\right)\left(\frac{\delta m^2}{7.5\times 10^{-5}\mathrm{eV}^2}\right)\frac{1\mathrm{MeV}}{E} \\ &= 3.75\times 10^{-11}\mathrm{eV}\left(\frac{\delta m^2}{7.5\times 10^{-5}\mathrm{eV}^2}\right)\left(\frac{1\mathrm{MeV}}{E}\right).\end{aligned} \tag{A.34}$$

On the other hand, electro-volt is related to length through the useful formula

$$197\mathrm{MeV}\cdot\mathrm{fm} = \hbar c = 1. \tag{A.35}$$

Thus we have the oscillation angular frequency written as

$$\begin{aligned}\omega_{v,21} &= 3.75\times10^{-11}\text{eV}\frac{\delta m^2}{7.5\times10^{-5}\text{eV}^2}\frac{1\text{MeV}}{E}\\ &= 3.75\times10^{-17}\text{MeV}\frac{\delta m^2}{7.5\times10^{-5}\text{eV}^2}\frac{1\text{MeV}}{E}\\ &= 1.90\times10^{-4}\text{m}^{-1}\frac{\delta m^2}{7.5\times10^{-5}\text{eV}^2}\frac{1\text{MeV}}{E}.\end{aligned} \tag{A.36}$$

Similarly for $\delta m_{32} = 2.4\times10^{-3}\text{eV}^2$ the frequency is

$$\omega_{v,32} = \frac{\delta m_{32}^2}{2E} = 6.3\times10^{-3}\text{m}^{-1}\frac{\delta m_{32}^2}{2.5\times10^{-3}\text{eV}^2}\frac{1MeV}{E}. \tag{A.37}$$

With the results for angular frequencies, the rescaled length $\hat{x}$ is restored using

$$x = \frac{\hat{x}}{\omega_v} = \frac{\hat{x}}{1.90\times10^{-4}\text{m}^{-1}\frac{\delta m^2}{7.5\times10^{-5}\text{eV}^2}\frac{1\text{MeV}}{E}} \tag{A.38}$$

$$= \frac{\hat{x}}{0.190}\text{km}\frac{7.5\times10^{-5}\text{eV}^2}{\delta m^2}\frac{E}{1\text{MeV}}. \tag{A.39}$$

Another important example is the 2 flavor neutrino oscillations in constant matter background potential $\lambda_c = \sqrt{2}G_\text{F}n_e$. The characteristic energy scale is $\omega_m$ which is calculated using

$$\omega_m = \omega_v\sqrt{\frac{\lambda_c}{\omega_v}^2 + 1 - 2\frac{\lambda_c}{\omega_v}\cos 2\theta_v}. \tag{A.40}$$

Meanwhile, the effective mixing angle $\theta_m$ is determined by

$$\tan 2\theta_m = \frac{\sin 2\theta_v}{\cos 2\theta_v - \frac{\lambda}{\omega_v}}. \tag{A.41}$$

Similar to vacuum equation of motion, we rescale the equation of motion in constant background using $\omega_m$

$$i\frac{d}{d\hat{x}}\Psi = \frac{1}{2}(-\cos 2\theta_m\boldsymbol{\sigma_3} + \sin 2\theta_m\boldsymbol{\sigma_1})\Psi, \tag{A.42}$$

we find out the scaled distance

$$\hat{x} = \omega_m x. \tag{A.43}$$

To reverse the process and find out the actual SI unit distance after the numerical calculation, we use

$$x = \frac{\hat{x}}{\omega_m}. \tag{A.44}$$

The procedure will be the following.

- Calculate $\omega_v$ using Eq. A.36.
- Calculate $\hat{\lambda}_c = \frac{\lambda_c}{\omega_v}$.
- Calculate $\omega_m$ using Eq. A.40.
- Find out the actual distance using Eq. A.44.

# Appendix B

# Rabi Oscillations

In this appendix we introduce flavor isospin [23] to Rabi oscillations and derive the transition probabilities as well as explain the resonance and width briefly.

A Rabi oscillation system is shown in Fig. B.1. The Hamiltonian for Rabi oscillation is

$$H_{\mathrm{R}} = -\frac{\omega_{\mathrm{R}}}{2}\sigma_3 - \frac{A_{\mathrm{R}}}{2}\left(\cos(k_{\mathrm{R}}t + \phi_{\mathrm{R}})\sigma_1 - \sin(k_{\mathrm{R}}t + \phi_{\mathrm{R}})\sigma_2\right), \tag{B.1}$$

in which $\omega_{\mathrm{R}}$ serves as the energy split of the two level system, while $A_{\mathrm{R}}$ and $k_{\mathrm{R}}$ are the strength and frequency of the driving field, respectively. A decomposition of the second term shows that

$$H_{\mathrm{R}} = -\frac{\boldsymbol{\sigma}}{2} \cdot (\mathbf{H}_3 + \mathbf{H}_+),$$

where $\boldsymbol{\sigma}$ is the the vector of Pauli matrices, and the three vectors are

$$\mathbf{H}_3 = \begin{pmatrix} 0 \\ 0 \\ \omega_{\mathrm{R}} \end{pmatrix}, \tag{B.2}$$

$$\mathbf{H}_+ = \begin{pmatrix} A_{\mathrm{R}} \cos(k_{\mathrm{R}} t + \phi_{\mathrm{R}}) \\ -A_{\mathrm{R}} \sin(k_{\mathrm{R}} t + \phi_{\mathrm{R}}) \\ 0 \end{pmatrix}. \tag{B.3}$$


Figure B.1: Schematic illustration of Rabi oscillations system. The two level system has two energy states at $E_1 = -\frac{\omega_0}{2}$ and $E_2 = \frac{\omega_0}{2}$, which indicating an energy gap of $\omega_0$. Incoming light has frequency $\omega$. Resonance happens when $\omega \sim \omega_0$.

The three vectors are mapped onto a Cartesian coordinate system, so that $\mathbf{H}_3$ is the vector aligned with the third axis, $\mathbf{H}_+$ is a rotating vectors in a plane perpendicular to $\mathbf{H}_3$. The wave function $\Psi = (\psi_1, \psi_2)^{\mathrm{T}}$ is also used to define the state vector $\mathbf{s}$

$$\mathbf{s} = \Psi^\dagger \frac{\boldsymbol{\sigma}}{2} \Psi \tag{B.4}$$

$$= \frac{1}{2} \begin{pmatrix} 2\,\mathrm{Re}\,(\psi_1^* \psi_2) \\ 2\,\mathrm{Im}\,(\psi_1^* \psi_2) \\ |\psi_1|^2 - |\psi_2|^2 \end{pmatrix} \tag{B.5}$$

The third component of $\mathbf{s}$, which is denoted as $s_3$, is within range $[-1/2, 1/2]$. The two limits, $s_3 = -1/2$ and $s_3 = 1/2$ stand for the system in high energy state and

low energy state respectively. $s_3 = 0$ if the system has equal probabilities to be on high energy state and low energy state. The Schrödinger equation becomes

$$\frac{\mathrm{d}}{\mathrm{d}t}\mathbf{s} = \mathbf{s} \times \mathbf{H}, \tag{B.6}$$

which is the precession equation. For static $\mathbf{H}$, the state vector $\mathbf{s}$ precess around $\mathbf{H}$.

In a frame that corotates with $\mathbf{H}_+$, which is described in Fig. B.2, the new Hamiltonian is

$$\frac{\mathrm{d}}{\mathrm{d}t}\mathbf{s} = \mathbf{s} \times (\mathbf{H}'_3 + \mathbf{H}_+), \tag{B.7}$$

where

$$\mathbf{H}'_3 = \begin{pmatrix} 0 \\ 0 \\ \omega_\mathrm{R} - k_\mathrm{R} \end{pmatrix}, \qquad \mathbf{H}'_+ = \begin{pmatrix} A_\mathrm{R} \\ 0 \\ 0 \end{pmatrix}. \tag{B.8}$$

The state vector $\mathbf{s}$ precess around a static vector $\mathbf{H}'_3 + \mathbf{H}'_+$ with a frequency $\Omega_\mathrm{R} = \sqrt{|A_\mathrm{R}|^2 + (k_\mathrm{R} - \omega_\mathrm{R})^2}$. A geometric analysis by projecting the state vector $\mathbf{s}$ on to the vertical axis shows that

$$s_3 = \frac{1}{2} - \frac{|A_\mathrm{R}|^2}{\Omega_\mathrm{R}^2} \sin^2\left(\frac{\Omega_\mathrm{R}}{2}t\right). \tag{B.9}$$

Resonance occurs when the term $\mathbf{H}_3$ disappears in this corotating frame, since the state vector $\mathbf{s}$ converts completely between $+1/2$ (low energy state) and $-1/2$ (high energy state).

Such a system has analytical transition probability from low energy state to high energy state

$$P(t) = \frac{1}{2}(1 - 2s_3(t)) = \frac{|A_\mathrm{R}|^2}{\Omega_\mathrm{R}^2} \sin^2\left(\frac{\Omega_\mathrm{R}}{2}t\right), \tag{B.10}$$

where

$$\Omega_\mathrm{R} = \sqrt{|A_\mathrm{R}|^2 + (k_\mathrm{R} - \omega_\mathrm{R})^2} \tag{B.11}$$

is known as Rabi frequency. The detuning, which is defined by $k_\mathrm{R} - \omega_\mathrm{R}$, determines how off-resonance the system is, and amplitude of driving field $A_\mathrm{R}$ determines the

resonance width,

$$\text{Detuning} = |k_{\mathrm{R}} - \omega_{\mathrm{R}}|, \tag{B.12}$$

$$\text{Resonance Width} = |A_{\mathrm{R}}|, \tag{B.13}$$

which is also shown in Fig. B.3 and Fig. B.4. The transition probability oscillates with frequency $\Omega_{\mathrm{R}}$. However, the amplitude $A_1$ is the dominate factor for oscillation frequency when the system is close to resonance. The phase of the matter potential $\phi_{\mathrm{R}}$ has no effect on the transition probability since it only determines the initial phase of driving Hamiltonian vector $\mathbf{H}_+$. We also notice that the transition amplitude is determined by relative detuning $D$, which is defined as

$$D = \left| \frac{k_{\mathrm{R}} - \omega_{\mathrm{R}}}{A_{\mathrm{R}}} \right|. \tag{B.14}$$

Given a Rabi oscillation system with two driving frequencies

$$\begin{aligned} H_{\mathrm{R}} = &- \frac{\omega_{\mathrm{R}}}{2}\sigma_3 - \frac{A_1}{2}\left(\cos(k_1 t + \phi_1)\sigma_1 - \sin(k_1 t + \phi_1)\sigma_2\right) \\ &- \frac{A_2}{2}\left(\cos(k_2 t + \phi_2)\sigma_1 - \sin(k_2 t + \phi_2)\sigma_2\right) \end{aligned}$$

we decompose it into $\mathbf{H}_{\mathrm{R}} = \mathbf{H}_3 + \mathbf{H}_1 + \mathbf{H}_2$, where

$$\mathbf{H}_1 = \begin{pmatrix} A_1 \cos(k_1 t + \phi_1) \\ A_1 \sin(k_1 t + \phi_1) \\ 0 \end{pmatrix}, \mathbf{H}_2 = \begin{pmatrix} A_2 \cos(k_2 t + \phi_2) \\ A_2 \sin(k_2 t + \phi_2) \\ 0 \end{pmatrix}.$$

Assume $\mathbf{H}_1$ is the on-resonance perturbation which requires $k_1 = \omega_{\mathrm{R}}$. The most general condition that we can drop the new perturbation $\mathbf{H}_2$ is to make sure $k_2$ is far from the resonance condition compared to the resonance width,

$$D \equiv \frac{|k_2 - \omega_{\mathrm{R}}|}{|A_2|} \gg 1. \tag{B.15}$$

The transition amplitude between the two states becomes

$$P(t) = \frac{1}{1 + D^2} \sin^2\left(\frac{\Omega_{\mathrm{R}}}{2} t\right). \tag{B.16}$$

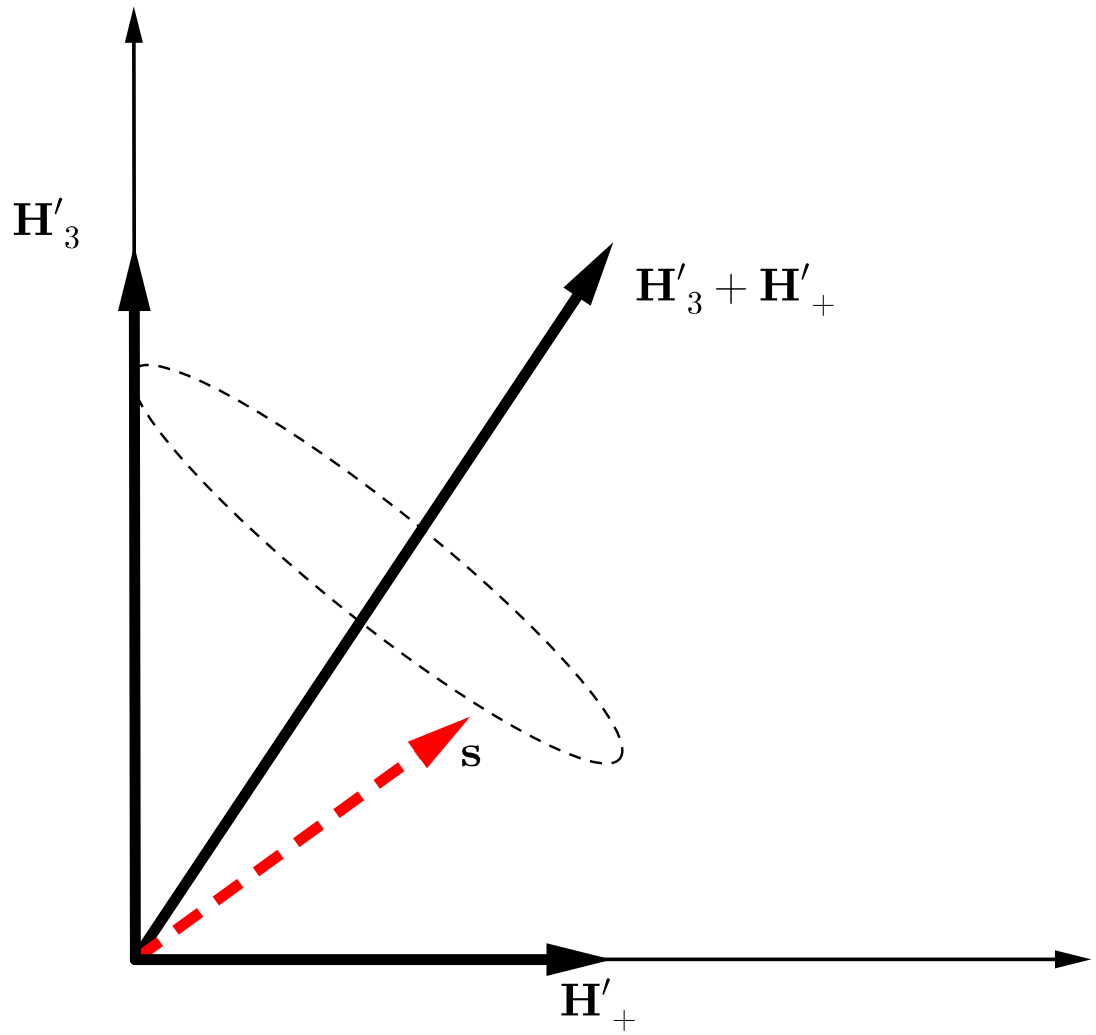


Figure B.2: Rabi oscillations in corotating frame. The red dashed vector is the flavor isospin, while the black solid vectors are the vectors of Hamiltonian. The flavor isospin vector is precessing around vector of total Hamiltonian $\mathbf{H}_3 + \mathbf{H}_+$.

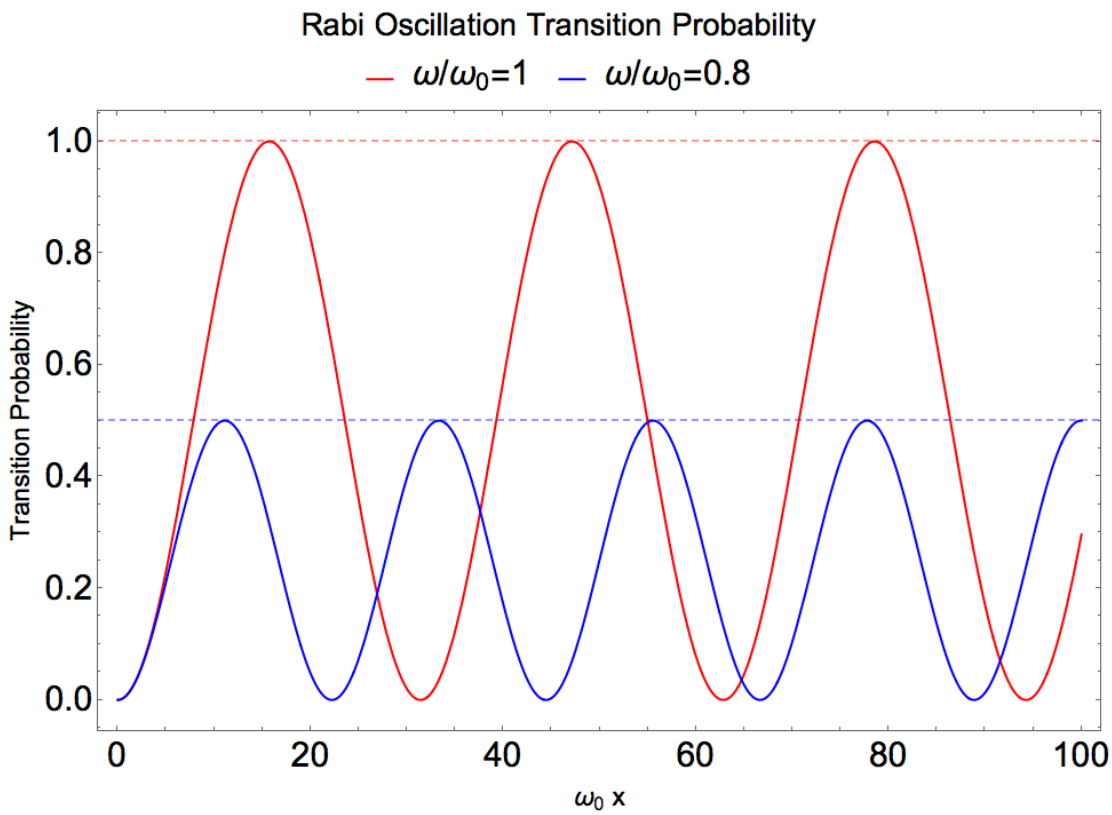


Figure B.3: Rabi oscillations for two different incoming light frequencies. $\omega/\omega_0 = 1$ is the resonance condition. As for $\omega/\omega_0 = 0.8$, the oscillation amplitude becomes 0.5.

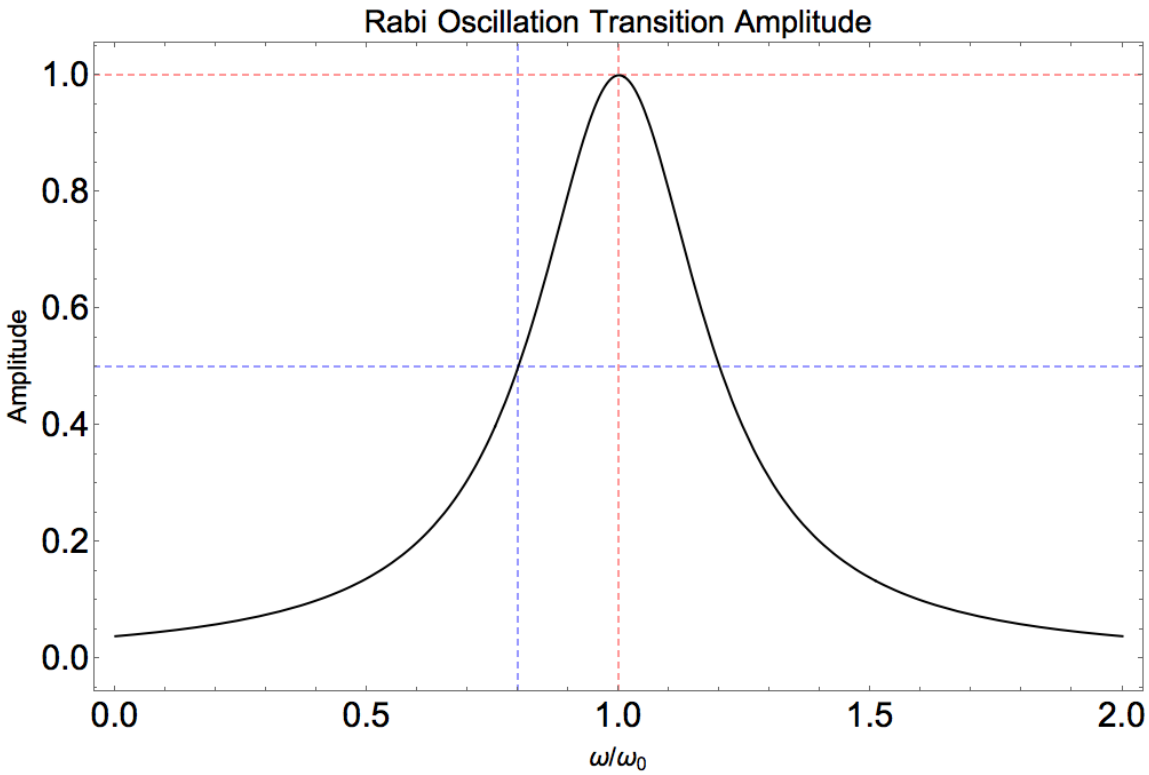


Figure B.4: Rabi oscillations for two different incoming light frequencies. $\omega/\omega_0 = 1$ is the resonance condition. The amplitude reach maximum when $\omega/\omega_0 = 1$. Resonance width is defined to be the width where amplitude becomes half of the maximum which is shown with blue dashed lines.

# Appendix C

# MSW Effect Revisited

## C.1 Flavor Basis

In terms of formalism, vacuum oscillations is already a Rabi oscillation at resonance with oscillation width $\omega_v \sin 2\theta_v$. As derived, neutrino oscillations in matter are determined by Hamiltonian in flavor basis

$$H^{(f)} = \left(-\frac{1}{2}\omega_v \cos 2\theta_v + \frac{1}{2}\lambda(x)\right)\sigma_3 + \frac{1}{2}\omega_v \sin 2\theta_v \sigma_1, \tag{C.1}$$

with the Schröding equation

$$i\partial_x \Psi^{(f)} = H^{(f)}\Psi^{(f)}. \tag{C.2}$$

To make connections to Rabi oscillations, we would like to remove the changing $\sigma_3$ terms, using a transformation

$$U = \begin{pmatrix} e^{-i\eta(x)} & 0 \\ 0 & e^{i\eta(x)} \end{pmatrix}, \tag{C.3}$$

which transform the flavor basis to another basis

$$\begin{pmatrix} \psi_e \\ \psi_x \end{pmatrix} = \begin{pmatrix} e^{-i\eta(x)} & 0 \\ 0 & e^{i\eta(x)} \end{pmatrix} \begin{pmatrix} \psi_a \\ \psi_b \end{pmatrix}. \tag{C.4}$$

The Schrodinger equation can be written into this new basis

$$i\partial_x(T\Psi^{(r)}) = H^{(f)}T\Psi^{(r)}, \tag{C.5}$$

which is simplified to

$$i\partial_x\Psi^{(r)} = H^{(r)}\Psi^{(r)}, \tag{C.6}$$

where

$$H^{(r)} = -\frac{1}{2}\omega_v \cos 2\theta_v\sigma_3 + \frac{1}{2}\omega_v \sin 2\theta_v \begin{pmatrix} 0 & e^{2i\eta(x)} \\ e^{-2i\eta(x)} & 0 \end{pmatrix}, \tag{C.7}$$

in which we remove the varying component of $\sigma_3$ elements using

$$\frac{d}{dx}\eta(x) = \frac{\lambda(x)}{2}. \tag{C.8}$$

The final Hamiltonian would have some form

$$H^{(r)} = -\frac{1}{2}\omega_v \cos 2\theta_v\sigma_3 + \frac{1}{2}\omega_v \sin 2\theta_v \begin{pmatrix} 0 & e^{i\int_0^x \lambda(\tau)d\tau + 2i\eta(0)} \\ e^{-i\int_0^x \lambda(\tau)d\tau - 2i\eta(0)} & 0 \end{pmatrix}, \tag{C.9}$$

where $\eta(0)$ is chosen to counter the constant terms from the integral.

For arbitrary matter profile, we could first apply Fourier expand the profile into trig function then use Jacobi-Anger expansion so that the system becomes a lot of Rabi oscillations. Any transformations or expansions that decompose $\exp\left(i\int_0^x \lambda(\tau)d\tau\right)$ into many summations of $\exp(iax + b)$ would be enough for an Rabi oscillation interpretation. As for constant matter profile, $\lambda(x) = \lambda_0$, we have

$$\eta(x) = \frac{1}{2}\lambda_0 x. \tag{C.10}$$

The Hamiltonian becomes

$$H^{(r)} = -\frac{1}{2}\omega_v \cos 2\theta_v\sigma_3 + \frac{1}{2}\omega_v \sin 2\theta_v \begin{pmatrix} 0 & e^{i\lambda_0 x} \\ e^{-i\lambda_0 x} & 0 \end{pmatrix}, \tag{C.11}$$

which is exactly a Rabi oscillation. The resonance condition is

$$\lambda_0 = \omega_v \cos 2\theta_v. \tag{C.12}$$

## C.2 Instantaneous Matter Basis

Neutrino oscillations can be calculated in instantaneous matter basis, where the Schrödinger equation is transformed to instantaneous matter basis by applying a rotation $U$,

$$i\partial_x \left(U\Psi^{(m)}\right) = H^{(f)}U\Psi^{(m)}, \tag{C.13}$$

where

$$U = \begin{pmatrix} \cos\theta_m & \sin\theta_m \\ -\sin\theta_m & \cos\theta_m \end{pmatrix}. \tag{C.14}$$

With some simple algebra, we can write the system into

$$i\partial_x\Psi^{(m)} = H^{(m)}\Psi^{(m)}, \tag{C.15}$$

where

$$H^{(m)} = U^\dagger H^{(f)}U - iU^\dagger\partial_x U. \tag{C.16}$$

By setting the off-diagonal elements of the first term $U^\dagger H^{(f)}U$ to zero, we can derive the relation

$$\tan 2\theta_m = \frac{\sin 2\theta_v}{\cos 2\theta_v - \lambda/\omega_v}. \tag{C.17}$$

Furthermore, we derive the term

$$iU^\dagger\partial_x U = -\dot{\theta}_m\sigma_2. \tag{C.18}$$

We can calculate $\dot{\theta}_m$ by taking the derivative of $\tan 2\theta_m$,

$$\frac{d}{dx}\tan 2\theta_m = \frac{2}{\cos^2 2\theta_m}\dot{\theta}_m, \tag{C.19}$$

so that

$$\dot{\theta}_m = \frac{1}{2}\cos^2(2\theta_m)\frac{d}{dx}\tan 2\theta_m \tag{C.20}$$

$$= \frac{1}{2}\frac{(\cos 2\theta_v - \lambda/\omega_v)^2}{(\lambda/\omega_v)^2 + 1 - 2\lambda\cos 2\theta_v/\omega_v}\frac{d}{dx}\frac{\sin 2\theta_v}{\cos 2\theta_v - \lambda/\omega_v} \tag{C.21}$$

$$= \frac{1}{2}\frac{(\cos 2\theta_v - \lambda/\omega_v)^2}{(\lambda/\omega_v)^2 + 1 - 2\lambda\cos 2\theta_v/\omega_v}\frac{\sin 2\theta_v}{(\cos 2\theta_v - \lambda/\omega_v)^2}\frac{1}{\omega)v}\frac{d}{dx}\lambda(x) \tag{C.22}$$

$$= \frac{1}{2}\sin 2\theta_m \frac{1}{\omega_m}\frac{d}{dx}\lambda(x). \tag{C.23}$$

## C.3 Bipolar Model

The nature of this section is to provide the linear stability analysis of bipolar model. Bipolar model is a model of neutrino oscillations with the presence of neutrino and antineutrinos. It is also called bimodal oscillations [13], which means two frequencies in the context. An example of such instability happens in a system composed of equal amounts of neutrinos and antineutrinos.

Neutrino oscillations has a small amplitude inside a SN core (suppressed by matter effects) [5], which basically pins down the flavour transformation. As the neutrinos reaches a further distance, matter effect could drop out. Neutrino self-interaction becomes more important. S. Samuel considers a system of neutrinos and antineutrinos with only vacuum and neutrino self-interactions [13]. The neutrinos and antineutrino forms a bipolar vector in flavor isospin space. The flavor isospin of neutrinos and that of antineutrinos are coupled.

The equation of motion is

$$i\partial_t\rho = \left[-\frac{\omega_v}{2}\cos 2\theta\sigma_3 + \frac{\omega_v}{2}\sin 2\theta\sigma_1 - \mu\alpha\bar{\rho}, \rho\right]$$
$$i\partial_t\bar{\rho} = \left[\frac{\omega_v}{2}\cos 2\theta\sigma_3 - \frac{\omega_v}{2}\sin 2\theta\sigma_1 + \mu\rho, \bar{\rho}\right].$$

For the purpose of linear stability analysis, we assume that

$$\rho = \frac{1}{2}\begin{pmatrix} 1 & \epsilon \\ \epsilon^* & -1 \end{pmatrix}$$
$$\bar{\rho} = \frac{1}{2}\begin{pmatrix} 1 & \bar{\epsilon} \\ \bar{\epsilon}^* & -1 \end{pmatrix}.$$

Plug them into equation of motion and set $\theta = 0$, we have the linearized ones,

$$i\partial_t \begin{pmatrix} \epsilon \\ \bar{\epsilon} \end{pmatrix} = \frac{1}{2}\begin{pmatrix} -\alpha\mu - \omega_v & \alpha\mu \\ -\mu & \mu + \omega_v \end{pmatrix}\begin{pmatrix} \epsilon \\ \bar{\epsilon} \end{pmatrix}.$$

To have real eigenvalues, we require

$$(-1+\alpha)^2\mu^2 + 4(1+\alpha)\mu\omega_v + 4\omega_v^2 < 0,$$

which is reduced to

$$\frac{-2\omega_v(1+\alpha) - 4\sqrt{\alpha}|\omega_v|}{(1-\alpha)^2} < \mu < \frac{-2\omega_v(1+\alpha) + 4\sqrt{\alpha}|\omega_v|}{(1-\alpha)^2}.$$

It is simplified to

$$\sqrt{-2\omega_v}(1-\sqrt{\alpha})^2 < \mu < \sqrt{-2\omega_v}(1+\sqrt{\alpha})^2,$$

assuming normal hierarchy, i.e., $\omega_v > 0$. We immediately notice that this can not happen.

For inverted hierarchy, we have $\omega_v < 0$, so that

$$\sqrt{2|\omega_v|}(1+\sqrt{\alpha})^2 < \mu < \sqrt{2|\omega_v|}(1-\sqrt{\alpha})^2,$$

Within this region, neutrinos experience exponential growth.

For completeness, we also write down the formalism in flavor isospin picture.

$$i\partial_t \mathbf{s} = \mathbf{s} \times (\eta\mathbf{H}_v + \alpha\mu\bar{\mathbf{s}}) \tag{C.24}$$
$$i\partial_t \bar{\mathbf{s}} = \bar{\mathbf{s}} \times (\eta\mathbf{H}_v + \mu\mathbf{s}), \tag{C.25}$$

where $\eta$ is the hierarchy, and $\alpha$ is the ratio of neutrino number density and antineutrino number density.

# Glossary

| | |
|---|---|
| $\nu_{e,\mu,\tau}$ | Electron, muon, tao flavor neutrinos |
| IH | Inverted hierarchy |
| NH | Normal hierarchy |
| DUNE | Deep Underground Neutrino Experiment |
| AGN | Active Galactic Nuclei |
| CNO | Carbon-Nitrogen-Oxygen |
| RWA | Rotating Wave Approximation |

# Bibliography


[1] C L Cowan et al. "Detection of the Free Neutrino: a Confirmation." In: *Science (New York, N.Y.)* 124.3212 (July 1956), pp. 103–4.

[2] B Pontecorvo. "Neutrino experiments and the problem of conservation of leptonic charge". In: *Sov. Phys. JETP* 26.5 (1968), pp. 984–988.

[3] J.N. Bahcall. "The solar neutrino problem". In: *Nuclear Instruments and Methods* 110 (July 1973), pp. 381–384.

[4] Elliott G Flowers and Peter G Sutherland. "Neutrino-neutrino scattering and supernovae". In: *The Astrophysical Journal* 208.1 (Aug. 1976), p. L19.

[5] L. Wolfenstein. "Neutrino oscillations in matter". In: *Physical Review D* 17.9 (May 1978), pp. 2369–2374.

[6] L. Wolfenstein. "Neutrino oscillations and stellar collapse". In: *Physical Review D* 20.10 (Nov. 1979), pp. 2634–2635.

[7] S. P. Mikheev and A. Yu. Smirnov. "Resonance Amplification of Oscillations in Matter and Spectroscopy of Solar Neutrinos". In: *Sov. J. Nucl. Phys.* 42 (1985). [Yad. Fiz.42,1441(1985)], pp. 913–917.

[8] J. N. Bahcall, A. Dar, and T. Piran. "Neutrinos from the recent LMC supernova". In: *Nature* 326.6109 (Mar. 1987), pp. 135–136.

[9] P.I. Krastev and A.Yu. Smirnov. "Parametric effects in neutrino oscillations". In: *Physics Letters B* 226.3-4 (Aug. 1989), pp. 341–346.

[10] T. K. Kuo and James Pantaleone. "Neutrino oscillations in matter". In: *Reviews of Modern Physics* 61.4 (Oct. 1989), pp. 937–979.

[11] G. Sigl and G. Raffelt. "General kinetic description of relativistic mixed neutrinos". In: *Nuclear Physics B* 406.1-2 (Sept. 1993), pp. 423–451.

[12] F. N. Loreti and A. B. Balantekin. "Neutrino oscillations in noisy media". In: *Physical Review D* 50.8 (Oct. 1994), pp. 4762–4770. arXiv: `9406003 [nucl-th]`.

[13] Stuart Samuel. "Bimodal coherence in dense self-interacting neutrino gases". In: *Physical Review D* 53.10 (May 1996), pp. 5382–5393. arXiv: `9604341 [hep-ph]`.

[14] S. T. Petcov. "Diffractive-like (or parametric-resonance-like?) enhancement of the Earth (day-night) effect for solar neutrinos crossing the Earth core". In: *Physics Letters B* 434.3-4 (Aug. 1998), pp. 321–332. arXiv: `9805262 [hep-ph]`.

[15] T. Totani et al. "Future Detection of Supernova Neutrino Burst and Explosion Mechanism". In: *The Astrophysical Journal* 496.1 (Mar. 1998), pp. 216–225.

[16] E.Kh. Akhmedov. "Parametric resonance of neutrino oscillations and passage of solar and atmospheric neutrinos through the earth". In: *Nuclear Physics B* 538.1-2 (Jan. 1999), pp. 25–51. arXiv: `hep-ph/9805272 [hep-ph]`.

[17] E. Kh Akhmedov. "Parametric resonance in neutrino oscillations in matter". In: *Pramana* 54.1 (Jan. 2000), pp. 47–63. arXiv: `9907435 [hep-ph]`.

[18] Michael F Altmann, Rudolf L Mößbauer, and Lothar J N Oberauer. "Solar neutrinos". In: *Reports on Progress in Physics* 64.1 (Jan. 2001), pp. 97–146.

[19] S.T. Petcov and M. Piai. "The LMA MSW solution of the solar neutrino problem, inverted neutrino mass hierarchy and reactor neutrino experiments". In: *Physics Letters B* 533.1-2 (May 2002), pp. 94–106. arXiv: `hep-ph/0112074 [hep-ph]`.

[20] Mathias Th. Keil. "Supernova Neutrino Spectra and Applications to Flavor Oscillations". PhD thesis. 2003. arXiv: 0308228 [astro-ph].

[21] Georg G. Raffelt et al. "Supernova neutrinos: Flavor-dependent fluxes and spectra". In: *Neutrino oscillations and their origin. Proceedings, 4th International Workshop, NOON2003, Kanazawa, Japan, February 10-14, 2003*. 2003, pp. 380–387. arXiv: astro-ph/0303226 [astro-ph].

[22] Huaiyu Duan, George M. Fuller, and Yong-Zhong Qian. "Analysis of collective neutrino flavor transformation in supernovae". In: *Physical Review D* 74.12 (Dec. 2006), p. 123004. arXiv: 0703776 [astro-ph].

[23] Huaiyu Duan, George M. Fuller, and Yong-Zhong Qian. "Collective neutrino flavor transformation in supernovae". In: *Physical Review D* 74.12 (Dec. 2006), p. 123004. arXiv: 0703776 [astro-ph].

[24] Huaiyu Duan et al. "Simulation of coherent nonlinear neutrino flavor transformation in the supernova environment: Correlated neutrino trajectories". In: *Physical Review D - Particles, Fields, Gravitation and Cosmology* 74 (2006), pp. 1–22. arXiv: 0606616 [astro-ph].

[25] Alexander Friedland and Andrei Gruzinov. "Neutrino signatures of supernova turbulence". July 2006.

[26] J. P. Kneller and G. C. McLaughlin. "Monte Carlo neutrino oscillations". In: *Physical Review D* 73.5 (Mar. 2006), p. 056003.

[27] R. W. Boyd. *Nonlinear Optics*. Third. Elsevier, 2008. ISBN: 978-0-12-369470-6.

[28] I. Ploumistakis, S. D. Moustaizis, and I. Tsohantjis. "Towards laser based improved experimental schemes for multiphoton e+e-pair production from vacuum". In: *Physics Letters, Section A: General, Atomic and Solid State Physics* 373.32 (2009), pp. 2897–2900. arXiv: 0907.2555v1.

[29] I. Ploumistakis, S.D. Moustaizis, and I. Tsohantjis. "Towards laser based improved experimental schemes for multiphoton pair production from vacuum". In: *Physics Letters A* 373.32 (2009), pp. 2897–2900.

[30] Huaiyu Duan, George M. Fuller, and Yong-Zhong Qian. "Collective Neutrino Oscillations". In: *Annual Review of Nuclear and Particle Science* 60.1 (Nov. 2010), pp. 569–594. arXiv: 1001.2799.

[31] James Kneller and Cristina Volpe. "Turbulence effects on supernova neutrinos". In: *Physical Review D* 82.12 (Dec. 2010), p. 123004. arXiv: 1006.0913.

[32] Eg Adelberger and a García. "Solar fusion cross sections. II. The pp chain and CNO cycles". In: *Reviews of Modern ...* 83.March (2011). arXiv: arXiv:1004.2318v3.

[33] John F. Cherry et al. "Neutrino scattering and flavor transformation in supernovae". In: *Physical Review Letters* 108.June (2012), pp. 1–5. arXiv: arXiv:1203.1607v1.

[34] Srdjan Sarikas et al. "Supernova neutrino halo and the suppression of self-induced flavor conversion". In: *Physical Review D - Particles, Fields, Gravitation and Cosmology* 85.11 (2012), pp. 1–5. arXiv: arXiv:1204.0971v1.

[35] James P. Kneller, Gail C. McLaughlin, and Kelly M. Patton. "Stimulated neutrino transformation with sinusoidal density profiles". In: *Journal of Physics G: Nuclear and Particle Physics* 40.5 (May 2013), p. 055002. arXiv: arXiv:1202.0776v1.

[36] Ilídio Lopes and Sylvaine Turck-Chièze. "Solar Neutrino Physics Oscillations: Sensitivity To the Electronic Density in the Sun's Core". In: *The Astrophysical Journal* 765.1 (2013), p. 14.

[37] Georg Raffelt, Srdjan Sarikas, and David De Sousa Seixas. "Axial Symmetry Breaking in Self-Induced Flavor Conversionof Supernova Neutrino Fluxes". In: *Physical Review Letters* 111.9 (Aug. 2013), p. 091101.

[38] a Malkus, A Friedland, and G. C. McLaughlin. "Matter-Neutrino Resonance Above Merging Compact Objects". In: 1 (Mar. 2014), pp. 1–6. arXiv: 1403.5797.

[39] Gianpiero Mangano, Alessandro Mirizzi, and Ninetta Saviano. "Damping the neutrino flavor pendulum by breaking homogeneity". In: *Physical Review D* 89.7 (Apr. 2014), p. 073017. arXiv: 1403.1892.

[40] Kelly M. Patton, James P. Kneller, and Gail C. McLaughlin. "Stimulated neutrino transformation through turbulence". In: *Physical Review D* 89.7 (Apr. 2014), p. 073022. arXiv: arXiv:1407.7835v1.

[41] Sean M. Couch and Christian D. Ott. "The Role of Turbulence in Neutrino-driven Core-collapse Supernova Explosions". In: *The Astrophysical Journal* 799.1 (Jan. 2015), p. 5.

[42] B. Muller and H.- T. Janka. "Non-radial instabilities and progenitor asphericities in core-collapse supernovae". In: *Monthly Notices of the Royal Astronomical Society* 448.3 (Feb. 2015), pp. 2141–2174.

[43] D. Vaananen and G. C. McLaughlin. "Uncovering the Matter-Neutrino Resonance". In: (Oct. 2015), pp. 1–16. arXiv: 1510.00751.

[44] Sovan Chakraborty et al. "Self-induced neutrino flavor conversion without flavor mixing". In: *Journal of Cosmology and Astroparticle Physics* 2016.03 (Mar. 2016), pp. 042–042. arXiv: 1602.00698.

[45] Hans-Thomas Janka, Tobias Melson, and Alexander Summa. "Physics of Core-Collapse Supernovae in Three Dimensions: A Sneak Preview". In: *Annual Review of Nuclear and Particle Science* 66.1 (2016), pp. 341–375. arXiv: 1602.05576.

[46] C. Patrignani et al. "Review of Particle Physics". In: *Chin. Phys.* C40.10 (2016), p. 100001.

[47] R. F. Sawyer. "Neutrino Cloud Instabilities Just above the Neutrino Sphere of a Supernova". In: *Physical Review Letters* 116.8 (2016), pp. 1–5. arXiv: 1509.03323.

[48] Meng-Ru Wu, Huaiyu Duan, and Yong-Zhong Qian. "Physics of neutrino flavor transformation through resonances". In: *Physics Letters B* 752 (Jan. 2016), pp. 89–94. arXiv: 1509.08975.

[49] Basudeb Dasgupta, Alessandro Mirizzi, and Manibrata Sen. "Fast neutrino flavor conversions near the supernova core with realistic flavor-dependent angular distributions". In: *Journal of Cosmology and Astroparticle Physics* 2017.02 (Feb. 2017), pp. 019–019. arXiv: 1609.00528.

[50] Ignacio Izaguirre, Georg Raffelt, and Irene Tamborra. "Fast Pairwise Conversion of Supernova Neutrinos: A Dispersion Relation Approach". In: *Physical Review Letters* 118.2 (Jan. 2017), p. 021101. arXiv: 1610.01612.

[51] E. Kemp. "The Deep Underground Neutrino Experiment: The precision era of neutrino physics". In: *Astronomische Nachrichten* 338.9-10 (2017), pp. 993–999.

[52] *The Garching Core-Collapse Supernova Archive, http://wwwmpa.mpa-garching.mpg.de/ccsna*